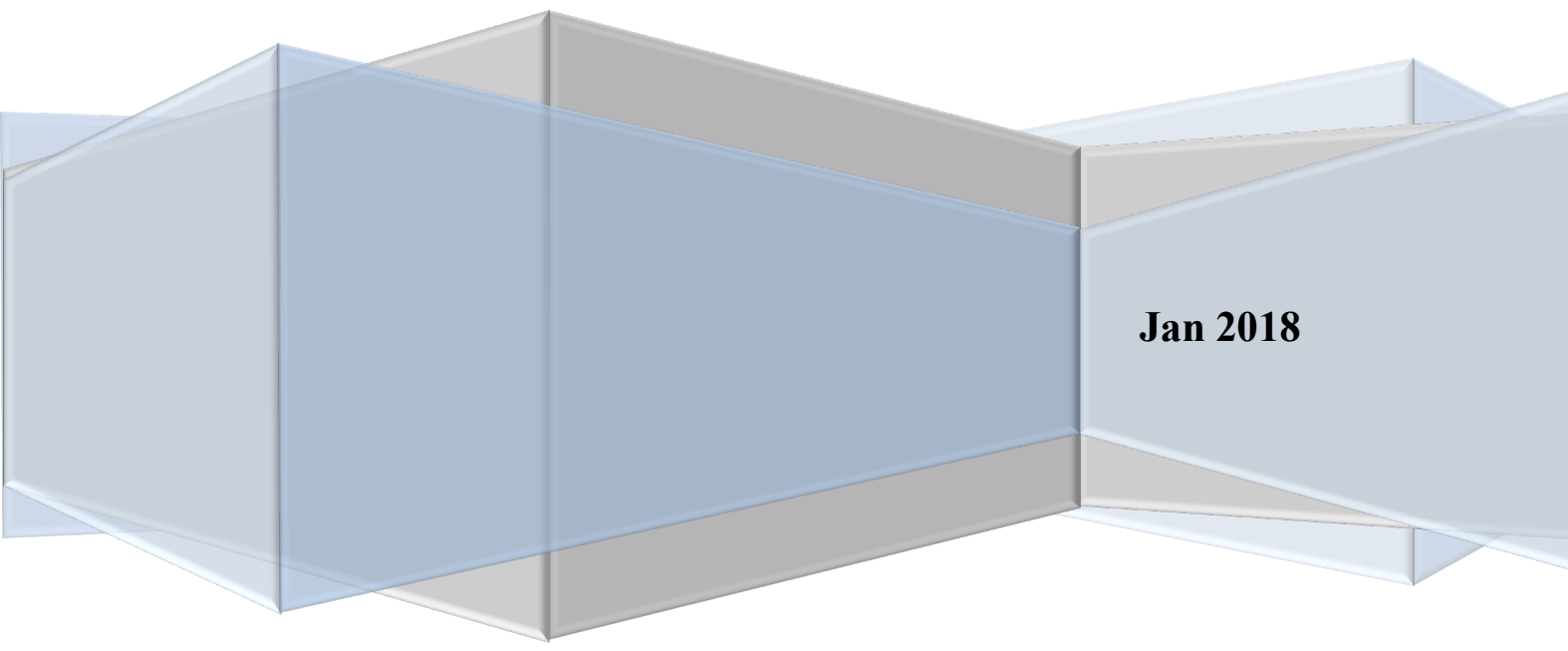


**Reservoir Management Improvement  
Under Current and Future Climate Conditions  
Based on Evolutionary Computation Technique Application  
for Calibrating Hydrological Model and Optimizing Rule Curves**

**NGUYEN THI THUY HANG**



**Jan 2018**

# ABSTRACT

The main objective of this study is to investigate the impacts of climate change on Thac Mo reservoir control and the reservoir operation improvements under current and future climate conditions by using the evolutionary computational technique, differential evolution (DE), for calibrating a hydrological model and optimizing reservoir operation rule curves. It was achieved by (1) evaluating the performance of differential evolution (DE) and evolution strategy (ES) in automatic calibration of a rainfall-runoff model called Long-and-Short Term runoff model (LST model) for Be River catchment in Vietnam, (2) analyzing the impact of climate change on inflow into reservoir and reservoir control of Thac Mo reservoir in the upper Be River catchment based on historical operation, (3) evaluating the performance of DE application in reservoir operation optimization for Thac Mo reservoir, and (4) analyzing the adaptive operation rules under climate change conditions compared with the current.

The results of using DE and ES in LST model calibration showed that both DE and ES algorithms are efficient methods for automatic calibration of the LST model. DE was proved to be slightly better than ES with the better obtained fitness indices and shorter computation time. Calibrated LST model using DE was integrated into reservoir operation model for Thac Mo reservoir.

The result of the inflow into the reservoir simulated by using the calibrated LST model and other parameters of reservoir control for the current and future climate scenarios showed that the inflow into the reservoir increases dramatically in the rainy season, but there is less change in the dry season. There is a less noticeable change in the reservoir storage and in the amount of water used for hydropower compared to the water spilled out of the reservoir for safety reasons during the flood season.

Improving Thac Mo reservoir operation rule in the dry season was investigated by employing DE using multi-objective function considering shortage index (*WSI*), annual power production (*APP*) and power production stability (*PPS*) in optimization. The simulations demonstrated that the performances by optimized rules were remarkably

improved in comparison with that by government existing rule and the historical operations. The RCP4.5 scenario resulted in the greatest changes in the balance distance, and the second best results were under the RCP8.5. The optimized rules showed better performances than that by the existing rule.

In overall, this study proved the efficiency of evolutionary technique especially DE in hydrological model calibration and reservoir operation optimization. Moreover, the study helped better understanding about evolutionary technique application in hydrology research as well as the impacts of climate change on runoff, reservoir control, and adaptive reservoir operation.

## ACKNOWLEDGEMENT

My PhD program was sponsored by the Japanese Government (Monbukagakusho). Research grant funded by Graduate School of Environmental and Life Science-Okayama University also supported for my research in collecting data and participating in academic conferences. During my PhD period, I have received supports from many individuals. It is pleasure to acknowledge to those who contributed to completion of my PhD research.

Firstly, I would like to thank to my supervisor Prof. Hidetaka Chikamori for the continuous support of the MEXT scholarship applying stage and during my PhD course, for his guidance, advice, and kindness. I have been lucky to have a supervisor who has not only cared much about my work and my life but also given me freedom to carry out my study through my time as his student.

Besides my supervisor, I would like to thank the rest of my co-supervisor: Prof. Moroizumi Toshitsugu, and Prof. Maeda Morihiro, for their comments and also for their willingness to review and evaluate my thesis.

I would like to express my gratitude to Assoc. Prof. Nguyen Thi Bay (University of Technology, VNU-HCMC), Assoc. Prof. Vu Van Nghi (University of Science, VNU-HCMC), Dr. Dao Nguyen Khoi (University of Science, VNU-HCMC), Msc. Nguyen Quang Long (University of Science, VNU-HCMC), Msc. Nguyen Tram Anh (Ho Chi Minh University of Natural Resources and Environment ), Dr. Nguyen Thi Phuong (Sub-Institute of Hydro-meteorological and Environment of South Vietnam), Mr. Vo Minh Thau (Thac Mo Hydro Power JSC), and other colleagues in Vietnam for their encouragement and support in data collection for my study.

Finally, I'm also thankful to family for their presence and loving support behind me throughout my life. My mother passed over many years before I started my PhD course; however, she deserves special mention not only for her sacrifice but also for the inspiration to face challenges of my life and my PhD completion.

# TABLE OF CONTENTS

ABSTRACT.....	i
ACKNOWLEDGEMENT .....	iii
TABLE OF CONTENTS.....	iv
LIST OF FIGURES.....	vii
LIST OF TABLES.....	viii
CHAPTER I.....	1
INTRODUCTION.....	1
1.1. Background.....	1
1.2. Literature review.....	2
1.2.1. Studies on evolutionary techniques applied in hydrological model calibration.....	2
1.2.2. Studies on reservoir operation optimization .....	4
1.2.3. Studies on reservoir operation under climate change.....	6
1.2.4. Studies in Vietnam .....	7
1.3. Research objectives.....	8
CHAPTER II.....	10
DIFFERENTIAL EVOLUTION AND EVOLUTION STRATEGY.....	10
2.1. Differential Evolution .....	10
2.1.1. Introduction.....	10
2.1.2. Population structure.....	11
2.1.3. Algorithm.....	11
2.2. Evolution Strategies .....	13
2.2.1. Introduction.....	13
2.2.2. Population structure.....	13
2.2.2 Algorithm.....	14
CHAPTER III.....	16
DIFFERENTIAL EVOLUTION AND EVOLUTION STRATEGY APPLICATION FOR THE LST MODEL TO THE BE RIVER CATCHMENT IN VIETNAM .....	16
3.1. Introduction .....	16
3.2. Materials and Methods.....	18
3.2.1. LST model .....	18
3.2.2. Study area and data.....	18
3.2.3. Objective functions for optimization.....	20
3.2.4. DE and ES experiments.....	21

3.3. Results and Discussion.....	22
3.3.1. Final calibration and validation performance.....	22
3.3.2. Comparison of evolutionary progress.....	27
3.3.3. Distribution of the best optimized indices .....	30
3.3.4. Computation time.....	31
3.4. Conclusions .....	32
CHAPTER IV .....	34
UNCERTAINTY IN THE IMPACT OF CLIMATE CHANGE ON STREAMFLOW AND RESERVOIR MANAGEMENT .....	34
4.1. Introduction.....	34
4.2. Method and materials .....	35
4.2.1. Study Area .....	35
4.2.2. LST Model.....	36
4.2.3. Reservoir Description and Reservoir Balance Modeling.....	36
4.2.4. Hydrological Model Performance Evaluation.....	38
4.2.5. Differential Evolution.....	38
4.2.6. Future Precipitation Projection .....	39
4.3. Results and discussion.....	39
4.3.1. LST Model Calibration and Validation in the Periods Without Reservoir Operation.....	39
4.3.2. LST Model Validation and Simulation of Thac Mo Reservoir Management .....	40
4.3.3. Streamflow Changes under Climate Change Scenarios.....	43
4.3.4. Possible Impacts of the Projected Streamflow Scenarios on Reservoir Control.....	44
4.4. Conclusions .....	46
CHAPTER V.....	47
DIFFERENTIAL EVOLUTION IN IMPROVING OPERATION RULE CURVES FOR THAC MO RESERVOIR.....	47
5.1. Introduction .....	47
5.2. Methods and materials .....	49
5.2.1. Optimization of rule curves .....	49
5.2.2. Multi-objective optimization and scenarios for optimization .....	51
5.2.3. Data .....	52
5.3. Results and discussions .....	52
5.3.1. Objective correlations and their impacts on the multi-objective optimization.....	52
5.3.2. Trade-off solution.....	55
5.3.3. Comparison to the existing rule and the observation.....	57
5.4. Conclusions .....	61
CHAPTER VI .....	63

RESERVOIR OPERATION OPTIMIZATION UNDER CLIMATE CHANGE.....	63
6.1. Introduction .....	63
6.2. Methods and materials .....	65
6.2.1. Rainfall-Runoff models .....	65
6.2.2. Data .....	65
6.2.3. Optimization and experiments .....	65
6.3. Results and discussions .....	66
6.3.1. Comparisons between the applied rules.....	66
6.3.2. Impact of climate change on reservoir operation objectives.....	68
6.3.3. Impacts of climate change and optimization on the monthly released discharge control.....	70
6.4. Conclusions .....	72
CHAPTER VII .....	74
CONCLUSIONS AND RECOMMENDATIONS .....	74
7.1. Conclusion.....	74
7.2. Limitation and recommendation for future works .....	77
REFERENCES.....	78

# LIST OF FIGURES

<b>Fig 3.1</b> Layout of the LST model .....	18
<b>Fig 3.2</b> Map of Vietnam and the Be River Catchment .....	19
<b>Fig 3.3</b> Observed and simulated daily flow hydrograph at Phuoc Hoa station, calibration (left) and validation (right).....	23
<b>Fig 3.4</b> The Improvements of the best NSE (left) MAE (right) by generation change with the population size as 40 (a), 80 (b), 160 (c), 320 (d) and 640 (e).....	29
<b>Fig 3.5</b> Distribution of the best NSE (a), MAE (b) and RMSE (c) by DE and ( $\mu+\lambda$ )-ES after 1000 generation simulation .....	30
<b>Fig 4.1</b> Map of Thac Mo catchment.....	35
<b>Fig 4.2</b> Observed and simulated daily flow hydrograph at Phuoc Long station during the calibration (1984-1988) and validation (1989-1991) periods.....	41
<b>Fig 4.3</b> Observed and simulated average monthly regime of storage (a), inflow (b) and outflow for power generation (c) in the Thac Mo reservoir .....	42
<b>Fig 4.4</b> The comparisons between simulated and observed data of monthly inflow (a), reservoir water level at beginning of the month (b) and monthly outflow for power generation (c).....	42
<b>Fig 4.5</b> The inflows into the reservoir under current (1981) and future (2046-2065) climate scenarios for different ensembles: r1i1p1 (a), r2i1p1 (b) and r3i1p1 (c) .....	43
<b>Fig 4.6</b> The simulation of average monthly storage (a), outflow for hydropower (b) and outflow spill (c) of the reservoir among three ensembles, r1p1i1, r2i1p1, r3i1p1 .....	45
<b>Fig 5.1.</b> Existing-Rule of Thac Mo reservoir issued by government.....	49
<b>Fig 5.2</b> Individual solutions represented by standardized objectives.....	57
<b>Fig 5.3</b> Existing and optimized rule curves.....	60
<b>Fig 6.1</b> Comparison of the reservoir operation objective indices for different cases of applied rule curves under the current (1981-2000) and future (2046-2065) climate scenarios .....	67
<b>Fig 6.2</b> Ensemble average released discharge by different solutions under the current (1981-2000) and future (2046-2065) climate scenarios for different cases of applied rule curves .....	71

# LIST OF TABLES

Table 3.1 Estimated parameters of the LST model by DE and ( $\mu+\lambda$ )-ES .....	21
<b>Table 3.2</b> Experiment conditions with different optimization population sizes .....	22
<b>Table 3.3</b> The best performances of the DE- and ES-calibrated models after 1,000-generation calibration for the calibration duration (The fitness of the calibrated discharge to the observed discharge was evaluated by Nash–Sutcliffe efficiency (NSE), root mean square error (RMSE) and mean absolute error (MAE)).....	24
<b>Table 3.4</b> The performance of the model in validation according to Nash–Sutcliffe efficiency (NSE), root mean square error (RMSE) and mean absolute error (MAE) using sets of parameters after calibration by different objective functions for optimization.....	25
<b>Table 3.5</b> Average computation times per one-generation simulation of DE and ( $\mu+\lambda$ )-ES optimization .	32
<b>Table 4.1</b> Parameters of LST model.....	41
<b>Table 4.2</b> Model performance for the simulation of LST model and reservoir management.....	41
<b>Table 5.1</b> List of parameters of objective indices obtained from the historical data and the optimized and existing rule curve operations.....	53

# CHAPTER I

## INTRODUCTION

### 1.1. Background

Water resources management has been indispensable for the continued existence of all humanity and our sustainable development. Importance of water resources management is internationally recognized in the sixth goal, “Sanitation of Water Supply”, of the Sustainable Development Goals (SDGs) which are a universal call to action to end poverty, protect the planet and ensure that all people enjoy peace and prosperity (UNDP).

Reservoirs take important roles in water resources management. Thus, each reservoir should be operated efficiently not only for maximizing available water resources for water supply and power production and so on but also for minimizing flood and drought damages in the downstream area.

Vietnam has many reservoirs in all regions from north to south which play the key roles in supplying water to downstream, controlling flood and generating power etc. With the complex topography and climate conditions in all area from the north to south and from the delta to mountain areas, Vietnam is facing many problems involving with water resources such as droughts, floods, and landslides. Moreover, being affected by climate change, Vietnam has experienced rise in temperature and variations in precipitation in all regions. The nationally annual average temperature increased by 0.62°C during the period of 1958 - 2014, and 0.42°C especially in the period of 1985-2014. The annual precipitation decreased in the Northern areas by 5.8-12.5% during 57 years from 1985 to 2014. However, rainfall increased by 6.9-19.8% in the south in the same that duration (MONRE 2016). It is anticipated that the climate change might more strongly affect the hydrological condition in future so that a water resources regulation rules should be changed to adapt to future climate condition.

This study focuses on the optimal management of reservoirs by calibrating hydrological models and optimizing reservoir operation rules in Vietnam. The streamflow and inflow into the reservoir have been estimated to be changed in any catchment in future. The prediction of the impacts of climate change on reservoir control as well as prediction of adaptive operation rule under climate change are the important factors for water management strategies in future. Rainfall-runoff processes in future are simulated by conceptual hydrological models by using projected future climate data.

Generally, a hydrological model has a number of parameters. The successful application of a hydrological model depends on how well the parameters are calibrated (Jiang *et al.* 2013). The same can be said for reservoir operation rules, which should be also calibrated for optimal operation for reservoirs. For these optimization problems, the traditional manual trial-and-error method can result in good model performance sometimes, however, it requires some experiences and detailed understanding of model structure. Additionally, it can be tedious and time-consuming, especially for inexperienced workers (Cohen *et al.* 2013). Automatic optimization techniques should be developed and applied to avoid these difficulties. Especially, Differential Evolution (DE), which has simple algorithm among evolutionary techniques, will be helpful in solving this problem if it is proved to be successfully applied.

## **1.2. Literature review**

### **1.2.1. Studies on evolutionary techniques applied in hydrological model calibration**

Mathematical optimization technique has been developed and successfully applied in various scientific and practical problems. Especially, evolutionary computation techniques have been increasingly attracted for solving complex optimization problems in recent decades. They can deal with complex optimization problems better than traditional optimization techniques (Ruhul Sarker *et al.* 2002). In recent years, a series of evolutionary methods have been found widespread use in the fields of water resources with both single and multi-objective optimization due to their robustness in such problems (Olofintoye *et al.* 2013).

Several techniques have been proved to be successfully applied in water resources researches such as Shuffled Complex Evolution (SCE-UA) (Duan *et al.* 1992), genetic algorithms (GAs) and evolution programming (EP). Differential evolution (DE) (Storn 1996), a simple powerful searching algorithm, has been successfully applied in many aspects of science; however, its application in hydrological studies was limited.

A large number of authors have investigated in model calibration procedures in the past decades and many automatic optimization procedures have been developed to address model calibration problems. One such early development is the genetic algorithm (GA) (Holland, 1975), which was reported to be an efficient and robust mean for the calibration of conceptual rainfall-runoff models by Wang (1991), and another is the shuffled complex evolution (SCE-UA) algorithm by Duan *et al.* (1992, 1993), who have proved its consistence, effectivity, and efficiency in locating parameter values of a hydrological model that optimizes a given objective function (Gupta *et al.* 1998). These methods then were developed and applied by other researchers (Vrugt *et al.* 2003, Zhang *et al.* 2015). Ndiritu *et al.* (2001) improved the GA algorithm by using three methods of automatic search space applied for a rainfall-runoff model calibration and compared with SCE performance. Cohen *et al.* (2013) compared the SCE and GA algorithms in calibrating a rainfall-runoff model called Australian Water Balance Model (AWBM) for Tasmania catchment. Zhang *et al.* (2015) presented SCE-UA global optimization method to calibrate the Xinanjiang model.

Particle swarm optimization (PSO) proposed by Kennedy and Eberhart (1995) is another well-known evolutionary algorithm applied in hydrology. PSO was firstly proposed based on the analogy of swarming animals, such as a flock of birds or school of fish, which is a simple and powerful heuristic method for solving nonlinear, non-differential and multi-modal optimization problem (Amjady & Soleymanpour 2010; Mandal *et al.* 2008). Since PSO utilized for parameter estimation in hydrology by Gill *et al.* (2006), a number of researchers have investigated PSO for hydrological model calibration (Zhang *et al.* 2009, Jiang *et al.* 2013) and it was demonstrated that PSO approach has many computational advantages over traditional evolutionary computing (Chau 2007; Jiang *et al.* 2006, 2007).

The evolution strategy (ES) has been used for system parameter estimation in many fields of research. Hatanaka *et al.* (1996) employed ES for parameter estimation of an autoregressive (AR) model and showed that the ES outperformed the recursive least square and recursive weighted least square methods, emphasizing that the adaptability and robustness of the ES exceeded those of other methods. Chen and Hsu (2006) and Fujihara *et al.* (2003) developed and applied ES for hydrological models and compared with GA. Lately, a study of applying the ES in calibrating hydrologic models for the Nong Saeng catchment in Thailand was found (Fujihara *et al.* 2011).

Differential Evolution (DE) proposed by Storn and Price (1996) is a fast and simple technique which performs well on a wide variety of problems. The DE algorithms claimed to be very efficient when they are applied to solve multimodal optimal control problems (Regulwar *et al.* 2010). Owing to the simplicity and powerfulness, DE has been successfully applied to problems across diverse fields such as physics (Pang *et al.* 2013), computer science (Zhong & Cai 2015), water resources (Zheng *et al.* 2015; Zahmatkesh *et al.* 2015; Guo 2014), environment (Kişi 2010; Niu *et al.* 2015), biology (Zhao *et al.* 2013) and economics (Glотиć *et al.* 2015). However, the investigations of DE in hydrological model calibration were rarely found.

### **1.2.2. Studies on reservoir operation optimization**

Reservoir operation forms an important role in water resources management and development. The improvement of operation policies has been investigated in recent years by many researchers (Afshar *et al.* 2011; Ostadrahimi *et al.* 2012; Goyaletal 2013; Ahmadietal 2014; Schaepli 2015). In reservoir management and operation, a series of methods and algorithms have been developed and applied such as Linear Programming (LP), Dynamic Programming (DP), and Nonlinear Programming (NLP) (Yeh 1985). Recently, GA has been well-known as the efficient algorithm for reservoir optimization. Oliveira and Loucks (1997) derived multi-reservoir operating policies by using the genetic search algorithms. Wardlaw and Sharif (1999) evaluated several alternative formulations of a genetic algorithm (GA) for reservoir system. Labadie (2004) assessed the state-of-the-art in the optimization of reservoir system management and operations, in which the application of heuristic programming methods using evolutionary and genetic

algorithms was described. Chang *et al.* (2005) investigated the efficiency and effectiveness of two genetic algorithms, binary coded and real coded, to derive multipurpose reservoir operating rule curves. Chen *et al.* (2007) developed the macro-evolutionary multi-objective genetic algorithm to deal with a two-objective problem of a multi-purpose reservoir system involving water supply and hydropower generation. Regulwa and Raji (2008) presented a multi-objective, multi-reservoir operation model for maximizing irrigation releases and hydropower production using GA.

Another increasingly focused evolutionary technique applied for reservoir operation is non-dominant-sorting genetic algorithm (NSGA II). Kim *et al.* (2006) applied non-dominated sorting genetic algorithm-II (NSGA-II) to a four-reservoir system in the Han River basin and demonstrated that it performed well in multi-reservoir system optimization. Chang and Chang (2009) coupled the NSGA-II with a reservoir simulation model to search optimal joint operating strategies for water supplies. Fallah-Mehdipour *et al.* (2012) employed the multi-objective PSO and NSGA-II as optimization tools to solve two construction project management problems and concluded that NSGA-II is more successful in determining optimal alternatives in both time–cost trade-off and time–cost–quality trade-off. Cioffi and Gallerano (2012) applied e-constraint and NSGA II methods to search for optimal solutions for water distribution between dam release flows in watercourses and hydropower supply flows. Shokri *et al.* (2013) integrated artificial neural networks with NSGA-II in multi-objective problems to reduce the number of simulations by the main simulator and demonstrated it an effective method to extract the Pareto front with much less simulation time. Ahmadi *et al.* (2014) employed NSGA-II to extract the real-time optimal operating rules considering the conflicting objectives of reliability and vulnerability in hydropower generation. Yang *et al.* (2016) optimized reservoir operation rule curves both by DP and NSGA-II methods. In these studies, the decision variables of operating rules were optimized by multi-objective optimization algorithm.

DE is a robust and easy to use in optimization and has been found efficient in water resources management (Vasan & Raju 2004, 2007). DE investigation on reservoir policies has been found to be attentioned in recent years. Reddy and Kumar (2007) studied Multi-Objective Differential Evolution (MODE) with an application to a

reservoir system optimization. The evolutionary operators used in DE algorithms are very much suitable for problems having interdependence among the decision variables. Vasan and Raju (2007) and Regulwar (2010) presented the application of DE for the optimal operation of the multipurpose reservoir. The objective of the study is to maximize the hydropower production. The results were compared with GA.

### **1.2.3. Studies on reservoir operation under climate change**

A large number of studies have focused on reservoir operation related to climate change in recent years. Brekke *et al.* (2009) presented climate change risk assessments involving reservoir operations for California's Central Valley Project and State Water Project systems. Li *et al.* (2009) investigated potential impacts of future climate change on streamflow and reservoir operation performance in a Northern American Prairie Watershed. López-Moreno *et al.* (2013) simulated the management of the Yesa reservoir based on its current capacity and its projected capacity under various climate and land cover change scenarios. Zhou and Guo (2013) proposed an integrated optimization model to develop operation rule curves of Danjiangkou Reservoir in a base period and three future periods. Ahmadi *et al.* (2014) proposed an adaptive method to revise reservoir operating rules for Karoon4 Reservoir in Iran as an adaptation strategy to climatic change. Fill *et al.* (2013) presented an evaluation of the combined dependable energy output of the hydropower plants located within the Brazilian part of the La Plata Basin, addressing the impact of future climate change on the energy output and allowing contributions to adjust planning strategies of the agencies responsible for the expansion and operation of the Brazilian electric power system. These studies mainly assessed the impacts of climate change in reservoir management without considering the adaptive operation policies.

Lately, several studies on adaptive operation policies under climate change based on traditional optimization methods such as dynamic programming (DP) and stochastic dynamic programming (SDP). For example, Raje and Mujumdar (2010) investigated the impacts of climate change on reservoir performance using a stochastic dynamic programming (SDP) model to derive the optimal monthly operating policy. Zhao *et al.* 2011 analyzed the effect of forecast uncertainty on real-time reservoir operations based on DP and SDP.

Investigations of reservoir operation with climate change conditions based on evolution optimization were found in a number of studies. Eumand and Simonovic (2010) developed the optimal rule curves for a multi-purpose reservoir for three different climate change conditions using the DE optimization algorithm. Yang *et al.* (2016) presented an adaptive multi-objective reservoir operation model based on multi-objective optimization NSGA-II method. Although evolutionary algorithms have been proved to be efficient in reservoir optimization, there are fewer studies on the effect of forecast uncertainty on reservoir operation based on evolutionary computational optimization and the application of DE was limited to be found.

#### **1.2.4. Studies in Vietnam**

Many studies on water resources using rainfall-runoff models in Vietnam use the commercial model developed by Danish Hydraulic Institute, Denmark (DHI), like MIKE NAM or MIKE BASIN, MIKE SHE (Vu & Nguyen 2015, Vu *et al.* 2017). Recently, a number of authors investigated in SWAT model (Khoi & Suetsugi 2012, 2013). The developed rainfall-runoff model using automatic calibration was also found; however, it is limited. Ngoc *et al.* (2013) investigated GA applied to calibrate parameters of two hydrological models, NAM model and Tank model, to improve the modeling efficiency applied for Dau Tieng catchment.

Reservoir optimization was found to be investigated by several researchers with both traditional and evolutionary techniques. Ngo *et al.* (2007) applied SCE for optimizing the reservoir operation in flood season for Hoa Binh reservoir in northern Vietnam. Castelletti *et al.* (2012) analyzed the historical operation of the Hoa Binh reservoir on the Da River and explored reoperation options corresponding to different tradeoffs among three main objectives (hydropower production, flood control, and water supply), using multi-objective GA optimization techniques. Ho *et al.* (2014) developed an algorithm combination of harmony search (HS) and incremental dynamic programming (IDP) for optimally operating Huong Dien Reservoir in Hue to maximize hydropower production, to prevent flood, and to ensure irrigation water availability. Babel *et al.* (2014) estimated the environmental flow requirements in La Nga River in Vietnam and simulated the operation of hydropower system for different alternative

scenarios to understand the impact of maintaining the natural flow regime on hydropower production. The trade-off between hydropower generation and environmental flow was considered in this study.

Vietnam has experienced climate changes and its effects on water resources clearly. The topics evolving with climate change have attracted attention of many researchers. Most of these studies have been based mainly on climate change scenarios for Vietnam (MONRE 2016) or on outputs from individual GCMs to assess the impacts of climate change on streamflow, sediment yield (Khoi & Suetsugi 2012, 2013, Manh *et al.* 2014, Dang *et al.* 2010, Le *et al.* 20017), saltwater intrusion (Hien *et al.* 2010, Rasmussen *et al.* 2013), flooding, inundate (Le *et al.* 2007). Studies on adaptive reservoir operation under climate change basing evolution optimization have been not found.

### **1.3. Research objectives**

The overall objective of this study is to investigate the evolutionary computation technique application in improving reservoir management under current and future climate change conditions by automatic calibration of a rainfall-runoff model, Long-and-Short Term Runoff Model (LST model) and reservoir operation rule curve optimization. Thac Mo reservoir in Be River catchment is the objective study area.

The sub-objectives are detailed as follows:

- (1) To calibrate and validate the LST model using DE and ES optimization methods applied for Be River catchment. Comparison between two algorithms is carried out.
- (2) To evaluate impacts of climate change on inflow into Thac Mo reservoir as well as the reservoir control basing on the historical operation.
- (3) To evaluate the DE optimization on improving Thac Mo reservoir operation rule and compare with the existing rule and historical operations.
- (4) To evaluate the possible impact of climate change on Thac Mo reservoir operation performance under the government existing-rule as well as adaptive rules based on DE optimization.



## CHAPTER II

# DIFFERENTIAL EVOLUTION AND EVOLUTION STRATEGY

### 2.1. Differential Evolution

#### 2.1.1. Introduction

DE is also one of the global optimization algorithms as ES, which was developed by Price and Storn (1997) as an effective optimization technique for multi-modal objective functions. Since its inception, DE has earned a reputation as a very effective global optimizer. While DE is not a panacea, its record of reliable and robust performance demands that it belongs to every scientist and engineers. Many other researchers in optimization became aware of DE's potential after reading, "Differential Evolution – A Simple and Efficient Heuristic for Global Optimization over Continuous Spaces", by Rainer and Ken. Published in the December 1997 issue of The Journal of Global Optimization (Price & Storn 1997), this paper gave extensive empirical evidence of DE's robust performance on a wide variety of test functions (Price & Storn 2005). The DE is started with an initial population of randomly chosen  $Np$  parent individuals. Algorithm for creating a new generation of DE includes mutation, crossover, and selection. In mutation step, new vectors are generated by adding the weighted difference between two parent vectors to third vectors that are chosen randomly. If the resulting vector yields a better solution of objective function than the parent's one, the parent is replaced. Otherwise, the parent is retained. The "evolution" process is terminated when required criterion is satisfied. The optimization performance by DE is influenced by the value of a number of population ( $Np$ ), and controlling the copied fraction of parameter values ( $Cr$ ) and rate of population evolves ( $F$ ). These variables must be selected to begin DE algorithm.

In this study application, the original DE algorithm (Price & Storn 1997) was applied and the procedure is specifically described as follow.

### 2.1.2. Population structure

DE's most versatile implementation maintains a pair of vector populations, both of which contain  $Np$   $D$ -dimensional vectors of real-valued parameters. The current population, symbolized by  $P_{x,g}$ , is composed of those vectors,  $x_{i,G}$ , that have already been found to be acceptable either as initial points or by comparison with other vectors:

$$P_{x,g} = (x_{i,g}), i=0,1,\dots,Np-1, g=0,1,2\dots g_{max} \quad (2.1)$$

$$x_{i,g} = (x_{j,i,g}), j=0,1,\dots,D-1$$

Indices start with 0 to simplify working with arrays and modular arithmetic. The index,  $G = 0, 1, \dots, g_{max}$ , indicates the generation to which a vector belongs. In addition, each vector is assigned a population index,  $i$ , which runs from 0 to  $Np-1$ . Parameters within vectors are indexed with  $j$ , which runs from 0 to  $D-1$ .

### 2.1.3. Algorithm

#### *Initialization*

Before the population can be initialized, both upper and lower bounds for each parameter must be specified. These  $2D$  values can be collected into two,  $D$ -dimensional initialization vectors,  $p_{j,min}$  and  $p_{j,max}$ , for which subscripts min and max indicate the lower and upper bounds, respectively. Once initialization bounds have been specified, a random number generator assigns each parameter of every vector a value from within the prescribed range. For example, the initial value ( $G = 0$ ) of the  $j$ th parameter of the  $i$ th vector is

$$x_{j,i,0} = rand_j(0,1) \cdot (p_{j,max} - p_{j,min}) + p_{j,min} \quad (2.2)$$

The random number generator,  $rand_j(0,1)$ , returns a uniformly distributed random number from within the range  $[0,1)$ , i.e.,  $0 \leq rand_j(0,1) < 1$ . The subscript,  $j$ , indicates that a new random value is generated for each parameter. Even if a variable is discrete or integral, it should be initialized with a real value since DE internally treats all variables as floating-point values regardless of their type.

### *Mutation*

The scale factor,  $F \in (0,1+)$ , is a positive real number that controls the rate at which the population evolves. While there is no upper limit on  $F$ , effective values are seldom greater than 1.0. The base vector index,  $r0$ , can be determined in a variety of ways, but for now, it is assumed to be a randomly chosen vector index that is different from the target vector index,  $i$ . Except for being distinct from each other and from both the base and target vector indices, the difference vector indices,  $r1$  and  $r2$ , are also randomly selected once per mutant.

### *Crossover*

To complement the differential mutation search strategy, DE also employs uniform crossover. Sometimes referred to as discrete recombination, (dual) crossover builds trial vectors out of parameter values that have been copied from two different vectors. In particular, DE crosses each vector with a mutant vector:

$$u_{i,g} = u_{j,i,g} = \begin{cases} v_{j,i,g}, & \text{rand}_j(0,1) \leq Cr \text{ or } j = j_{rand} \\ x_{j,i,g}, & \text{otherwise} \end{cases} \quad (2.4)$$

The crossover probability,  $Cr \in [0, 1]$ , is a user-defined value that controls the fraction of parameter values that are copied from the mutant. To determine which source contributes a given parameter, uniform crossover compares  $Cr$  to the output of a uniform random number generator,  $\text{rand}_j(0,1)$ . If the random number is less than or equal to  $Cr$ , the trial parameter is inherited from the mutant,  $v_{i,g}$ ; otherwise, the parameter is copied from the vector,  $x_{i,g}$ . In addition, the trial parameter with randomly chosen index,  $j_{rand}$ , is taken from the mutant to ensure that the trial vector does not duplicate  $x_{i,g}$ . Because of this additional demand,  $Cr$  only approximates the true probability, that a trial parameter will be inherited from the mutant.

### *Selection*

If the trial vector,  $u_{i,g}$ , has an equal or lower objective function value than that of its target vector,  $x_{i,g}$ , it replaces the target vector in the next generation; otherwise, the target retains its place in the population for at least one more generation (Eq. 2.5). By

comparing each trial vector with the target vector from which it inherits parameters, DE more tightly integrates recombination and selection than do other EAs:

$$x_{i,g+1} = \begin{cases} u_{i,g}, & \text{if } f(u_{i,g}) \leq f(x_{i,g}) \\ x_{i,g}, & \text{otherwise} \end{cases} \quad (2.5)$$

Once the new population is installed, the process of mutation, recombination, and selection is repeated until the optimum is located, or a prespecified termination criterion is satisfied or the number of generations reaches a preset maximum,  $g_{max}$ .

## 2.2. Evolution Strategies

### 2.2.1. Introduction

Evolution Strategy (ES) is one of global optimization algorithms that was created in the early 1960s (Rechenberg, 1971) and developed further in the 1970s and later. Optimization by the ES is started with an initial population of  $\mu$  parents that are randomly chosen. Each parent individual is composed of vectors, each of which is a set of parameters to be calibrated. In each new generation, an offspring composed of  $\lambda$  new individuals are generated from randomly selected parent individuals by mutation which is normally performed by adding normal random value to each individual vector component. After mutation, their fitness is evaluated and the better individuals are selected as parents for the next generation. For ES, a variety of mutation and selection ways have been proposed. In this study,  $(\mu, \mu+\lambda)$ -ES algorithm was applied by referring to Fujihara *et al.* (2003). By this algorithm, both offspring individuals and current parents may survive to reproduce in the next generation.

### 2.2.2. Population structure

Denote an individual to be optimized as  $\mathbf{a}$ . The  $\mathbf{a}$  is composed of a set of parameters,  $\mathbf{x}$ , and standard deviations,  $\boldsymbol{\sigma}$ , as follows:

$$\mathbf{a} = (\mathbf{x}, \boldsymbol{\sigma}) \quad (2.6)$$

$$\mathbf{x} = (x_1, \dots, x_D)$$

$$\sigma = (\sigma_1, \dots, \sigma_n)$$

where  $x_i$  is  $i$ -th parameter, and  $\sigma_i$  is standard deviation for mutation of  $i$ -th parameter,  $D$  is the number of parameter

### 2.2.2 Algorithm

Algorithm is as follows:

- 1) Generate an initial parent group composed of  $\mu$  individuals:  $P(0) = \{a_1, a_2, \dots, a_\mu\}$ , where  $a_i$  is the  $i$ -th individual whose elements are parameters to be optimized and standard deviations. The first generation is denoted as  $T=0$ , that is a parent group.
- 2) Evaluate an objective function for each individual of the parameters for the first generation.
- 3) Generate an offspring group,  $P(T)$ , composed of  $\lambda$  new individuals generated from the parent group by mutation and crossover. Denote the offspring group as  $P''(T) = \{a_1''(T), a_2''(T), \dots, a_\lambda''(T)\}$ , where  $a_i''(T)$  is the  $i$ -th individual of  $T$ -th generation whose elements are parameters to be optimized.
- 4) Evaluate an objective function for each individual for the first generation,  $P''(T)$ .
- 5) Select  $\mu$  individuals of minimum values of the objective function, which compose  $(T+1)$ -th generation group.

*Crossover:*

Generate offsprings  $x_i''$  from selected two parents  $x'_{k_1,i}$  and  $x'_{k_2,i}$  as follows:

$$x_i'' = x'_{k_1,i} + \chi_i(x'_{k_2,i} - x'_{k_1,i}) \quad (2.7)$$

where  $\chi_i$  is random number between 0 and 1.

Crossover of standard deviation is performed as follows:

$$\sigma'_i = \frac{1}{\mu} \sum_{k=1}^{\mu} \sigma_{k,i} \quad (2.8)$$

where  $\mu$  is the number of individuals included in a parent group.

*Mutation:*

Mutation is performed by using the following equations:

$$x_i'' = x_i' + \sigma_i'' N_i(0,1) \quad (2.9)$$

$$\sigma_i'' = \sigma_i' \exp\{\tau' N(0,1) + \tau N_i(0,1)\} \quad (2.10)$$

where  $\sigma_i$  represents mutation parameters,  $N_i(0,1)$  represents normal random variables for each decision parameter,  $N(0,1)$  is a normal random parameter, and  $\tau'$  and  $\tau$  are operation parameters that are expressed as  $\tau' = (2D)^{-1/2}$  and  $\tau = (2D^{1/2})^{-1/2}$ , respectively.

## CHAPTER III

# DIFFERENTIAL EVOLUTION AND EVOLUTION STRATEGY APPLICATION FOR THE LST MODEL TO THE BE RIVER CATCHMENT IN VIETNAM

### 3.1. Introduction

Mathematical optimization techniques have been developed and applied to solving complex problems across a wide range of scientific fields. In recent decades, evolutionary computation techniques, such as shuffled complex evolution (SCE-UA) (Duan *et al.* 1992), genetic algorithms (GAs), evolution programming (EP), and differential evolution (DE), have been increasingly employed for optimization problems. Evolutionary algorithms are powerful optimization techniques based on the principle of natural selection. These algorithms are easy to implement and have the capacity to converge to a global optimum with relatively low computational effort (Chakraborty 2008). Among these evolution algorithms, DE is an efficient method for optimizing real-valued optimization problems (Storn 1996), with overall excellent performance for a wide range of criterion problems. Furthermore, because of its simple but powerful searching algorithm, DE has a number of real-world applications (Price *et al.* 2005) and has been successfully applied to problems across diverse fields such as physics (Pang *et al.* 2013), computer science (Zhong and Cai 2015), water resources (Zheng *et al.* 2015; Zahmatkesh *et al.* 2015; Guo 2014), environment (Kişi 2010; Niu *et al.* 2015), biology (Zhao *et al.* 2013) and economics (Glотиć *et al.* 2015). Zhong and Cai (2015) used DE with sensitivity analysis and Powell's method to calibrate a crowd model for industry, academia, and government. Pang *et al.* (2013) employed DE for calibration of three-axis magnetometers which are widely employed in the magnetic field measurement systems used in aircraft and marine applications.

The evolution strategy (ES) has increasingly been used for system parameter estimation in many fields of research. Among the many versions of the ES, the  $(\mu+\lambda)$ -ES,

in which both  $\mu$  parent individuals and  $\lambda$  offspring are ranked together by objective function values, has been evaluated as an elitist strategy (Eiben and Smith 2003). It has been stated that the  $(\mu+\lambda)$ -ES always performs better than the  $(\mu, \lambda)$ -ES, in which only  $\lambda$  generated offspring individuals are ranked (Beyer and Schwefel 2002). Hatanaka *et al.* (1996) employed the  $(\mu+\lambda)$ -ES for parameter estimation of an autoregressive (AR) model, and showed that the ES outperformed the recursive least square and recursive weighted least square methods, emphasizing that the adaptability and robustness of the ES exceeded those of other methods. In the study entitled, “A multi-objective optimization solver using rank-niche evolution strategy”, Chen and Hsu (2006) developed a rank-niche ES (RNES) algorithm to solve unconstrained multi-objective optimization problems using Pareto-optimal solutions. For some test problems, the Pareto-optimal solutions obtained using the RNES are better than those obtained using GA-based algorithms. The ES was found to be useful for parameter calibration in a hydrological model by Fujihara *et al.* (2003), who applied  $(\mu+\lambda)$ -ES for parameter estimation of tank models for the Eigenji, Osako, and Syorenji dam basins in Japan. These results show that the searching ability of the ES is far superior to that of a binary GA. Later, they also applied the ES in calibrating hydrologic models in their study applying to the Nong Saeng catchment in Thailand (Fujihara *et al.* 2011)

Hydrological modeling simulation is a major field in water resources research. Every hydrological model has a number of parameters that need to be estimated through calibration to achieve good agreement between simulated and observed data. Optimization techniques, particularly SCE-UA, have attracted the attention of hydrologists for automatic calibration for many years (Duan *et al.* 1992, Duan *et al.* 1994, Vrugt *et al.* 2003; Tang *et al.* 2006; Zhang *et al.* 2008, Zhang *et al.* 2015). Although searching optimal algorithms are widely used in parameter estimation, the  $(\mu+\lambda)$ -ES and DE algorithms, which are simple and easy to implement, have been investigated only in a limited number of studies on hydrological model calibration.

The aim of this work was to introduce application of the  $(\mu+\lambda)$ -ES and DE to automatic calibration of parameters in a hydrological model, namely the long-and-short term runoff model (LST model) (Kadoya & Tanakamaru 1989). The efficiency of the two methods was compared after conducting a number of experiments. The original DE

introduced by Storn (1996) and the  $(\mu+\lambda)$ -ES algorithm described by Fujihara *et al.* (2003) were applied in this study, because the simplicity of a calibration algorithm is an important factor for practical implementation.

### 3.2. Materials and Methods

#### 3.2.1. LST model

The LST model (Kadoya & Tanakamaru 1989) is a storage-type rainfall–runoff model structured on the basis of a Tank model (Sugawara 1995). Figure 3.1 shows its structure, consisting of three tanks, the first (top) of which is divided into two layers. The LST model has 11 parameters that need to be calibrated, including runoff coefficients  $a_1, a_2, a_3, a_4, a_5$ , an infiltration coefficient  $b_1$ , percolation coefficients  $b_2, b_3$ , and the heights of side outlets  $Z_1, Z_2, Z_3$ . The initial storage depths of each layer of the top tank,  $S_1$  and  $S_2$ , and those of the second and third (bottom) tanks,  $S_3$  and  $S_4$ , also require calibration. In this study, potential evapotranspiration was calculated using the Penman equation, which relies on temperature, humidity, wind speed, and sunshine duration data. Table 3.1 shows the minimum and maximum values of each coefficient used for optimization selection.

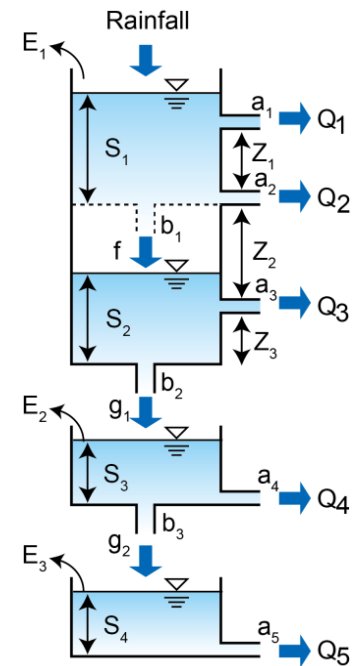


**Fig 3.1** Layout of the LST model

#### 3.2.2. Study area and data

The LST model was applied to the Be River catchment of the Dong Nai River system located in southern Vietnam. Figure 3.2 shows the Be River catchment and the locations of the hydrometeorological stations. The catchment area of the Phuoc Hoa discharge gauging station is about 5,988 km<sup>2</sup>, encompassing the Dak Nong, Binh Phuoc, Binh Duong, and Dong Nai provinces of Vietnam, as well as some Cambodian territory near the border of Dak Nong Province. The catchment is a mix of plain and highland areas with elevations ranging from 100 to 1,000 m. The average temperature of this area is about 25.5–26.7°C, and the maximum and minimum temperatures are approximately

36.6°C and 17.3°C, respectively. The rainy season lasts from May to November and accounts for 85–90% of the total annual precipitation, with the highest precipitation usually occurring from August to October. The mean annual precipitation is about 2,250 mm, ranging from 1,700 mm over the plain to 2,700 mm in mountainous areas. The annual potential evapotranspiration is about 1,100 mm and the annual sunshine duration amounts to 2,500–3,000 h.

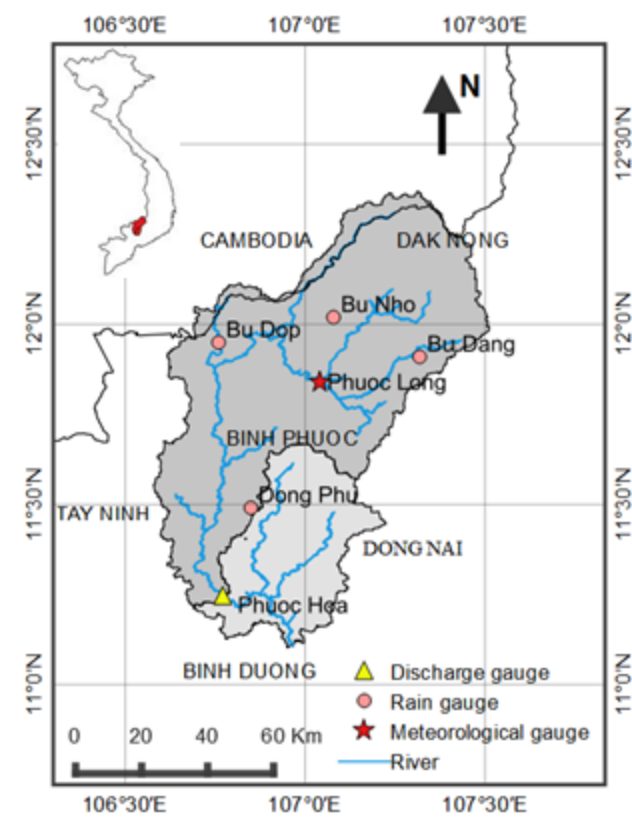


**Fig 3.2** Map of Vietnam and the Be River Catchment

The data used for calibration and validation of the LST model were as follows: (i) daily precipitation observed at four rain gauge stations (Dong Phu, Bu Dang, Bu Dop, and Bu Nho); (ii) monthly meteorological data including temperature, humidity, wind speed, and sunshine hours at Phuoc Long station to estimate evaporation; and (iii) daily discharge observed at Phuoc Hoa station for calibration and validation (Fig 3.2). In this study, the catchment average rainfall was estimated using arithmetic-mean method. The data observation period was from January 1985 to December 1991. The data from the first 5 years (1985–1989) were used for model calibration and those from the following 2 years (1990–1991) were used for validation. A digital elevation model (DEM) with 30-m resolution, as determined using the Advanced Spaceborne Thermal Emission and

Reflection Radiometer (ASTER), Global Digital Elevation Model (GDEM) (Japan Space System), was used to delineate the watershed and specify the size of the objective area using QGIS software, a cross-platform, free, open-source desktop geographic information system (GIS) application licensed under the GNU general public license (QGIS Development Team).

### 3.2.3. Objective functions for optimization

To achieve successful calibration using an automatic optimization technique as well as to evaluate performance through calibration and validation, it is crucial to select appropriate objective functions that assess the error or fitness of the simulated to observed data. Dawson *et al.* (2007) assembled 20 performance measures used in hydrology. In the present study, the accuracy of simulated discharge by the LST model was evaluated using the following three indices: the Nash–Sutcliffe efficiency (NSE) (Nash & Sutcliffe 1970), mean absolute error (MAE), and root mean square error (RMSE). These indices are defined as follows:

$$NSE = 1 - \frac{\sum_{i=1}^N (Q_{sim,i} - Q_{obs,i})^2}{\sum_{i=1}^N (Q_{obs,i} - \bar{Q}_{obs})^2} \quad (3.1)$$

$$MAE = \frac{1}{N} \sum_{i=1}^N |Q_{sim,i} - Q_{obs,i}| \quad (3.2)$$

$$RMSE = \sqrt{\frac{1}{N} \sum_{i=1}^N (Q_{sim,i} - Q_{obs,i})^2} \quad (3.3)$$

where  $i$  is the time step number (day),  $N$  is the total number of data records,  $Q_{obs,i}$  is the observed discharge at the  $i$ -th time step,  $Q_{sim,i}$  is the simulated discharge at the  $i$ -th time step, and  $\bar{Q}_{obs}$  is the average observed discharge. The NSE quantitatively describes the accuracy of the model output for variables, and ranges between  $-\infty$  and 1. The simulated values completely correspond to observed values when the NSE is 1. The RMSE and MAE describe the difference between the observed and simulated variables, ranging between 0 and  $+\infty$ . The simulated values completely correspond to the observed values when the RMSE and MAE are both 0.

### 3.2.4. DE and ES experiments

Usually, in evolution algorithms, after evaluating the objective function values, they are compared to the convergence condition. If this condition is satisfied, the optimization procedure is terminated; otherwise, it is continued and new offspring generations are reproduced. In this study, reproduction of new offspring generation by the DE or  $(\mu+\lambda)$ -ES algorithms was terminated after the 1,000th generation without considering convergence. The performances of the DE and  $(\mu+\lambda)$ -ES optimized models after 1,000 generations were compared by considering the variation in fitness or error indices. The detail of DE and ES was introduced in chapter 2.

Table 3.1 Estimated parameters of the LST model by DE and  $(\mu+\lambda)$ -ES

Parameter	Bounds	DE			$(\mu+\lambda)$ -ES		
	Lower - Upper	Min	Max	Average	Min	Max	Average
$a_1$ ( $\text{m}^{-2/3}\text{d}^{-1}$ )	0.001 – 0.05	0.00105	0.00201	0.00136	0.00113	0.00367	0.00182
$a_2$ ( $\text{d}^{-1}$ )	0.01 – 0.1	0.0313	0.0507	0.0416	0.0329	0.0526	0.0422
$a_3$ ( $\text{d}^{-1}$ )	0.001 – 0.1	0.0111	0.0149	0.0130	0.0067	0.0153	0.0115
$a_4$ ( $\text{d}^{-1}$ )	0.0005 – 0.02	0.00357	0.00626	0.00488	0.00153	0.00398	0.00300
$a_5$ ( $\text{d}^{-1}$ )	0.00001 – 0.001	0.00039	0.00054	0.00048	0.00007	0.00081	0.00037
$b_1$ ( $\text{d}^{-1}$ )	0.01 – 0.02	0.0377	0.1151	0.0703	0.0465	0.1214	0.0795
$b_2$ ( $\text{d}^{-1}$ )	0.001 – 0.04	0.00938	0.01661	0.01158	0.00844	0.01511	0.01021
$b_3$ ( $\text{d}^{-1}$ )	0.001 – 0.01	0.00846	0.00999	0.00941	0.00101	0.00806	0.00444
$Z_1$ (mm)	5 - 200	84.18	165.79	106.68	78.80	174.20	115.93
$Z_2$ (mm)	5 - 500	320.40	491.37	427.90	395.65	493.70	435.42
$Z_3$ (mm)	5 - 200	132.28	199.98	169.40	41.88	177.69	131.89
$S_1$ (mm)	0 - 20	0.18	19.18	10.16	0.53	16.01	7.369
$S_2$ (mm)	0 - 200	100.01	196.70	179.97	19.41	177.53	109.76
$S_3$ (mm)	0 -1000	31.35	137.63	65.37	5.28	420.83	193.94
$S_4$ (mm)	0 - 1000	959.29	999.27	986.15	364.65	955.07	726.76

DE calibration results are influenced by the size of the population,  $N_p$ , the controlling copied fraction of parameter values,  $Cr$ , and the scaling factor or the rate of population evolution,  $F$ , whereas those of the  $(\mu+\lambda)$ -ES are affected by the parent population size,  $\mu$  and the offspring size,  $\lambda$ . In this study,  $Cr$  and  $F$  were respectively set as 0.2 and 0.7 based on previous studies (Storn 1996; Gämperle *et al.* 2002; Storn and Price 1997; Rönkkönen *et al.* 2005) as well as the results of several trials. For a fair comparison of the values of fitness indices and computation times obtained from the DE and  $(\mu+\lambda)$ -ES methods, the population size, that is,  $N_p$  for DE and  $\mu+\lambda$  for  $(\mu+\lambda)$ -ES, should be equal. The ratio of  $\lambda$  to  $\mu$  was set as  $\lambda = 7\mu$ , referring to Fujihara *et al.* (2003) and Eiben and Smith (2005). Five experiments with similar initial selected parents were

conducted for different population sizes (40, 80, 160, 320, and 640) for each fitness index used in each optimization technique. The optimization parameters are shown in Table 3.2. The case of population size  $Np = \mu + \lambda = 160$  was taken as an example for 100 independent runs started with different initial populations for each fitness function, to compare the distributions of the optimized fitness indices. The minimum and maximum values of each parameter of LST model which needs to be calibrated is shown in Table 3.1.

**Table 3.2** Experiment conditions with different optimization population sizes

Experiment No.	DE			$(\mu + \lambda)$ -ES	
	$Np$	$Cr$	$F$	$\mu$	$\lambda$
1	40	0.2	0.7	5	35
2	80	0.2	0.7	10	70
3	160	0.2	0.7	20	140
4	320	0.2	0.7	40	280
5	640	0.2	0.7	80	560

$Np$ : population size,  $Cr$ : crossover rate,  $F$ : rate of population evolution,  $\mu$ : parent population,  $\lambda$ : offspring population.

### 3.3. Results and Discussion

#### 3.3.1. Final calibration and validation performance

To compare the efficiency of DE and  $(\mu + \lambda)$ -ES optimization, the performance of the LST model calibrated using the DE (DE-calibrated model) and  $(\mu + \lambda)$ -ES (ES-calibrated model) algorithms was compared. Figure 3.3 shows examples of the simulated and observed daily flow hydrographs for the calibration and validation periods at Phuoc Hoa station in the case of  $Np = 320$  for DE and  $\mu = 40$  and  $\lambda = 280$  for  $(\mu + \lambda)$ -ES. The objective fitness index for automatic calibration was the NSE. Both simulated hydrographs seem to fit the observed values well in both the calibration and validation periods. No significant differences were observed between the simulated hydrographs. Table 3.3 shows the results of the calibration, with the objective fitness index set respectively to the NSE, MAE, and RMSE. This table shows the parent and offspring population sizes, the best values of the target fitness index, and the values of the other indices. The average and standard deviation  $\sigma$  values of all of the indices under all population-size conditions are also shown.

In cases where the NSE was optimized using  $(\mu+\lambda)$ -ES, all of the fitness indices (NSE, MAE and RMSE) were identical to those found when optimizing RMSE for all population sizes. In the case where the NSE was optimized by the DE, all of the fitness indices were close to those of the RMSE cases; that is, the calibrated parameter sets obtained by optimizing the NSE were the same or very close to those obtained by optimizing RMSE for both the  $(\mu+\lambda)$ -ES and DE methods.

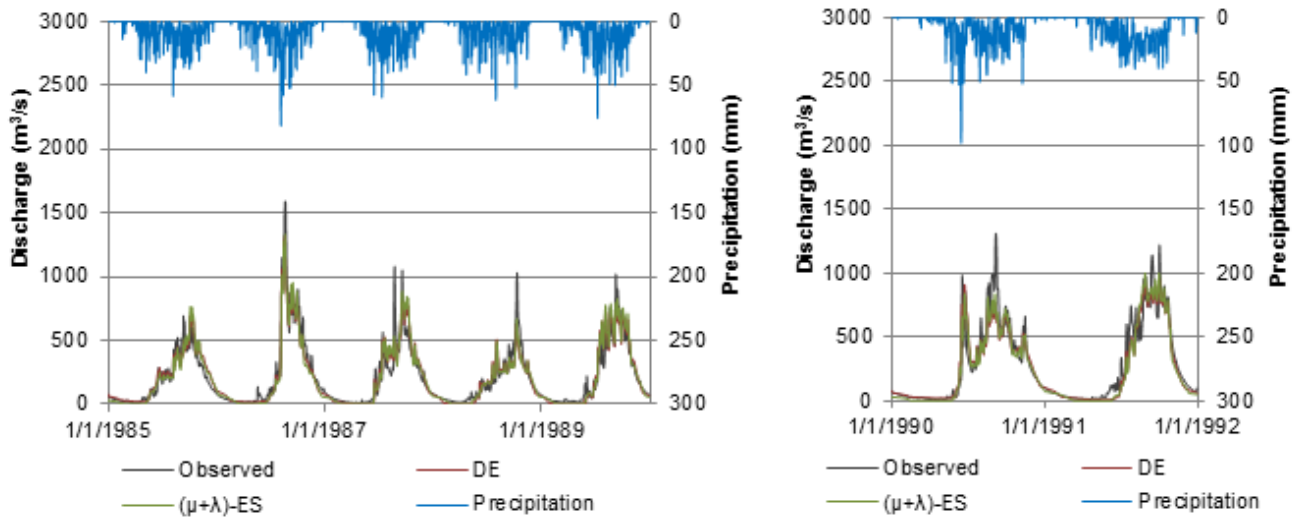


**Fig 3.3** Observed and simulated daily flow hydrograph at Phuoc Hoa station, calibration (left) and validation (right)

When using the NSE as an objective function, the average NSE of simulated discharge by the DE-calibrated model in all population size cases was 0.9089. The average MAE and RMSE values for the cases where the NSE was optimized were 44.27  $\text{m}^3/\text{s}$  and 72.82  $\text{m}^3/\text{s}$ , respectively. The ES-calibrated model showed a slightly weaker performance in NSE, MAE and RMSE values compared to the DE-calibrated model (Table 3.3).

When using MAE as an objective function, the DE-calibrated model performed slightly better than the ES-calibrated model, because almost all of the minimum MAE and RMSE of simulated discharge values obtained using the DE-calibrated model were lower than those obtained using the ES-calibrated model, and the maximum NSE values from the DE-calibrated model were slightly greater than those from the ES-calibrated model (Table 3.3). The average NSE, MAE, and RMSE values from the simulation performed using the DE-calibrated model were 0.9003, 42.80  $\text{m}^3/\text{s}$ , and 76.16  $\text{m}^3/\text{s}$  respectively. The same index values obtained from the simulation using the ES-calibrated

model were worse than those obtained using the DE-calibrated model, with values of 0.8986, 44.91m<sup>3</sup>/s, and 76.82 m<sup>3</sup>/s respectively.

**Table 3.3** The best performances of the DE- and ES-calibrated models after 1,000-generation calibration for the calibration duration (The fitness of the calibrated discharge to the observed discharge was evaluated by Nash–Sutcliffe efficiency (NSE), root mean square error (RMSE) and mean absolute error (MAE))

Optimized Index	DE			$(\mu+\lambda)$ -ES				
	Parent population	Fitness indices			Parent and offspring population	Fitness indices		
		NSE	MAE (m <sup>3</sup> /s)	RMSE (m <sup>3</sup> /s)		NSE	MAE (m <sup>3</sup> /s)	RMSE (m <sup>3</sup> /s)
NSE	$Np = 40$	0.9084	44.84	73.03	$\mu = 5, \lambda = 35$	0.9039	44.62	74.80
	$Np = 80$	0.9090	44.26	72.80	$\mu = 10, \lambda = 70$	0.9048	47.08	74.44
	$Np = 160$	0.9092	43.95	72.70	$\mu = 20, \lambda = 140$	0.9055	46.16	74.15
	$Np = 320$	0.9088	44.46	72.85	$\mu = 40, \lambda = 280$	0.9045	47.12	74.58
	$Np = 640$	0.9091	43.83	72.74	$\mu = 80, \lambda = 560$	0.9048	46.32	74.43
	Average	0.9089	44.27	72.82	Average	0.9047	46.26	74.48
	Standard deviation, $\sigma$	0.0003	0.36	0.12	Standard deviation, $\sigma$	0.0005	0.91	0.21
MAE	$Np = 40$	0.8992	43.18	76.61	$\mu = 5, \lambda = 35$	0.8950	44.94	78.18
	$Np = 80$	0.8954	42.86	78.02	$\mu = 10, \lambda = 70$	0.9016	45.49	75.69
	$Np = 160$	0.9027	42.61	75.27	$\mu = 20, \lambda = 140$	0.9001	44.71	76.25
	$Np = 320$	0.9003	42.70	76.17	$\mu = 40, \lambda = 280$	0.8965	44.69	77.61
	$Np = 640$	0.9041	42.63	74.70	$\mu = 80, \lambda = 560$	0.8999	44.72	76.34
	Average	0.9003	42.80	76.16	Average	0.8986	44.91	76.82
	Standard deviation, $\sigma$	0.0030	0.21	1.15	Standard deviation, $\sigma$	0.0025	0.31	0.93
RMSE	$Np = 40$	0.9077	45.20	73.30	$\mu = 5, \lambda = 35$	0.9039	44.62	74.80
	$Np = 80$	0.9089	44.04	72.82	$\mu = 10, \lambda = 70$	0.9048	47.08	74.44
	$Np = 160$	0.9090	44.27	72.82	$\mu = 20, \lambda = 140$	0.9055	46.16	74.15
	$Np = 320$	0.9091	44.54	72.72	$\mu = 40, \lambda = 280$	0.9045	47.12	74.58
	$Np = 640$	0.9092	44.05	72.71	$\mu = 80, \lambda = 560$	0.9048	46.32	74.43
	Average	0.9088	44.42	72.87	Average	0.9047	46.26	74.48
	Standard deviation, $\sigma$	0.0005	0.43	0.22	Standard deviation, $\sigma$	0.0005	0.91	0.21

When using RMSE as an objective function, the results were identical to those obtained when using the NSE for the ES algorithm, and similar to those obtained when using the DE algorithm. Table 3.3 shows that there were no significant differences in

calibration performance indicated by optimizing the NSE or RMSE for each population size when using either the DE-calibrated or ES-calibrated model.

**Table 3.4** The performance of the model in validation according to Nash–Sutcliffe efficiency (NSE), root mean square error (RMSE) and mean absolute error (MAE) using sets of parameters after calibration by different objective functions for optimization

Optimized Index	DE			$(\mu+\lambda)$ -ES				
	Parent population	Fitness indices		Parent and offspring population	Fitness indices			
		NSE	MAE (m <sup>3</sup> /s)		RMSE (m <sup>3</sup> /s)	NSE	MAE (m <sup>3</sup> /s)	RMSE (m <sup>3</sup> /s)
NSE	$Np = 40$	0.9041	53.13	94.46	$\mu = 5, \lambda = 35$	0.8963	55.17	98.22
	$Np = 80$	0.9008	53.67	96.10	$\mu = 10, \lambda = 70$	0.9049	56.83	94.09
	$Np = 160$	0.9006	53.43	96.18	$\mu = 20, \lambda = 140$	0.9067	54.11	93.17
	$Np = 320$	0.8994	54.37	96.75	$\mu = 40, \lambda = 280$	0.9038	56.03	94.61
	$Np = 640$	0.9038	53.46	94.60	$\mu = 80, \lambda = 560$	0.8951	57.39	98.81
	Average	0.9017	53.61	95.62	Average	0.9014	55.90	95.78
	Standard deviation, $\sigma$	0.0019	0.42	0.92	Standard deviation, $\sigma$	0.0047	1.17	2.29
MAE	$Np = 40$	0.8819	56.82	104.83	$\mu = 5, \lambda = 35$	0.8817	60.18	104.91
	$Np = 80$	0.8793	56.89	106.00	$\mu = 10, \lambda = 70$	0.9029	55.11	95.08
	$Np = 160$	0.8912	54.58	100.60	$\mu = 20, \lambda = 140$	0.8942	55.38	99.21
	$Np = 320$	0.8886	54.96	101.80	$\mu = 40, \lambda = 280$	0.8791	58.83	106.07
	$Np = 640$	0.8960	53.61	98.38	$\mu = 80, \lambda = 560$	0.8981	54.86	97.37
	Average	0.8874	55.37	102.32	Average	0.8912	56.87	100.53
	Standard deviation, $\sigma$	0.0061	1.29	2.78	Standard deviation, $\sigma$	0.0093	2.20	4.27
RMSE	$Np = 40$	0.9075	52.44	92.76	$\mu = 5, \lambda = 35$	0.8963	55.17	98.22
	$Np = 80$	0.9016	53.40	95.70	$\mu = 10, \lambda = 70$	0.9049	56.83	94.09
	$Np = 160$	0.9065	52.09	93.30	$\mu = 20, \lambda = 140$	0.9067	54.11	93.17
	$Np = 320$	0.9008	53.61	96.08	$\mu = 40, \lambda = 280$	0.9038	56.03	94.61
	$Np = 640$	0.8996	54.12	96.63	$\mu = 80, \lambda = 560$	0.8951	57.39	98.81
	Average	0.9032	53.13	94.90	Average	0.9014	55.91	95.78
	Standard deviation, $\sigma$	0.0032	0.75	1.56	Standard deviation, $\sigma$	0.0047	1.17	2.29

The minimum, maximum and average values of parameters obtained by the DE and  $(\mu+\lambda)$ -ES among different trials of population size and objective function NSE, MAE and

RMSE, are shown in Table 3.1. Except the parameter  $S_3$  where the average value obtained by DE optimization was clearly 3 times smaller than that by  $(\mu+\lambda)$ -ES, there were 0.5-2.0 times of differences between average parameters found by DE and the respective parameters found by ES. The Table 3.1 also shows that the range widths of some parameters,  $a_4$ ,  $b_1$ ,  $b_2$ ,  $Z_2$ ,  $S_1$ , obtained by DE-calibrated model were slightly greater than those by ES-calibrated. However, the ranges of the other parameters obtained by the DE-calibrated were totally narrower than those by the ES-calibrated. This suggests the stability of the DE-calibrated superior to that of the ES-calibrated.

Table 3.4 shows the performance of the calibrated models for simulation in the validation period. The DE-calibrated model performed better than the ES-calibrated model during validation, although compared to the calibration period, the advantage of the DE-calibrated model over the ES-calibrated model in simulation accuracy was reduced. The NSE, MAE, and RMSE statistical indices of the discharge simulated by the DE-calibrated model were not always better than those from the ES-calibrated model in equivalent experiments. However, the average NSE values using the DE-calibrated model were slightly greater than those using the ES-calibrated model, and the average MAE and RMSE values were both slightly smaller using the DE-calibrated model than using the ES-calibrated model. For example, comparison of the three fitness indices of the discharges simulated by the two models calibrated by optimizing NSE produced the following results. Discharge simulated using the DE-calibrated model produced NSE values during validation ranging from 0.8994 to 0.9041, while the range using the ES-calibrated model was slightly wider, varying from 0.8951 to 0.9067. The range of the best MAE of simulated discharge was wider using the DE-calibrated model than using the ES-calibrated model; the best MAE values from the DE-calibrated model during validation ranged from 53.13 m<sup>3</sup>/s to 54.37 m<sup>3</sup>/s, whereas those from the ES-calibrated model ranged from 54.11 m<sup>3</sup>/s to 57.39 m<sup>3</sup>/s. The best RMSE values from the DE-calibrated model ranged from 94.46 m<sup>3</sup>/s to 96.75 m<sup>3</sup>/s, while those from the ES-calibrated model ranged from 93.17 m<sup>3</sup>/s to 98.81 m<sup>3</sup>/s. The average values of these indices were all slightly better using the DE-calibrated model than using the ES-calibrated model. The values of the NSE, MAE, and RMSE were 0.9017, 53.61 m<sup>3</sup>/s, 95.62 m<sup>3</sup>/s respectively using the DE-calibrated model, whereas these indices were slightly worse using the ES-calibrated model, at 0.9014, 55.90 m<sup>3</sup>/s, 95.78 m<sup>3</sup>/s,

respectively. During validation, the fitness of the simulated data changed with population size. For some middle-population-size experiments, from  $Np = \mu + \lambda = 80$  to 320, the NSE and RMSE values using the ES-calibrated model showed better fitness than those derived from the DE-calibrated model. For smaller and larger population size experiments ( $Np = \mu + \lambda = 40$  and 640), the performance of the DE-calibrated model was better than that of the ES-calibrated model. The best MAE values were better using the DE-calibrated model than using the ES-calibrated model under all experimental conditions, but the inverse trend was observed for some fitness indices. Similar to the calibration period, the fitness indices of the discharge simulated by the calibrated models were similar regardless of the target index selected. It is evident from Table 3.4 that all of the fitness indices of simulated discharge by the DE-calibrated model using RMSE were close to those of the DE-calibrated model using NSE. For the ES-calibrated model, the RMSE of the simulated discharge by the LST model calibrated by optimizing NSE was the same as that obtained by optimizing RMSE. Similar results were found in the cases where the model was calibrated by optimizing the MAE or RMSE. In both cases, the DE-calibrated model performed better than the ES-calibrated model.

The standard deviation value,  $\sigma$ , of each fitness index shown in Tables 3.3 and 3.4 is smaller for the DE-calibrated model than the ES-calibrated model. This suggests that the distribution range of each fitness index of the DE-calibrated model was narrower than that of the ES-calibrated model; that is, calibration results using DE were not significantly affected by population size. In Table 3.3, the NSE  $\sigma$  values were mostly equal to zero in calibration. The MAE values were also small, accounting for 0.36 m<sup>3</sup>/s when optimizing the NSE, 0.21 m<sup>3</sup>/s when optimizing MAE, and 0.43 m<sup>3</sup>/s when optimizing RMSE. A similar situation was observed for RMSE, with a very small standard deviation,  $\sigma$ , in all cases. Tables 3.3 and 3.4 show that the standard deviations of almost all of the fitness indices were larger using  $(\mu + \lambda)$ -ES calibration than using DE calibration. This suggests that calibration results obtained using  $(\mu + \lambda)$ -ES are more affected by population size than those from DE.

### 3.3.2. Comparison of evolutionary progress

The evolutionary progress of DE and  $(\mu + \lambda)$ -ES was compared. Here, the optimization of the NSE and MAE are discussed, because the evolutionary progress of

the NSE and RMSE were similar. Figure 3.4 shows the change in the best NSE and MAE by generation during the DE and  $(\mu+\lambda)$ -ES optimization processes. The results are shown for each population size. The changes in the fitness indices were larger using the ES-calibrated model than using the DE-calibrated model. The best NSE from the DE-calibrated model increased by only around 0.03–0.05 from the initial generation. The best MAE decreased by around 11 m<sup>3</sup>/s in the cases of  $Np = 40, 80,$  and 160 and around 8 m<sup>3</sup>/s for larger population sizes. In contrast, the changes in the NSE using the ES-calibrated model varied from 0.047 ( $\mu+\lambda = 640$ ) to over 0.5 ( $\mu+\lambda = 40$ ), and the changes in MAE were from over 9 m<sup>3</sup>/s ( $\mu+\lambda = 640$ ) to 55 m<sup>3</sup>/s ( $\mu+\lambda = 40$ ). The changes in the NSE and MAE decreased with increasing population size, because fitness indices tend to be worse for  $(\mu+\lambda)$ -ES calibration than for DE calibration at the initial generation, particularly for small population sizes.

However, during early generations for small population sizes, the objective functions were improved using the ES-calibrated model more rapidly than using the DE-calibrated model. Using the  $(\mu+\lambda)$ -ES algorithm, the fitness indices improved significantly and were comparable to those using the DE algorithm in the earliest four or five generations, and exceeded the fitness indices produced by DE in some cases ( $Np = 40$  and 640 for optimization of the NSE;  $Np = 80$  and 160 for optimization of the MAE). However, they then improved slowly in later generations. The best NSE from the ES-calibrated model changed from only over 0.01 ( $\mu+\lambda = 640$ ) to slightly over 0.03 ( $\mu+\lambda = 40$ ) from the fifth to the final generation. The change in the best MAE using the ES-calibrated model was from around 4.3 m<sup>3</sup>/s ( $\mu+\lambda = 320, 640$ ) to 8.93 m<sup>3</sup>/s ( $\mu+\lambda = 40$ ).

As mentioned above, the NSE of the initial generation was better using the DE-calibrated model than using the ES-calibrated model, particularly for small population sizes. This gap lessened with increasing population size. This is because the parent sizes, which affect the probability of finding a better set of parameters in the initial generation, were different; that is,  $Np$  in the DE-calibrated model was larger than  $\mu$  in the ES-calibrated model. In the first three to five generations, both the best NSE and the best MAE from the ES-calibrated model rapidly improved.

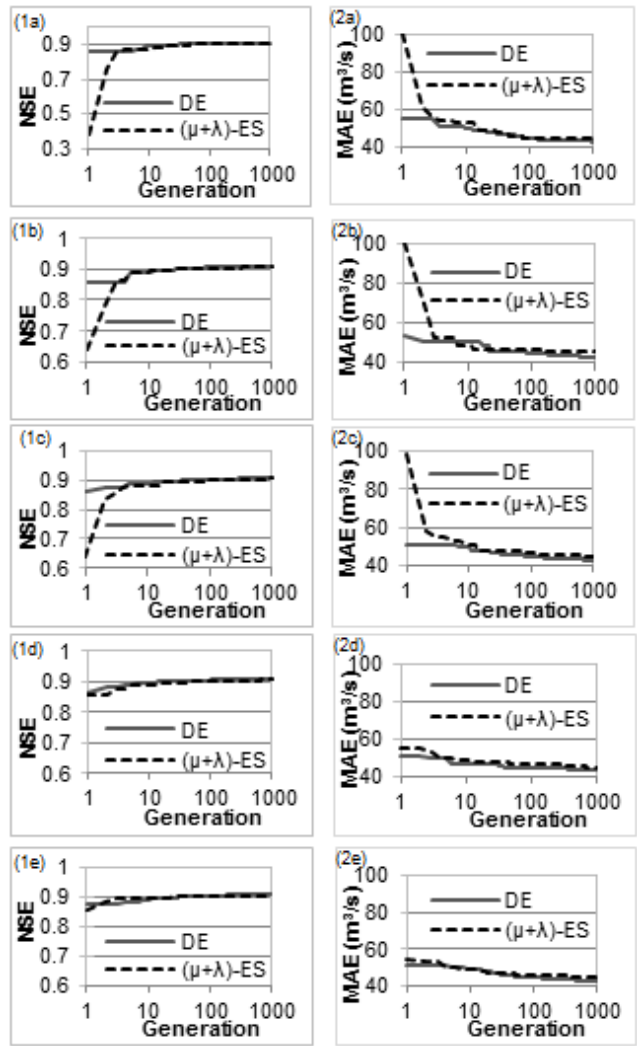


**Fig 3.4** The Improvements of the best NSE (left) MAE (right) by generation change with the population size as 40 (a), 80 (b), 160 (c), 320 (d) and 640 (e)

After the third to fifth generations, when the NSE or MAE of the discharge produced using the ES-calibrated model caught up with those produced using the DE-calibrated model, the NSE and MAE improved gradually in both the DE and  $(\mu+\lambda)$ -ES cases. From several to several dozens of generations after the catch-up, the fitness indices resulting from the ES-calibrated model were superior to those from the DE-calibrated model in some population cases. However, the fitness indices resulting from the DE-calibrated model improved slightly faster than did those from the ES-calibrated model in later generations, in which the  $(\mu+\lambda)$ -ES optimization needed more generations to obtain better-optimized indices than DE optimization. As a consequence, the performance improvement in NSE and MAE values resulting from the DE-calibrated model were greater than those from the ES-calibrated model. The best NSE values resulting from the DE-calibrated model were about 0.003–0.004 higher than those from the ES-calibrated

model. The best MAE values resulting from the DE-calibrated model were around 1.32 m<sup>3</sup>/s to 2.13 m<sup>3</sup>/s lower than those from the ES-calibrated model.

### 3.3.3. Distribution of the best optimized indices

Distributions of the fitness index of simulated discharge from the 100 different LST models calibrated for 1,000 generations are shown in Figure 3.5. The calibration of these models was started from 100 different randomly generated populations of independent individuals. Figure 3.5 shows the distributions of the final fitness indices, the NSE, RMSE and MAE, optimized using the DE- and ES-calibrated models after 1000 generations. A population size of 160 is shown as an example.

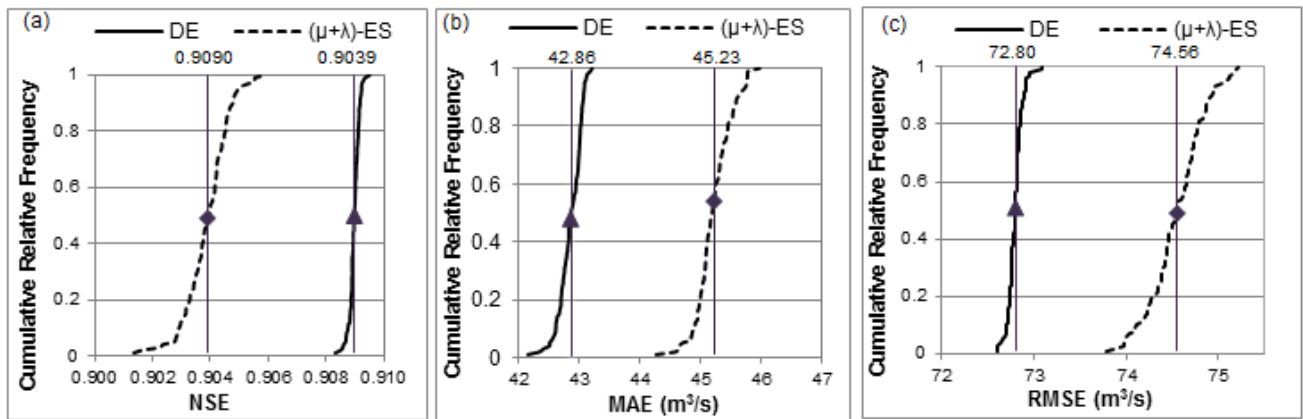


**Fig 3.5** Distribution of the best NSE (a), MAE (b) and RMSE (c) by DE and  $(\mu+\lambda)$ -ES after 1000 generation simulation

The averages of all of the fitness indices show the superiority of the DE algorithm over the  $(\mu+\lambda)$ -ES algorithm. Moreover, Figure 3.5 clearly shows that the distribution range of each optimal 100 fitness index was narrower using the DE-calibrated model than using the ES-calibrated model. In other words, the optimal fitness indices estimated using the DE-calibrated model were more stable than those resulting from the ES-calibrated model. According to the results of 100 independent optimization tests for NSE using the DE-calibrated model, the distribution range of NSE values in the final generation was 0.0012, and the worst and best NSE values were 0.9083 and 0.9095, respectively, with an average of 0.9090. The results of the same optimization tests using the ES-calibrated model show a distribution range of NSE values of 0.0046, 0.0034 larger than that from the DE-calibrated model. The best and worst NSE values were 0.9014 and 0.9060 respectively, and the average was 0.9039, which was 0.005 smaller than that resulting from the DE-calibrated model. The results of the same tests for MAE show that the

optimal MAE value from the DE-calibrated model was 1.06 m<sup>3</sup>/s; this value was 0.65 m<sup>3</sup>/s smaller than that from the ES-calibrated model (1.71 m<sup>3</sup>/s). The average MAE resulting from the DE-calibrated model was 42.86 m<sup>3</sup>/s, 2.4 m<sup>3</sup>/s smaller than that from the ES-calibrated model (45.23 m<sup>3</sup>/s). The tests for RMSE optimization showed that the distribution range of the RMSE value in the final generation using the DE-calibrated model was 0.49 m<sup>3</sup>/s, smaller than that resulting from the ES-calibrated model (1.43 m<sup>3</sup>/s). The average RMSE resulting from the DE-calibrated model, 72.80m<sup>3</sup>/s, was 1.75 m<sup>3</sup>/s lower than that from the ES-calibrated model (74.56m<sup>3</sup>/s).

### 3.3.4. Computation time

To evaluate the efficiency of the DE and ES algorithms in calibrating the LST model, the required computation times were compared. The programs were written in Fortran 95 and executed using a computer with an Intel Core i3 3.30GHz processor and 8.00GB RAM. Table 3.5 shows the average computation time for optimization of the NSE, the MAE, and the RMSE for each-generation calibration. The computation time for calibration using ( $\mu+\lambda$ )-ES calibration was longer than that using DE calibration for the same population size ( $Np = \mu+\lambda$ ). Moreover, the ratio of the computation time for one generation using the ES-calibrated model to that using the DE-calibrated model generally increased with increasing population size. As shown in Table 3.5, computation times for ( $\mu+\lambda$ )-ES calibration were between 1.45 and 1.58 times longer than those for DE calibration.

The computation time for one generation using the DE optimization technique was very short. For example, the average computation times for one generation were 0.0069s for  $Np = 40$  and 0.1094s for  $Np = 640$ . The computation time was approximately proportionate to the population size. In addition, the calibration results using DE were not significantly affected by population size as discussed above. As a result, the lowest population size  $Np=40$  in DE optimization resulted in the highest efficiency in optimizing model parameters for Be river catchment in this study.

The computation times were longer for ( $\mu+\lambda$ )-ES calibration than for DE calibration, ranging from 0.0103s for the smallest population to 0.1721s for the largest. The DE-calibrated model had faster calibration times than the ES-calibrated model for equivalent population size experiments. The computation times were around 1.5 times longer for

$(\mu+\lambda)$ -ES calibration than for DE calibration. The ratio of the computation time for ES-calibration to that for DE-calibration tended to increase slightly with increasing population size ( $Np = \mu+\lambda$ ). For either the DE or  $(\mu+\lambda)$ -ES calibration process, although the computation time differed with the objective fitness index, with MAE being the shortest and NSE the longest, there were no significant differences in computation times for each generation between these indices, which varied between less than 1% and nearly 10%.

**Table 3.5** Average computation times per one-generation simulation of DE and  $(\mu+\lambda)$ -ES optimization

DE		$(\mu+\lambda)$ -ES			(5)/(2)
(1) $Np$	(2) Time (s)	(3) $\mu$	(4) $\lambda$	(5) Time (s)	
40	0.0069	5	35	0.0103	1.4936
80	0.0141	10	70	0.0205	1.4476
160	0.0276	20	140	0.0433	1.5675
320	0.0546	40	280	0.0862	1.5792
640	0.1094	80	560	0.1721	1.5729
Average	0.0425			0.0665	1.5629

### 3.4. Conclusions

In this study, we evaluated the performance of optimization techniques using the original versions of the DE and  $(\mu+\lambda)$ -ES algorithms to calibrate the LST model. The results show that both algorithms can be successfully applied to automatic calibration of the LST model. The DE algorithm requires three optimization parameters,  $Np$ ,  $Cr$ , and  $F$ , for operation, whereas the  $(\mu+\lambda)$ -ES algorithm needs only two optimization parameters,  $\mu$  and  $\lambda$ , for calibration. However, the DE algorithm is simpler to execute than the  $(\mu+\lambda)$ -ES algorithm because in the process of generating offspring in DE calibration, only the offspring population is improved step-by-step by crossover, mutation and selection, whereas the ES-calibrated model requires intermediate calculation of standard deviations to generate offspring. In consequence, the computation time for calibration is shorter using the DE algorithm than using the  $(\mu+\lambda)$ -ES algorithm. The DE optimization technique is slightly more efficient than  $(\mu+\lambda)$ -ES in calibrating the LST model. Comparisons of the simulation accuracy of DE- and ES-calibrated models after 1000

generations, indicated by fitness indices, showed that during calibration the simulated discharge was more accurate using the DE-calibrated model than using the ES-calibrated model. The performance of the DE-calibrated model was also slightly better than that of the ES-calibrated model during validation. Furthermore, the computation time was shorter for DE calibration than for  $(\mu+\lambda)$ -ES calibration. The robustness of the DE technique in calibrating the LST model was better than that of the  $(\mu+\lambda)$ -ES technique. The results of the optimal fitness indices achieved by the DE-calibrated model were not significantly affected by population size, whereas the simulation accuracy of the ES-calibrated model was more sensitive to parent and offspring population conditions. The difference in robustness was also illustrated by differences in the values of the standard deviations of fitness indices. The results of the calibration tests started with 100 different initial populations of parameter sets showed that the distribution ranges and standard deviations of the optimal fitness indices estimated by the DE-calibrated model were smaller than those estimated by the ES-calibrated model. This suggests that the variety of parameters of the DE-calibrated model is smaller than that of the ES-calibrated model. In this study, the original DE and  $(\mu+\lambda)$ -ES evolutionary algorithms were applied to calibration of the LST model for the Be River catchment. The calibration parameters were set with reference to previous studies as well as the results of trials. The results suggest the high performance and practicability of the DE algorithm and support the application of the DE algorithm to calibration of rainfall-runoff models for other catchments.

# CHAPTER IV

## UNCERTAINTY IN THE IMPACT OF CLIMATE CHANGE ON STREAMFLOW AND RESERVOIR MANAGEMENT

### 4.1. Introduction

Thac Mo Sub-basin, which is separated from the downstream sub-basin by the Thac Mo Reservoir, is one of the major sub-basins of the Be River Basin in Vietnam. This basin is very rich in water resources, and the Thac Mo Reservoir has an important role in supplying water not only for hydropower but also for irrigation, municipal use and industrial activities in the downstream areas.

There have been a number of studies on the hydrological environment and water resources of the Be River Basin, some of which concerned the impact of climatic changes (Khoi & Suetsugi, 2012, 2013, 2014; Vu & Nguyen, 2015). However, these studies did not focus on specific sub-catchments. Khoi & Suetsugi (2012) used a SWAT model and projected future climate from Global Climate Models (GCMs) to assess the impacts of climate change and land-use change on the hydrological processes and sediment yield in the Be River Catchment. In the study by Vu & Nguyen (2015), the hydropower operation was considered, but this work was aimed at assessing the water transfer capacity from the Be River Basin to Dau Tieng Reservoir through the Phuoc Hoa Hydraulic-Works. Only a limited number of studies on the effects of streamflow change on the management of the Thac Mo Reservoir have been found.

Clearly, water resources have enormous consequences for the social-economic system in all areas. Furthermore, it is known that small meteorological changes can result in relatively large changes in runoff and water availability (Conway 2005; Beyene *et al.* 2010).

The above arguments show the importance of a study on the impact of climate change in specific Thac Mo Sub-basin. This study investigates the impact of the projected precipitation under the different climate scenarios, called Representative Concentration Pathways (RCPs), according to the Intergovernmental Panel on Climate Change (IPCC 2013), as compared with the current conditions (1981–2000). Three future scenarios, RCP2.6, RCP4.5, and RCP8.5, which cover the years 2046–2065, were selected. The Long- and Short-Term Runoff Model (LST Model) (Kadoya & Tanakamaru 1989) was applied to simulate the runoff, and was calibrated by a differential evolution (DE) optimization algorithm. Simulation of the reservoir operation was carried out on the basis of reservoir balance modeling, and the reservoir’s operation rules.

## 4.2. Method and materials

### 4.2.1. Study Area

The Thac Mo Hydropower Reservoir was created by construction of a dam across the Be River, in Bu Gia Map District, Binh Phuoc Province, Vietnam. The reservoir has a catchment area of 2,200 km<sup>2</sup>, located in the upper Be River Catchment, which belongs to the Dong Nai river system in the south of Vietnam (Figure 4.1). The mean annual precipitation in the catchment is about 2,600 mm. The rainy season lasts from May to

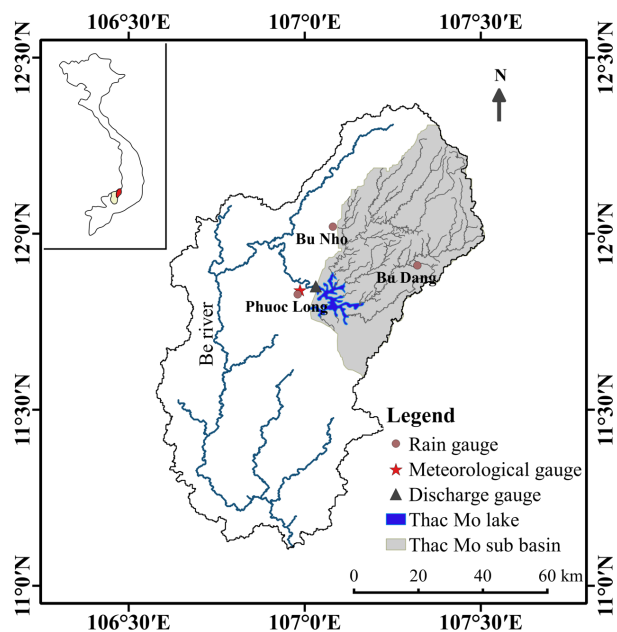


**Fig 4.1** Map of Thac Mo catchment

November and accounts for 85%–90% of the total annual precipitation with the largest monthly precipitation usually occurring from August to October. The flows in the rainy season are important for meeting water demand throughout the year. The average

temperature, humidity, and wind speed of this area are about 25°C, 80%, and 1.7 m/s, respectively. The annual sunshine duration amounts to 2,800 h.

The data used for calibration and validation of the LST model in the period before the hydropower plant began generation were as follows: (i) daily precipitation observed at three rain gauge stations (Phuoc Long, Bu Dop, and Bu Nho); (ii) monthly meteorological data including temperature, humidity, wind speed, and sunshine hours at Phuoc Long station to estimate evaporation; and (iii) daily discharge observed at Phuoc Long station for calibration and validation (Figure 4.1). The data observation period was from January 1984 to December 1991. The data from the first five years (1984–1988) were used for model calibration, and those from the following 3 years (1989–1991) were used for validation. For calibrating the regimes of inflow, outflow, and reservoir storage, the daily precipitation and monthly meteorological data of the above stations from 1996 to 2004 were used. Observed monthly data from 1996 to 2004, on water level, and reservoir inflows and outflows, were used to compare the simulation with the actual reservoir operation.

#### **4.2.2. LST Model**

In this study, the rainfall-runoff LST model was used as application for parameter calibration. The detail of LST model was presented in chapter 3. LST model applied in this sub-catchment was calibrated using DE.

#### **4.2.3. Reservoir Description and Reservoir Balance Modeling**

##### **4.2.3.1. Thac Mo Reservoir**

Construction of the Thac Mo hydropower dam was completed in January 1995. The dam has an effective storage capacity of  $1.25 \times 10^9$  m<sup>3</sup>. The normal and dead water levels in the reservoir are 218 m and 198 m with corresponding water surface areas of 109 km<sup>2</sup> and 25 km<sup>2</sup>, respectively. The capacity of the installed power plant is 150 MW ( $2 \times 75$  MW), and the target capacity is 55 MW.

The aims of the Thac Mo Hydropower Reservoir are to control the annual flow into the downstream area and to generate power for the national electricity system. In addition,

the regulatory regime of the Thac Mo hydropower plant will provide water for irrigation, and for municipal and industrial use downstream. There is no major water control infrastructure upstream of Thac Mo Reservoir. The water surface of the reservoir covers up to about 5% of the catchment during the highest storage levels in the flood season.

#### 4.2.3.2. Reservoir operation model

The reservoir operating policies are based on the reservoir rule curves and the principles of water balance concept.

- *The water balance equation:*

$$S_{t+1} = S_t + I_t + P_t - R_t - EV_t - L_t \quad (4.1)$$

where,  $S_t$  and  $S_{t+1}$  ( $m^3$ ) represent the reservoir storages at the beginning of period  $t$  and  $t+1$ , respectively.  $I_t$ ,  $P_t$ ,  $R_t$ ,  $EV_t$  and  $L_t$  are the volume ( $m^3$ ) of inflow, precipitation over the reservoir, release, evaporation, and water leakage through the dam, respectively

- *Usable storage capacity:*

$$S_t \leq S_{max} - S_{dead} \quad (4.2)$$

where  $S_{max}$  and  $S_{dead}$  are the reservoir maximum and dead storages respectively.

- *The upper limit on power production:*

$$9.81 \times Q_t \times H_t \times \eta_t \leq P_{cap} \quad (4.3)$$

where  $P_{cap}$ ,  $Q_t$ ,  $H_t$ ,  $\eta_t$  are the maximum power production of Thac Mo hydropower plant ( $150 \times 10^3 kW$ ), released discharge for power generation ( $m^3/s$ ), waterfall height (m), and overall system efficiency, respectively.

Operational rules for water release from the reservoir, issued in 1994, could not be found. The rules applied in this study were based on Decision 1892/QD-TTg, issued by the government in 2014 (Vietnamese Government, 2014), and the measured monthly reservoir water levels from 1996–2004.

Water discharge for producing power was based on the rules described in Decision 1892/QD-TTg. However, it was found in the observation data that there are many days when the operation was different from the issued rule. This may be due to that the operators relied on not only the reservoir storage level but also the other factors such as system electricity demand which could not be collected in this study. The regulation was modified so as to gain the better calibration compare to that by used origin issued rule. For example, for the safety of the reservoir during the flood season, it is required that if a flood warning is issued by the Southern National Centre for Hydro-Meteorological Forecasting, water must be spilled out to lower the water level to below the normal level three days before the flood (Decision 1892/QD-TTg). In this study, water is only spilled out to the normal water level. In case of sudden flooding, the spilled water level is set at 216.5 m in July, to reduce the risk to the reservoir.

#### **4.2.4. Hydrological Model Performance Evaluation**

To achieve successful calibration using an automatic optimization technique, as well as to evaluate performance through calibration and validation, it is crucial to select appropriate objective functions that assess the error or fitness of the simulated data with respect to the observed data. Dawson *et al.* (2007) assembled 20 performance measures used in hydrology. In the present study, the Nash–Sutcliffe efficiency (NSE) (Nash & Sutcliffe 1970) was optimized in calibration. The mean absolute error (MAE), and root mean square error (RMSE) were also calculated to evaluate the performance of the model. Three above fitness indices were presented in chapter 3.

#### **4.2.5. Differential Evolution**

In this study, DE was used to optimize the set of model parameters. The original DE algorithm (Storn, 1996) was applied to calibrate the LST model for the timespan 1984–1988, before the hydropower plant began operation, by maximizing the objective function NSE. The set of calibrated parameters was used for simulation in the validation periods, before and after the reservoir began operation, in the study catchment. In this study,  $Np$ ,  $Cr$ , and  $F$  were respectively set as 160, 0.2, and 0.7 as results from chapter 3.

#### **4.2.6. Future Precipitation Projection**

Future projections of daily runoff into the dam and simulation of dam operation under future climate conditions were performed with the calibrated LST model using projected daily precipitation by the GCM, MIROC5, developed by the University of Tokyo. For each future scenario mentioned below, future precipitation time series generated by three different ensemble members, r1i1p1, r2i1p1, and r3i1p1, were used for the simulations. The projected precipitation data used in this study was downloaded from the Data Integration and Analysis System (DIAS, n. d.).

The future precipitation scenarios were generated under future scenarios known as Representative Concentration Pathways (RCPs). The RCPs are representative scenarios including time series of emissions and concentrations of greenhouse gases, aerosols and chemically active gases, as well as land use or land cover. These were adopted for future projections of climate change in the Fifth Assessment Report of the IPCC (IPCC, 2013). In this study, scenarios RCP2.6, RCP4.5, and RCP8.5 were used, where RCP2.6 is the lowest radiative-forcing scenario, RCP4.5 is the low-middle one, and RCP8.5 is the highest one (IPCC, 2013). Bias in the future daily rainfall generated by MIROC5 was corrected by using the ratio of the monthly rainfall generated by MIROC5 under present climate conditions to the observed monthly rainfall. Bias correction was performed by CMIP5 data analysis system (n.d.) on the DIAS.

In this study, future changes in other climatic elements, such as temperature, humidity, etc. were not considered. Although the impacts of changes in these other elements are not negligible, we only considered the effects of future changes in rainfall, because it is the most important element impacting on the hydrological cycle in river basins of humid areas such as Vietnam.

### **4.3. Results and discussion**

#### **4.3.1. LST Model Calibration and Validation in the Periods Without Reservoir Operation**

After calibrating the LST model using DE through a 1,000-generation simulation, the

set of parameters for the LST model applied to the Thac Mo basin was optimized, as shown in Table 4.1. The 160 parent sets of parameters resulted in values of NSE ranging from  $-0.72$  to  $0.79$  at the 1st generation. The maximum value of NSE obtained from optimized parameters gradually improved from  $0.79$  to over  $0.86$  at the 1,000th generation. After simulating streamflow using these optimized parameters in the LST model over the calibration period, the RMSE and MAE were calculated for fitness evaluation. The calibrated set of parameters was applied for the validation periods. The evaluation coefficients for calibration and validation are shown in Table 4.2. In Figure 4.3, the simulated and observed daily discharges are compared for the calibration period and for the validation period at Phuoc Long station. The simulated daily flow seems to match the observed data well in both the calibration and validation periods, except on some days, especially in the year 1987, when the simulated flows fall far below the observed one. The values of observed discharge were high, but there were no noticeable increases in observed precipitation on these days. However, the values of the fitness indices for daily calibration and validation, NSE, RMSE, and MAE, which are illustrated in Table 4.2, indicate good performance of the LST model according to the criteria given by Moriasi *et al.* (2007). The agreement between the daily simulated and observed flow was marked by  $\text{NSE} = 0.86$ ,  $\text{RMSE} = 48.61 \text{ m}^3/\text{s}$ , and  $\text{MAE} = 23.95 \text{ m}^3/\text{s}$  for the calibration period; and  $\text{NSE} = 0.84$ ,  $\text{RMSE} = 57.44 \text{ m}^3/\text{s}$ , and  $\text{MAE} = 29.05 \text{ m}^3/\text{s}$  for the validation period. It can be concluded that the LST model can simulate the flow reasonably well for Thac Mo basin using the above optimized parameters.

#### **4.3.2. LST Model Validation and Simulation of Thac Mo Reservoir Management**

The inflow, outflow for power generation, and change in storage of the Thac Mo Reservoir were simulated for validation of the LST model, evaluation of the reservoir balance model, and assessment of future effects of streamflow change on the reservoir operation, using the projected precipitation.

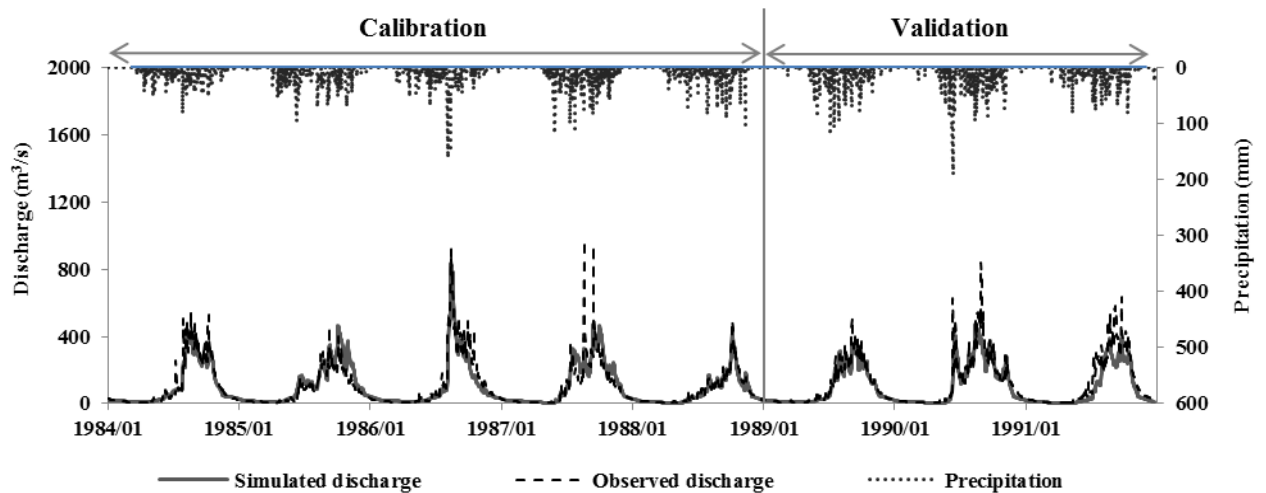
The simulated discharge by the calibrated LST model was used as input for the reservoir balance model, and the reservoir control rules described above were applied. The daily change in reservoir storage was simulated in order to consider the water spilled through the flood control, and the monthly values of three hydrological variables (inflow and outflow for power generation, and storage in the Thac Mo Reservoir) were calculated, and compared with the observed monthly data, as shown in Figure 4.4. Figure 4.5 shows the series of monthly simulated and measured values of these three variables.

**Table 4.1** Parameters of LST model

Parameter	Min - Max	Optimized value
a <sub>1</sub>	0.001 – 0.05	0.00142
a <sub>2</sub>	0.01 – 0.1	0.021265
a <sub>3</sub>	0.001 – 0.1	0.00397
a <sub>4</sub>	0.0005 – 0.02	0.00056
a <sub>5</sub>	0.00001 – 0.001	0.00076
b <sub>1</sub>	0.01 – 0.2	0.09660
b <sub>2</sub>	0.001 – 0.04	0.00665
b <sub>3</sub>	0.001 – 0.01	0.00207
Z <sub>1</sub>	5 - 200	134.76
Z <sub>2</sub>	5 - 500	377.33
Z <sub>3</sub>	5 - 200	155.07
S <sub>1</sub>	0 - 20	14.53
S <sub>2</sub>	0 - 200	36.50
S <sub>3</sub>	0 - 1000	297.65
S <sub>4</sub>	0 - 1000	781.18

**Table 4.2** Model performance for the simulation of LST model and reservoir management

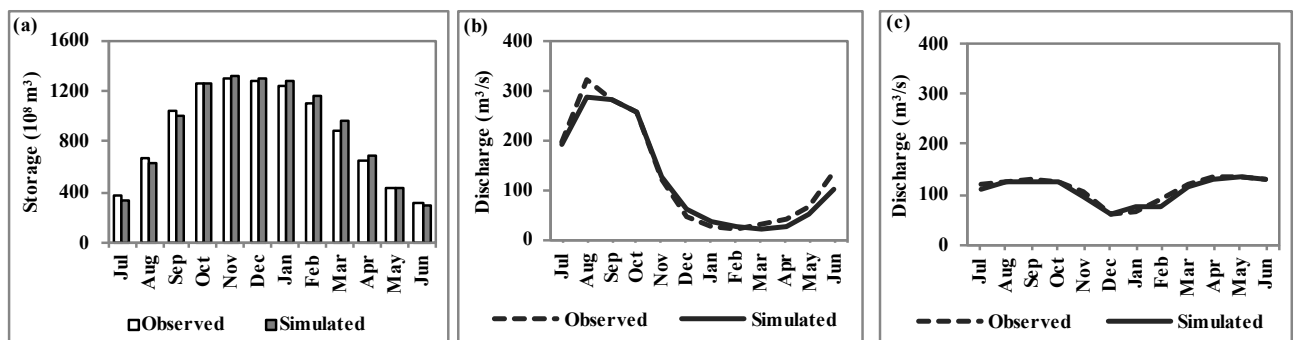
Period	Time step	NSE	RMSE	MAE
LST model calibration (1984-1988)	Daily	0.86	48.61 (m <sup>3</sup> /s)	23.95 (m <sup>3</sup> /s)
LST model validation (1989-1991)	Daily	0.84	57.44 (m <sup>3</sup> /s)	29.05 (m <sup>3</sup> /s)
Reservoir inflow (1996-2004)	Monthly	0.94	28.68 (m <sup>3</sup> /s)	20.32 (m <sup>3</sup> /s)
Reservoir water lever (1996-2004)	Monthly	0.95	1.23 (m)	0.88 (m)
Outflow for hydropower (1996-2004)	Monthly	0.65	21.69 (m <sup>3</sup> /s)	16.16 (m <sup>3</sup> /s)



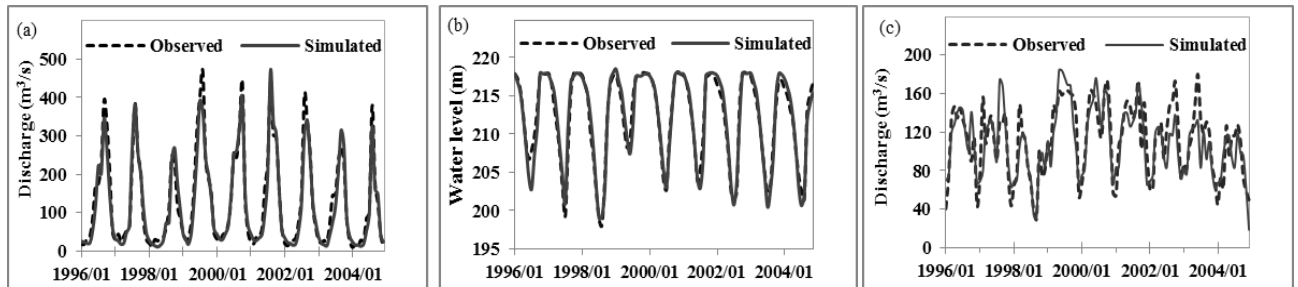
**Fig 4.2** Observed and simulated daily flow hydrograph at Phuoc Long station during the calibration (1984-1988) and validation (1989-1991) periods

Figure 4.3 shows that monthly changes in inflow, storage, and outflow for hydropower can be simulated accurately, although there was a slight variation between the observed and simulated storage levels of several months, a small difference in inflow particularly at the peak of the flood season, and a slight discrepancy in outflow for power

generation in several months are found in this figure. Moreover, Figure 4.4 shows the simulated seasonality of water inflow and the water use for power generation and downstream supply. The rainy season starts in May, and the water is mainly retained during the flood season from August to October. The water level usually reaches the normal elevation (218 m) at the beginning of November as shown in Figure 4.4b. It is kept stable or releases slightly more than the inflow until January, and noticeably decreases in the dry season, particularly from February. Then, it falls close to the dead water elevation (198 m) in July, before the flood season.



**Fig 4.3** Observed and simulated average monthly regime of storage (a), inflow (b) and outflow for power generation (c) in the Thac Mo reservoir



**Fig 4.4** The comparisons between simulated and observed data of monthly inflow (a), reservoir water level at beginning of the month (b) and monthly outflow for power generation (c)

The simulation accuracy of the monthly flow prediction using the LST model was validated from 1996 to 2004 with the observed reservoir inflow. As shown in Figure 4.4a, although there are some differences between the simulated and observed values, particularly in the flood season and at the peak of streamflow, the simulated monthly inflow matched the observed data well, with NSE over 0.94. The RMSE and MAE were approximately 28.68 m<sup>3</sup>/s and 20.32 m<sup>3</sup>/s, respectively. The statistical evaluation of the fitness between the simulated reservoir water level and the measured water level at the beginning of each month was good, as NSE = 0.95, RMSE = 1.23 m, and MAE = 0.88 m. The simulated release for hydropower was fairly accurate, as indicated by acceptable

values of  $NSE = 0.65$ ,  $RMSE = 21.69 \text{ m}^3/\text{s}$ , and  $MAE = 16.16 \text{ m}^3/\text{s}$ .

### 4.3.3. Streamflow Changes under Climate Change Scenarios

The unbiased GCM data indicated that the average annual precipitation in the future scenario RCP2.6 approximates to the current precipitation for the first ensemble member, r1i1p1, with 2600 mm. Those of subsequent members were slightly over 2800 mm. There was an obvious increase in annual precipitation for scenario RCP8.5, with an average annual precipitation of 2680 mm for the r1i1p1 and over 3000 mm for the others. The greatest growth in future annual precipitation was found in scenario RCP4.5, with over 2800 mm, 3200 mm, and 3000 mm for the first, second, and third members, respectively. The projected rainfall suggested little change in precipitation from December to March of

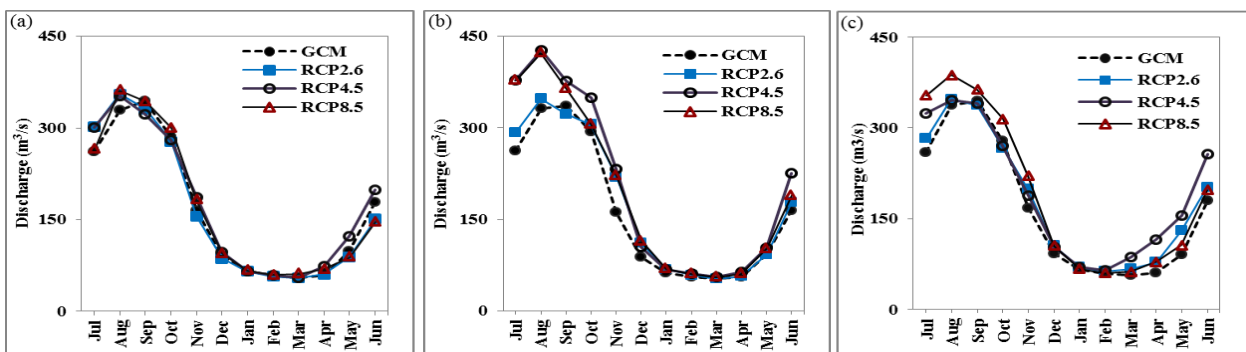


**Fig 4.5** The inflows into the reservoir under current (1981) and future (2046-2065) climate scenarios for different ensembles: r1i1p1 (a), r2i1p1 (b) and r3i1p1 (c)

the dry season. More marked change appeared in the rainy season.

As a consequence, the inflow to the Thac Mo Reservoir was changed under the climate scenarios. Figure 4.5 shows the average monthly inflows simulated by the LST model, with the projected precipitation by MIROC5 under climate change scenarios RCP2.6, RCP4.5, and RCP8.5 for the period 2046–2065, and the simulated inflow based on unbiased simulated precipitation by MIROC5 under the climate conditions of 1981–2000. In general, the discharge under the future climate change scenarios was predicted to increase considerably during the rainy season, but change during the dry season was insignificant. The results indicate similarity between the future average monthly discharges and the current ones, from December to March for the first ensemble member (r1i1p1), from January to April for the second (r2i1p1), and from January to February for the third (r3i1p1). It can be seen that the projected discharge under the scenario RCP8.5 was greatest from August to October for the r1p1i1 (Figure 4.5a) and from July to

November for the r3p1i1 (Figure 4.5c). In comparison, the estimated discharge under the scenario RCP4.5 had the greatest rise in the dry season, accounting for 45% in April (Figure 4.5c). It appeared greater than the others from April to July for the r1i1p1 ensemble, from May to November for the r2i1p1, and from March to Jun for the r3i1p1. In general, the increase in the projected discharge compared to current discharge under scenario RCP2.6 was less than the others during most months and across all the ensembles, although it was found to climb in July and August for the first and second ensembles, and from April to July for the third. It also appeared to decrease in June, September, and November for the first ensemble (Figure 4.5a), and in September for the second (Figure 4.5b). The average discharge of the three runs r1i1p1, r2i1p1, and r3i1p1 over 12 months were projected to go up 6.4%, 18.5%, and 11.7% under the RCP2.6, RCP4.5, and RCP8.5 scenarios, respectively. Evidently, there was inflow growth of 5% to 7% in January, February, June (except the RCP4.5 scenario), September, and October. The upward trend was estimated from 5% to 11.8% for the RCP2.6, from 12.5% to 44.5% for the RCP4.5, and from 15.4% to 27% for the RCP8.5 scenario in the other months.

#### **4.3.4. Possible Impacts of the Projected Streamflow Scenarios on Reservoir Control**

Figure 4.6 shows the long-term monthly average of the water storage (a), outflow for hydropower (b), and outflow spilled out of the reservoir (c) of the current (1981–2000) and future (2046–2065) periods for the RCP2.6, RCP4.5, and RCP8.5 scenarios. In Figure 4.6a, slight increase in the storage of the reservoir in the future scenarios can be found from the late dry season to the beginning of the rainy season; and the similar storage can be found in the late flood season (September and October) and early dry season (November to February). This is because the water level is controlled so as not to exceed the normal water level, although there are huge variations in the inflow in the future scenarios, particularly in the flood season. The water level control raises the future simulated discharge rises by over 10% in December, while an inconsiderable rise is found in January and February. As a consequence, annual variation in the reservoir storage was almost unchanged, while release for hydropower was increased in this period. The storage in the future scenarios clearly exceeds the current one from the beginning to the middle of the rainy season (May to August). The increase was particularly noticeable

in scenario the RCP4.5. The rate of increase was from 4.3% to 8.7 % for the scenario RCP2.6, from 16.5% to 35% for the scenario RCP4.5, and from 6.2% to 11.9 % for the scenario RCP8.5.

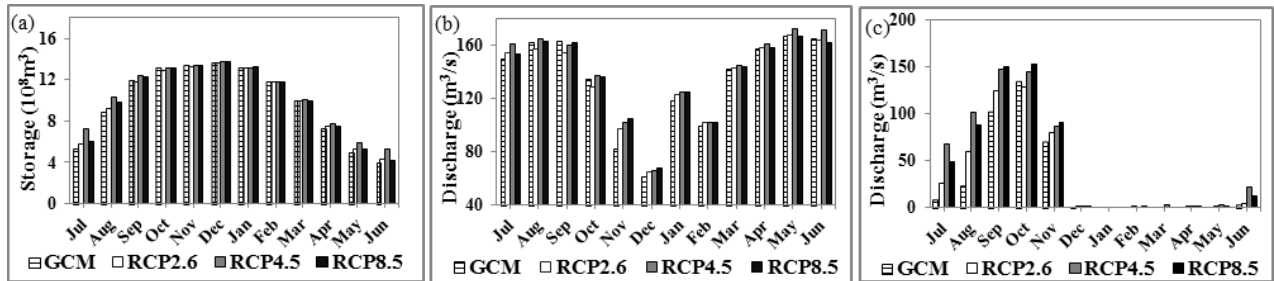


**Fig 4.6** The simulation of average monthly storage (a), outflow for hydropower (b) and outflow spill (c) of the reservoir among three ensembles, r1p1i1, r2i1p1, r3i1p1

For the release for hydropower, the discharge under the scenario RCP2.6 was somewhat higher than the current in July and from November to February of the following year, with the largest rise of 18.8% in November and the smallest of 2.7% in February. There was a decrease of within 5% in the flood season (August to October). An insignificant change was found during other periods. For the RCP4.5 and RCP8.5 scenarios, the release presented a marked variation in the same months as the RCP2.6 scenario; up to 25.4% and 28.6% increase in November for the scenarios RCP4.5 and RCP8.5, respectively. Another interesting point is that the release for hydropower under the RCP4.5 and RCP8.5 scenarios was projected to increase in all months of the year except September for the RCP4.5 and June for the RCP8.5. The rule for the reservoir simulation was set based on its actual operation. According to that rule, the water used for hydropower is lowered in the early dry season to retain water for downstream supply in the dry season. Therefore, although the reservoir storage increases, or even reaches maximum value in December (Figure 4.3), the used flow decreases (Figure 4.5b).

The most interesting point is that the simulated results of the spilled flow under the future scenario became much larger in the rainy season compared to the current situation. There are also some small spilled flows even in the dry season, as shown in Fig 4.6c. The reservoir was designed to be safe within the normal water level; therefore, the differences in storage and release for hydropower between the future and current scenarios are not remarkable as illustrated in Figure 4.6a and Figure 4.6b although inflow became greater in the rainy season. As a consequence, a considerable increase in spilled water was found

in the rainy season, particularly from June to November; the spill-out water was nearly 200% more than the current value in July under the RCP2.6 scenario, over 650% under the RCP4.5 scenario, and nearly 450% under the RCP8.5 scenario. The apparent increase in spill-out also appeared in June, August, September, and November. As shown in Figure 4.5c, the inflow discharge was projected to ascend markedly in the dry season under the scenario RCP4.5 with the third ensemble (r3i1p1), which explains why there was a small amount of spill water even in the dry season, as shown in Figure 4.6c.

#### **4.4. Conclusions**

To investigate the effects of change in precipitation under climate change on the inflow into the reservoir and reservoir control in Thac Mo basin, we simulated discharge under both current climate conditions and future climate change scenarios. Discharge was simulated by using the LST model, and projected precipitation data by a GCM, MIROC5, under current and future scenarios.

It was shown that the LST model could be successfully applied to streamflow simulation in Thac Mo basin, and that DE was suitable for calibrating this model for the basin. The simulated results emphasized that the flow coming into the reservoir under the future scenarios, particularly RCP4.5 and RCP8.5, increases remarkably in the rainy season, compared to under the current condition, although some remarkable rises were also found in the dry season, particularly under the scenario RCP4.5. The future reservoir storage was projected to insignificantly change compared to the present condition, especially in the flood season and early dry season. The future estimated release for hydropower slightly increased in comparison with under the current condition, especially for the RCP4.5 and RCP8.5. The spilled flow was projected to ascend markedly. The increase in inflow in the dry season is beneficial for hydropower generation as well as for downstream supply. However, the noticeable increase in the flood season is a matter of concern because it is not only wasteful but also may affect crop production, as well as the security of downstream communities. The results emphasize the importance of future management strategies for water resources in this catchment. The results obtained in this study can serve as a reference for further studies on water resources, as well as informing the management of water resources in this region.

## CHAPTER V

# DIFFERENTIAL EVOLUTION IN IMPROVING OPERATION RULE CURVES FOR THAC MO RESERVOIR

### 5.1. Introduction

Reservoir operation which is to effectively control the released water for supply takes an important role in water resource management. In general, the operators follow the rule curves which are typically designed from the data statistics and the simulation models considering the operating policies.

A series of studies on mathematical optimization methods have been focused on solving reservoir operation problems since the early 1950s (Mao 2016) and continuously focused in recent decades (Lin et al., 2005; Celeste & Billib 2009; Chu et al. 2015; Rosbjerg & Madsen 2009). Especially, the evolutionary algorithms especially GAs have been increasingly used (Chang 2005; Karamouz et al. 2009). Hormwichian et al. (2009) applied a conditional genetic algorithm to determine the optimal rule curves of Lampao reservoir in the Northeast region of Thailand, the minimum average water shortage was selected as the single objective for optimization. Chang (2005) considered water release deficit and hydropower as the multi-purpose for rule curve optimization applying to the Shih-Men reservoir in Taiwan and the results show that the GAs provide an adequate, effective and robust way for searching the rule curves. Different evolution (DE) is an efficient evolutionary algorithm for optimization in various complex problems (Storn, 1996). It has been successfully applied across diverse fields including water resources (Zheng et al. 2015; Zahmatkesh et al. 2015; Guo et al. 2014). GAs have been proved to be efficient for reservoir operation rule curves with both single objective and multi-objective optimization approach, whereas, there was a limited number of studies on using DE for reservoir operation.

A research of using DE for reservoir optimization was found (Regulwar et al. 2010). In this study, the authors applied DE for single objective of maximizing the hydropower production and its results were comparable with those by GA and that was helpful for the decision maker to take decisions regarding operation policy of the reservoir. In order to construct the rule curves or the operation policies, there are generally more than one purposes such as the water shortage, flood, hydropower, etc. to be considered. A number of researchers have addressed this issue by using multi-objective optimization (Yang et al. 2016; Chu et al. 2015; Rosbjerg & Madsen 2009). However, the investigation of differential evolution (Storn & Price 1997) in reservoir operation multi-objective optimization was rarely found.

A typical characteristic of climate in many regions in the world that there are two separate durations of huge precipitation and none or less precipitation which are so-called dry season and flood season in southern Vietnam. Thus, there are two separate durations of releasing and storing water in reservoir operation in these regions. The operation purposes in two mentioned durations of a year are significantly different because of the big difference in amount of water resources and climate condition. Generally, to control flood is the most important purpose to operate in flood season and that in the dry season is adequate water supply. The application of rule curve optimization for these reservoirs, therefore, should be considered in separate duration.

Thac Mo reservoir which separates the Thac Mo sub-basin from the downstream sub-basin of Be River Basin in Vietnam was chosen as the objective area. This basin is very rich in water resources, and the Thac Mo Reservoir has an important role in supplying water for the environment, human activities in the downstream areas and also for hydropower. The existing operation rule curves of this reservoir were established when the reservoir operation was started more than 20 years ago. The rule curves should be optimized to improve the usage of water resources in this catchment.

In this study, a multi-objective optimization using DE was applied to optimize rule curves for Thac Mo reservoir in the dry season. The considered objectives are to minimize the water shortage, to maximize the sum of power production and to improve the power stability.

## 5.2. Methods and materials

### 5.2.1. Optimization of rule curves

The rule curves of Thac Mo reservoir were optimized by using DE in this study. There are two clearly separated seasons, dry season and flood season, in this sub-catchment, and the purposes to be gained by released regulation in each season are different. The optimization for this reservoir rule curves, therefore, should be carried out for two divided durations of a year. In this study, only dry season lasting from the beginning of December to the end of June of the following year is taken into account.

As illustrated in Figure 5.1, there are four piecewise-linear operating rule curves of each of which has 12 inflection points presenting the operating storage level rule values on the first day of each month. However, only two middle curves which show respectively the upper and lower limits of target power production are considered for optimizing in this study. The dry season lasts from the beginning of December to the end of June of the following year. Indeed, there are 8 inflection points of each piecewise-linear which indicate the regulating storage level rule values on the first day of December to that of July are required to be optimized in this study. So, the total number of inflection points is 16, in other words, there are 16 parameters to be optimized to maximize the system performance.

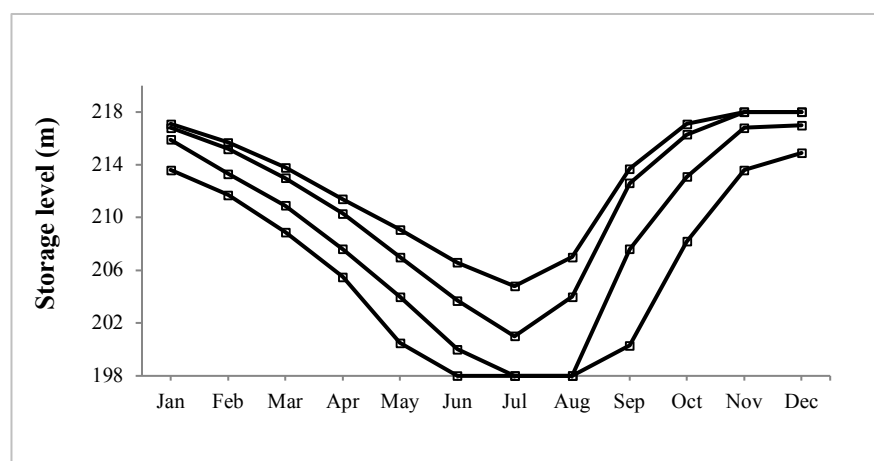


**Fig 5.1.** Existing-Rule of Thac Mo reservoir issued by government

One set of parameters requires constraints that the coordinate values of the upper limit of target power production should exceed its lower limit. On the other hand, all the

values must be within the minimum and the maximum boundary of storage levels. After several trials, the existing rule curves of the upper limit of increasing power production and lower limit of decreasing power production were selected as the maximum and minimum boundaries, respectively. It is because they were able to result in objective convergences with the least numbers of generations in optimizations. The parameters of DE optimization scheme were as follows: population size = 150, crossover probability = 0.2 and scale factor = 0.7, with reference to the previous studies (Storn 1996; Storn & Price 1997; Gämperle *et al.* 2002; Rönkkönen *et al.* 2005) as well as the results of several trials

The purposes for optimizing the rule curves are to minimize water shortage index (*WSI*), maximize total power production (*APP*) and minimize the index of power production stability (*PPS*) which are expressed as follows:

$$WSI = \frac{1}{N} \sum_{i=1}^N \frac{Q_{deficit}^i}{Q_{demand}^i} = \frac{1}{N} \sum_{i=1}^N \frac{Q_{demand}^i - Q^i}{Q_{demand}^i}, Q^i < Q_{demand}^i \quad (5.1)$$

$$APP = \frac{1}{n} \sum_{i=1}^M P_i \times 1000 \times 24; P_i = g \cdot \eta_f \cdot \eta_{tb} \cdot Q^i \cdot H_{head}^i \quad (5.2)$$

$$PPS = \frac{1}{n} \sum_{k=1}^7 \frac{|E_j^k - E_j^a|}{E_j^a} \quad (5.3)$$

where *WSI*, *APP*, *PPS* are respectively the water shortage index, average annual electricity production (kWh) and the electricity production stability index. The  $Q_{deficit}^i$ ,  $Q_{demand}^i$ ,  $Q^i$  are respectively average water deficit (m<sup>3</sup>/s), water demand (m<sup>3</sup>/s) and released discharged of *i*-th day.  $P_i$ ,  $g$ ,  $\eta_f$ ,  $\eta_{tb}$ ,  $Q^i$ ,  $H_{head}^i$  are respectively the average power productivity (MW), gravity (9.81 m/s<sup>2</sup>), electric generator efficiency, turbine efficiency, released discharge through turbine (m<sup>3</sup>/s), average hydraulic head (m) of the *i*-th day.  $n$ ,  $M$ ,  $N$  are the number of year, the number of day of a dry season, the total number of day of dry season of  $n$  year.  $E_j^k$  is the electricity production (kWh) of the  $k$ -th month and  $j$ -th year;  $E_j^a$  is the monthly average electricity production of the  $j$ -th year.

These objectives are typically conflicting with each other: high electricity production requires high hydraulic head and discharge released through a turbine, but this would result in worse electricity production stability and water shortage in the other durations. Therefore, the “trade-off” solutions should be considered. Because of the differences in water resources of every year, it is needed to calculate the power stability every year individually in order to minimize waste in water use.

### 5.2.2. Multi-objective optimization and scenarios for optimization

The multi-objective optimization is usually required in case that several objectives need to be optimized simultaneously. The objectives are, however, often in conflict with each other and are represented by different units. The fitness of the multi-objective system is evaluated by single objective function calculated by transforming and combining several objectives. In multi-objective optimization, there are a number of methods that can transform multi-objectives into single objective (Rosbjerg & Madsen 2009). In this study, the weighting function-based method was applied. By performing single optimizations with different weight combinations, the distribution of Pareto solutions can be explored and the best solution (Pareto optimum) can be found. Besides the contribution weight of each objective, the standardizing all objective into the same unit is required. In this study, the minimum and maximum objective values which are obtained from single objective optimization were used in transforming.

The formulation of transformation and the weight objective function is given as follows:

$$MO = \alpha \frac{WSI_{max} - WSI}{WSI_{max} - WSI_{min}} + \beta \frac{APP - APP_{min}}{APP_{max} - APP_{min}} + (1 - \alpha - \beta) \frac{PPS - PPS_{min}}{PPS_{max} - PPS_{min}}, 0 \leq \alpha + \beta \leq 1 \quad (5.4)$$

where  $MO$  is the multi-objective function;  $\alpha$ ,  $\beta$  are the weight of water shortage and power generation objective, respectively. The weight of produced electricity stability is  $1 - \alpha - \beta$ .  $WSI_{obs}$ ,  $APP_{obs}$ ,  $PPS_{obs}$  are respectively the values of average water shortage, yearly electricity production (kWh) and the average yearly electricity production stability index.

This study designs scenarios for optimization with different weight of objective contribution in multi-objective function. The step of objective weight was 0.2.

### **5.2.3. Data**

The data over the period from 1995 to 2013 used for hydrological simulation was as follow: (i) daily precipitation observed at four rain gauge stations (Phuoc Long, Bu Dop, Bu Nho and DakNong), (ii) monthly meteorological data including temperature, humidity, wind speed, and sunshine hours at Phuoc Long station to estimate evaporation. 1995 – 2013 monthly data of released discharge, electricity production used to calculate the historical obtained values of water shortage, electricity production, and electricity production stability indices which. Only the data of dry season from December to June in the following year was used. The simulation of the duration from December 2010 to Jun 2011 was eliminated in order to avoid the influence of the unusual data of the reservoir storage level in the end of flood season of 2010. In total, 17-year-of-dry-season data was used in this study.

The reservoir rule curve in this study was optimized for effective use of the water for multi purposes during the dry seasons in every year. In fact, the water storage levels reaching at the beginning of the dry seasons, that needs to be identified as the initial condition for simulation, are changed year by year belonging to inflow and outflow during the previous flood season. In this study, the observed storage at the end of November was used as the initial condition of the respective year for simulation.

## **5.3. Results and discussions**

### **5.3.1. Objective correlations and their impacts on the multi-objective optimization**

Different weight values,  $\alpha$ , and  $\beta$ , in Eq. (5.4) were respectively changed from 0 to 1 with the step of 0.2. In total, 21 optimization scenarios were carried out in order to get the trade-off among three objectives mentioned above. When  $\alpha=1$ ,  $\beta=1$  or  $\alpha+\beta=0$ , the multi-objective functions become the single objectives, the water shortage index (*WSI*), the average yearly power production (*APP*), and the average power production stability (*PPS*), respectively.

The real objective indices obtained by 21 optimized scenarios were standardized for forming the multi-objective function as Eq. (5.4) and shown in the three-dimensional scatter as Figure 5.2.

Table 5.1 details the results of optimizations with objective contribution weight sets  $(\alpha, \beta, 1-\alpha-\beta)$ , respectively to the water shortage, average total electricity production, and monthly electricity production stability. The three above single objective indices obtained from the optimized solutions are respectively illustrated in the columns of  $WSI$ ,  $APP$ , and  $PPS$ .  $S-WSI$ ,  $S-APP$ ,  $S-PPS$  and  $MO$  indicate the standardized water shortage, average total electricity production and monthly electricity production stability and multi-objective correspondingly.

**Table 5.1** List of parameters of objective indices obtained from the historical data and the optimized and existing rule curve operations

$\alpha$	$\beta$	$1-\alpha-\beta$	$WSI$	$APP$ ( $10^8$ kWh)	$PPS$	$S-WSI$	$S-APP$	$S-PPS$	$MO$	Distance
0	0	1	0.0057	4.1666	0.8896	0.0221	0.4274	0.0034	0.0034	0.4279
0	0.2	0.8	0.0082	4.2877	0.8895	0.0466	0.1193	0.0033	0.0265	0.1281
0	0.4	0.6	0.0101	4.3040	0.8991	0.0644	0.0778	0.0144	0.0398	0.1021
0	0.6	0.4	0.0169	4.3174	0.9249	0.1308	0.0436	0.0445	0.0440	0.1449
0	0.8	0.2	0.0195	4.3220	0.9479	0.1566	0.0319	0.0713	0.0398	0.1750
0	1	0	0.0647	4.3346	1.7405	0.5986	0.0000	0.9947	0.0000	1.1609
0.2	0	0.8	0.0051	4.1580	0.8897	0.0160	0.4491	0.0035	0.0060	0.4494
0.2	0.2	0.6	0.0070	4.2833	0.8879	0.0348	0.1305	0.0014	0.0339	0.1351
0.2	0.4	0.4	0.0099	4.3040	0.9000	0.0631	0.0779	0.0155	0.0500	0.1014
0.2	0.6	0.2	0.0131	4.3135	0.9204	0.0936	0.0537	0.0393	0.0588	0.1148
0.2	0.8	0	0.0201	4.3281	1.1406	0.1626	0.0163	0.2959	0.0456	0.3380
0.4	0	0.6	0.0048	4.1473	0.8924	0.0133	0.4763	0.0067	0.0093	0.4766
0.4	0.2	0.4	0.0066	4.2828	0.8900	0.0309	0.1316	0.0039	0.0402	0.1352
0.4	0.4	0.2	0.0091	4.3023	0.9009	0.0547	0.0822	0.0166	0.0581	0.1001
0.4	0.6	0	0.0096	4.3089	1.0633	0.0600	0.0654	0.2058	0.0632	0.2241
0.6	0	0.4	0.0041	4.1192	0.8971	0.0056	0.5478	0.0121	0.0082	0.5480
0.6	0.2	0.2	0.0063	4.2803	0.8929	0.0277	0.1380	0.0073	0.0457	0.1409
0.6	0.4	0	0.0077	4.3017	1.3639	0.0408	0.0837	0.5560	0.0580	0.5638
0.8	0	0.2	0.0040	4.1195	0.8987	0.0047	0.5470	0.0140	0.0066	0.5472
0.8	0.2	0	0.0047	4.2727	1.3749	0.0121	0.1575	0.5688	0.0412	0.5904
1	0	0	0.0035	4.1546	1.5296	0.0000	0.4578	0.7491	0	0.8779
Existing rule operation			0.0253	4.1353	1.4706	0.2134	0.5071	0.7067	-	0.8956
Historical operation			0.0734	4.3116	2.1194	0.6836	0.0585	1.4362	-	1.5917

It can be found from the Table 5.1 that there is a clear conflicting performance between the water shortage *WSI* and electricity production *APP*. It is strongly evidenced by the contrast in the better and worse tendency of those indices. The electricity production stability *PPS* obtained from the optimized solutions showed conflicting with the total electricity production objective *APP* and agreeable with the water shortage *WSI* in general although these correlations were less clear than the conflicting between performances of *WSI* and *APP* mentioned above.

From the table data, we can see that the increase in the optimized total electricity production was proportionate to its weight  $\beta$  and it resulted in the worse water shortage and electricity production stability indices at the constant weight  $\alpha$ . When  $\alpha=0$ , the values of average yearly electricity production gained from optimal solutions increased from  $4.167 \times 10^8$  kWh at weight  $\beta=0$  to  $4.335 \times 10^8$  kWh at  $\beta=1$ . The optimized water shortage got worse from approximate 0.006 to 0.065 respectively. Those values for the electricity production stability were from approximate 0.89 to 1.74. It is interesting that there are some cases that the obtained *PPS* of the higher weight  $1-\alpha-\beta$  was higher than that by the lower weight of  $1-\alpha-\beta$  scenario. For example, the value of *WSI* by the scenario  $(\alpha, \beta, 1-\alpha-\beta)=(0, 0, 1)$  was slightly higher than that by the scenario  $(0, 0.2, 0.8)$ . They proved that the weaker contribution of the objective *PPS* in the multi-objective. This can be explained that the water resources were different from year by year. When the potential water was higher than the water required for downstream, the contribution of the power stability objective in multi-objective become stronger. In contrast, the contribution of the power stability objective becomes weak because the required discharge for downstream from this reservoir was insignificantly different month by month.

Making the similar comparisons among optimal solutions with the constant weights of electricity production  $\beta$  and electricity production stability  $1-\alpha-\beta$ , we can see the similar increase or decrease tendencies of three above indices between solutions. The weaker correlations between the electricity production stability with two other objectives can also be realized. The increase and decrease tendencies in *PPS* value were contrary to those in *WSI* and *APP* in some cases. For example, the values of *WSI* and *APP* of the scenario  $(\alpha, \beta) = (0.2, 0.4)$  were lower than those of the scenario  $(\alpha, \beta)=(0.4, 0.4)$ . However, the value of *PPS* of the former solution was higher than that of the latter one.

When satisfying 100% priority of the water for downstream ( $\alpha=1$ ), the obtained water shortage index was about 0.0035, accounting for 18.61 times better than those by using 100% priority ( $\beta=1$ ) of power production, and 1.65 times better than those by 100 priority of power production stability ( $1-\alpha-\beta=1$ ).

The best power production was  $4.3346 \times 10^8$  kWh obtained by using the highest power production priority of  $\beta=1$ . It was around 4.03% higher than the case to prioritize downstream supply ( $\alpha=1$ ) and that of power production stability priority of 100% ( $1-\alpha-\beta=1$ ) in which obtained *APP* was approximately  $4.17 \times 10^8$  kWh and  $4.18 \times 10^8$  kWh.

The best power production stability index obtained among optimal solutions was 0.888. It is interesting that this was not the case of using highest power production stability priority ( $1-\alpha-\beta=1$ ) in optimization but the case of the objective weight set ( $\alpha, \beta, 1-\alpha-\beta$ ) = (0.2, 0.2, 0.6).

It strongly emphasizes that the impact of power production stability objective component in the multi-objective function was weaker than that of two others. The highest impact was water shortage objective when it resulted in the big gaps in obtained values with different weight contribution  $\alpha$ . Moreover, the obtained water shortage index *WSI* is clearly improved by the increase in the weight  $\alpha$ .

### 5.3.2. Trade-off solution

The trade-off performances among solutions can be evaluated by comparing the distances of each solution point to the ideal origin (0, 0, 0). The distance to the origin of coordinates can be observed by the 3-D scatter plot as well in Table 5.1. The smaller value of distance, the more balanced the solution it is. The optimal solution which gave the lowest value of the distance between that point and the origin became the trade-off solution. It can be found from the Table 5.1 that the trade-off solution was achieved at the weight set ( $\alpha, \beta$ ) = (0.4, 0.4) with the distance to the origin in 3D Cartesian coordinates was 0.1001. It is shown by the red circle point in Figure 5.2. The final value of the multi-objective function, *MO*, obtained after 1000 generations by DE using this weight set was 0.0581. The real obtained indices were *WSI*=0.0091 *APP*= $4.3023 \times 10^8$ kWh and *PPS*=0.9009. Interestingly, the multi-objective value *MO* of the trade-off solution was

observed to be greater than those of many other solutions (Table 5.1). Only two obtained values of  $MO$  was found to be greater than that of the trade-off solution. They are 0.0588 obtained by the scenario  $(\alpha, \beta) = (0.2, 0.6)$  and 0.0632 obtained by the scenario  $(\alpha, \beta) = (0.4, 0.6)$  (Table 5.1). Comparing to the obtained distance to the origin of coordinates in case of using single objectives ( $\alpha=1, \beta=1$  or  $\alpha=\beta=0$ ), it was 4.27 times lower than that for using water shortage objective, 11.60 times for using total power production  $APP$  objective and 8.77 times for using power production stability  $PPS$  objective and 3.56 times lower than the average value over all scenario optimal solutions.

The water shortage index obtained from this trade-off solution  $WSI = 0.0091$ , was 7.11 times better than that obtained by using single objective of power production ( $\beta=1$ ). Interestingly, it was 63% worse than that by using single objective of power production ( $\alpha=\beta=0$ ). This again highlights the strong conflicting correlation between the objective of reducing water shortage and increasing the power production.

The power production of the trade-off solution was  $APP=4.3023 \times 10^8$ kWh, accounting for 3.26% and 3.56 % higher than those of the single objective solution at  $\alpha=\beta=0$  and  $\alpha=1$  respectively. It was only 0.75% lower than the single objective solution of power production.

The power production stability was  $PPS=0.9009$ . This value was only 1.26% worse compared to that by using single objective power production stability. However, it was 93.19% and 69.79% better than the values obtained by other single objectives of water shortage and power production.

So, the real objective indices obtained by the trade-off solution were better than the average values over all scenarios. Besides, they were not much different from the best one of each indices among values obtained by all scenarios. However, there were significant differences between those obtained by the trade-of and those from other worst ones.

### 5.3.3. Comparison to the existing rule and the observation

The data derived from the historical operation and the government existing rule curve operation was shown in the two bottom rows of Table 5.1. Their performances were also viewed as the orange-circle point (historical operation) and the green point (existing rule curve operation) in Figure 5.2.

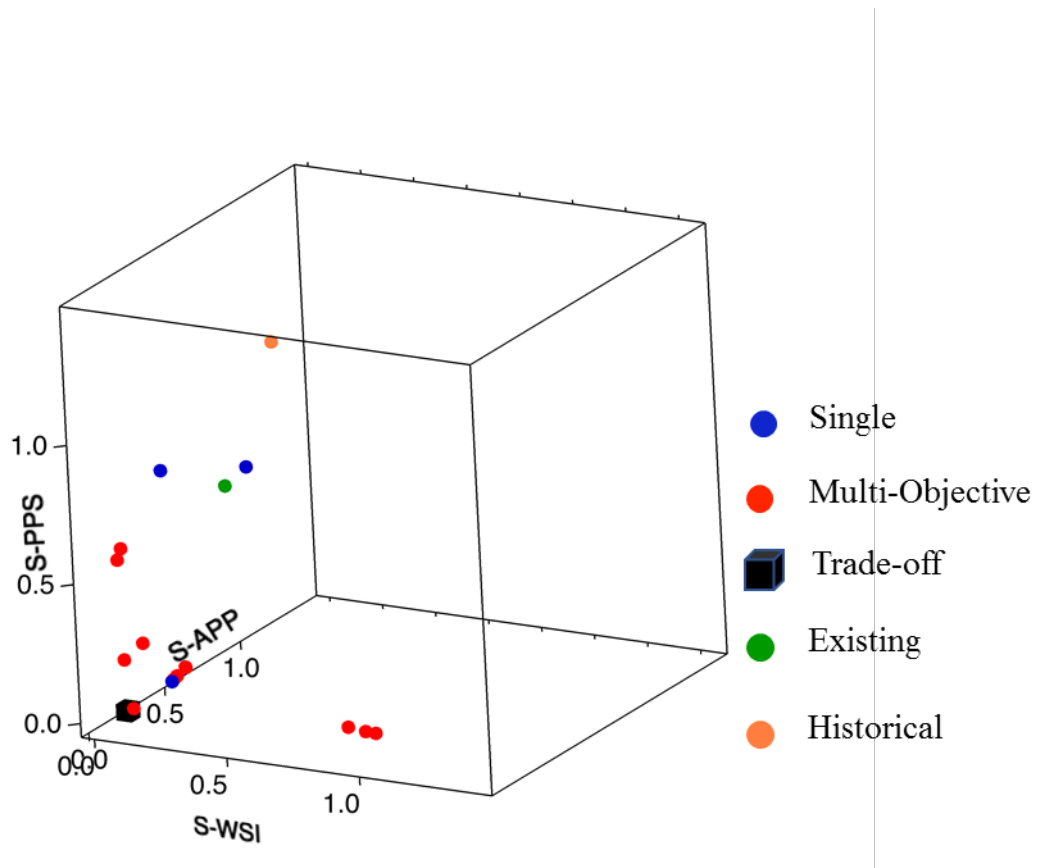


**Fig 5.2** Individual solutions represented by standardized

As shown in Table 5.1, three indices extracted by the observed historical data were 0.0734,  $4.3116 \times 10^8$  kWh/year and 2.1194 for the water shortage, total power production and power production stability respectively. These figures for the existing rule curve operation were 0.0253,  $4.1353 \times 10^8$  kWh/year and 1.4933 respectively. There was a significant difference between two above sets of values. The reason is that the real historical operation relied not only on the water storage level but also on the requirement of national electricity system as well as the contracts of supplying electricity for industry and municipal while the existing government rule relies only on the water level. The average produced power was clearly greater than that expected by the operation

following the government's issued rule curved. However, the water supply and the power production stability indices extracted from the historical data were about 320% and 142% worse than those by the existing rule curve operation, respectively. It demonstrated that the historical operation had focused on the electricity requirement more than the water supply for the downstream in several durations. Even the power production by the existing rule operation was lower than that by the historical one, the existing rule operation indicated more balance than the historical one with the lower distance to the origin.

In order to evaluate the efficiency of the optimized solutions, a comparison was carried out between the optimized solutions and the existing rule operation. The historical data of the reservoir operation was also taken into account for comparison with the optimized ones. It's apparent from the **Figure 5.2** and the Table 5.1 that the optimization scenarios resulted in the better performances compared to those by the historical and the existing operations in general.

It is evident that the distance from the points by the historical operation (the orange point) and by the existing rule curve operation (green point) are significantly greater than those by the optimization scenarios (Figure 5.2). This can also be seen from the Table 5.1. That means all optimization scenarios resulted in the more balanced performances compared to those by the existing rule and the historical operation. The distance from the origin to the solution for the existing rule curve operation and that for the historical operation are 0.8956 and 1.5917, respectively. The results are accounting for approximately 10 and 16 times greater than the value obtained by the trade-off solution. The above value by the existing rule operation was worse than those by all optimal scenarios. That by the historical operation was worse than those by all the optimal scenarios except the scenario of  $\beta=1$  when the obtained distance to the origin was 1.1609. The average distance from the origin to all optimal solutions were about 4.47 and 8.95 times better than those by the historical and the existing rule operation, respectively. The water storage index by the trade-off solution was around 2.79 times and 8.09 times better than those by the existing rule and the historical operations. These figures for the power production stability were 1.66 times and 2.35 times. The power production obtained by the trade-off solution was 3.89% better than that by the existing rule operation but it was

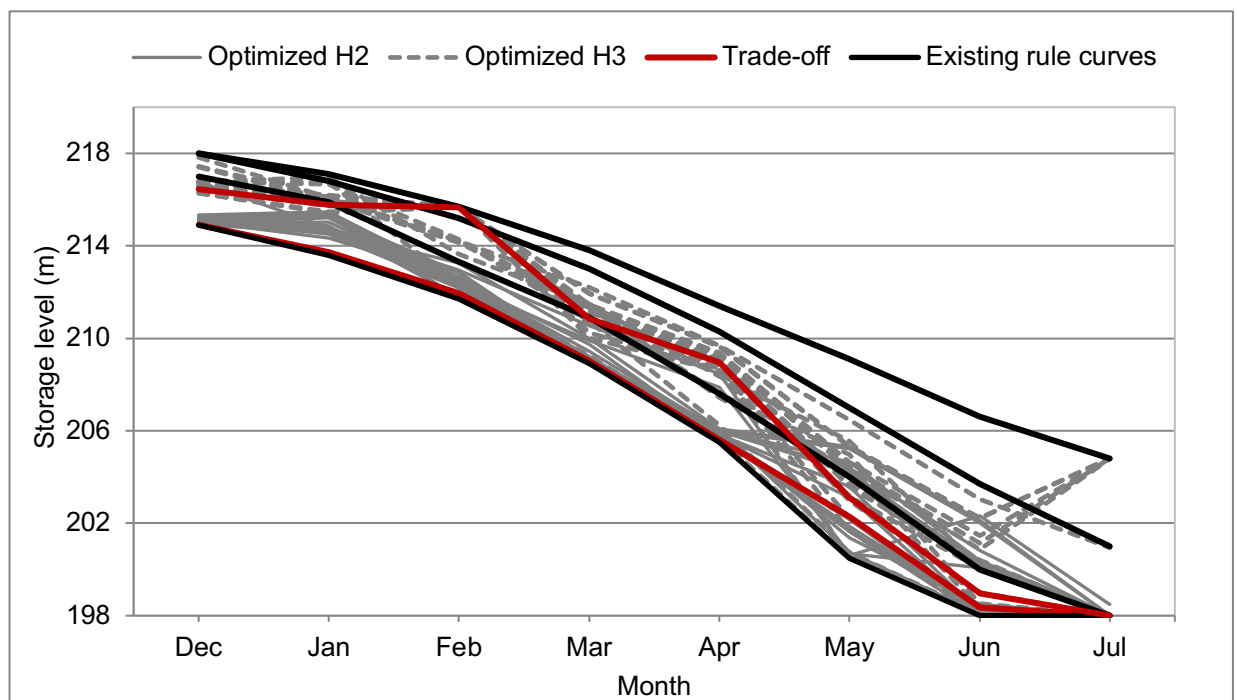
0.22% slightly worse than that by the historical operation. The rather worse power production of the trade-off solution compared to the historical operation arose from the policy to prioritize production of hydropower as discussed above.

Table 5.1 shows that the water shortage index, *WSI*, and the power production stability index, *PPS*, obtained by optimal solutions, which shows the better performances than those by the historical and those by the existing rule curve operations except at the scenarios of  $\beta=1$ . The power production, *APP*, by the existing rule curve operation was worse than the optimal ones in only two cases of  $(\alpha, \beta) = (0.6, 0)$  and  $(\alpha, \beta) = (0.8, 0)$ . It is interesting that the power production by the historical operation was not only significantly greater than that by the government rule curve operation but also mostly higher than those by the optimized solutions except the ones with the more priority in power production such as the scenarios of  $(\alpha, \beta) = (0, 0.6), (0, 0.8), (0, 1), (0.2, 0.6), (0.2, 0.8)$  (Table 5.1). In other words, the performances in water shortage reduction and the power stability could be significantly improved by most all the optimization scenarios, and the total power production could be improved by operations based on the optimized rule curve compared to by that based on the existing rule operation.

Figure 5.3 describes the existing rule curves by the government as well as the optimized rule curves of 21 scenarios. Red lines show the trade-off solutions in which the lower line indicates the lower limit of target power production curve ( $H_2$ ) and the upper line is the upper limit of target power production one ( $H_3$ ). The grey dash lines are the optimized upper limit of target power production curves (optimized  $H_3$ ) and the other solid grey lines are for the optimized lower limit of target power production (optimized  $H_2$ ). It is easy to see that the optimized  $H_2$  line and optimized  $H_3$  line tend to be lower than those of the existing rule. The target power capacity between two lines,  $H_2$  and  $H_3$ , was designed as 55MW. This capacity of the hydropower plant results in the released discharge which is approximate to the required for downstream in the dry season. However, the water storage level of the reservoir was not high enough to satisfy the supplying demand for the downstream if following the existing operation rule in practice. Moreover, when the  $H_3$  became lower the power production would be increased. These are the reasons why the optimal rule curves tend to be lower than the existing ones. As the trade-off solution, the water level seems to gradually decline from beginning of

December to beginning of February and from beginning of June to July while it significantly falls from February to May. It is due to the period from February to April is the driest duration in a year while May is the beginning stage of the rainy season and the precipitation in December and January is not very scarce. The distance between two lines of optimized solution especially the trade-off ones became narrow in the end of the dry season because the rainy season starts from May and the incoming water was higher than the required water for downstream and these optimized of these curved become lower to increase the power production. On the contrary, it was bigger at the beginning of the dry season because the precipitation condition and the initial water storage at the beginning of the dry season were different year by year. Especially, Figure 5.3 clearly shows that the gap between two optimized points of February is wide with the very high water level of the optimized H<sub>3</sub>. This is to reduce to release water to the downstream to save for the following dry duration.

There were some optimized solutions that the water level jumped up between June and July. Those cases were the scenarios that there was no contribution of power production objective in the multi-objective function ( $\beta=0$ ). The release of water in these scenarios mainly satisfied the water supply for downstream to reduce the water shortage index.



**Fig 5.3** Existing and optimized rule curves

## 5.4. Conclusions

This study presents an application of an evolutionary optimization method, DE, using a multi-objective function to optimize the operation rule curves for the Thac Mo Reservoir located in southern Vietnam. Climate condition of the catchment is clearly divided into the dry season and flood season so that reservoir operation should follow the different operation rules with different purposes. This study focused on optimization of reservoir operation in the dry season, and three objectives were optimized, including the water shortage was minimized, the power production was maximized, and the index of stability was minimized for the derivation of optimal rule curves. The performances of optimized and trade-off solutions were analyzed. Findings from this study are summarized as follows:

The objective of reducing the water shortage and that of increasing the total power production were proved to be in conflict each other, and the impact on the decision of the trade-off solution more strongly than the objective of stabilizing power production. The objective of the power production stability conflicts with that of the total power production. Increase in power production stability tends to decrease the water shortage objective, although its correlation is weak.

The optimized solutions resulted in the better-balanced objectives than those by the historical and the existing rule operation in most of all scenarios. Most of the values of the indices of water shortage, *WSI*, annual power production, *APP*, and power production stability, *PPS*, by the operation following the optimized rule curves were better than those by the operations by the historical and the existing rule. It was proved by the result that the distance between the optimized solution and the origin (0, 0, 0) is shorter than that of the historical and that of the existing rule operations. The distance of the solution by the existing rule was shorter than that by the optimized scenario only in one case of  $\beta=1$ . The trade-off solution was about 10 and 16 times better those by the historical and the government existing rule operations. The result emphasized that the multi-objective optimization carried by using DE optimization method can be efficiently applied for finding the better rule curves in the dry season for Thac Mo reservoir operation.

The comparison among the trade-off solutions, historical operating results and existing operation results shows that the historical operation put a higher priority on power production than on the other objectives compared to the existing rule as well as the optimized operations.

The water level of the optimized rule curves tended to be lower than those of the existing ones in order to reduce the water shortage to downstream as a requirement as well as to increase power production in several months with higher precipitation such as December, January, May, June. There were the wide or narrow gaps between the rule curve by the trade-off optimized curve,  $H_2$ , and optimized curve,  $H_3$ . The narrow one in May and June is to use more water to improve the power production because these months have greater precipitation. The wide one is to reduce the water release to downstream to save for the following drought duration.

## CHAPTER VI

# RESERVOIR OPERATION OPTIMIZATION UNDER CLIMATE CHANGE

### 6.1. Introduction

Climate change has been known as one of the greatest environmental threats facing the world today. Especially, it is an important factor influencing hydrometeorological conditions. According to the Intergovernmental Panel on Climate Change (IPCC) Fifth Assessment Report (AR5), the global average combined land and ocean surface temperature data as calculated by a linear trend shows a warming of 0.85°C over the period 1880 to 2012. Extreme precipitation events over wet tropical regions were projected to be very likely become more intense and more frequent. Changes in precipitation and temperature affect the hydrological cycle as well as the water resources in a basin that may lead to challenging on management in the future.

Reservoir is one of the most powerful elements for water resources management. Each reservoir has its operation rule formulated for a long-term duration application. Under climate change, the operation rule should be reset up with considering many objectives such as flood control, hydropower and water supply for adapting to change in water use environment. The improvement of operation rule curves has been investigated in recent decades by many authors (Hejazi *et al.* 2011, Wu *et al.* 2013, Mao *et al.* 2016, Ahmadianfar *et al.* 2016). Many approaches have been developed and applied such as dynamic programming (DP) and non-dominant-sorting genetic algorithm (NSGA II) (Cioffi *et al.* 2012, Yang *et al.* 2016), stochastic dynamic programming (SDP) (Hejazi *et al.* 2011, Raje & Mujumdar 2010), harmony search (HS) and incremental dynamic programming (IDP) (Ho *et al.* 2014).

Recently, GA has been increasingly focused by many researchers as an effective optimization approach. For example, Karamouz *et al.* (2009) applied GA to the Satarkhan reservoir in the north-western part of Iran and demonstrated that the models could be

used as effective tools in reservoir operation optimization. Xie *et al.* (2012) used progressive optimality algorithm (POA) in combination with the GA for establishing the rules power generation dispatching and emphasized the effectiveness and practical applicability of this approach. Kangrang *et al.* (2011) indicated that GA performed well when being applying for Kaeng Loeng Chan reservoir in Thailand. DE was demonstrated to be a good performance in reservoir operation optimization in some studies (Regulwar *et al.* 2010; Eumand and Simonovic 2010). However, the number of investigations on DE was still limited.

Vietnam is one of the most threatened countries by climate change effects involving with both rising in temperature and that in precipitation. The nationally annual average temperature was reported to be increased by 0.62°C during the period 1958-2014, and 0.42°C especially in the period of 1985-2014. The annual precipitation decreased in the Northern areas by 5.8-12.5% in the duration of 57 years from 1985 to 2014. However, rainfall increased by 6.9-19.8% in the south in the same that duration (MONRE 2016). A great number of studies have been investigated on water resources involved with climate change in Vietnam. However, most of these studies have focused on change in streamflow (Khoi & Suetsugi 2012, Thi & Hang, 2015), sediment dynamics (Khoi & Suetsugi 2014; Manh *et al.* 2014), saltwater intrusion (Rasmussen *et al.* 2013). A few studies on reservoir optimization are found. Babel *et al.* (2012) analyzed the impact of alternative scenarios of a hydropower system operation on energy production and natural flow regime in the La Nga river basin in Vietnam by using Range of Variability Approach (RVA). Ho *et al.* (2014) developed hybrid algorithms that are the combination of harmony search (HS) and incremental dynamic programming (IDP) for Huong Dien hydroelectric dam investigation. Ngo *et al.* (2007) applied SCE algorithm to find the trade-off between flood control and hydropower generation for the Hoa Binh reservoir operation in flood seasons and the reservoir level at the beginning of the dry season. Research of DE application on reservoir operation has not been investigated in Vietnam and there are very few studies of considering climate change involved with the reservoir operation.

This study applied DE for optimizing the rule curves considering multi-objectives, that is, to mitigate water shortage, to maximize power production and to stabilize power

production for the operation of Thac Mo reservoir in Vietnam in the releasing duration. The impact of climate change and the adaptive rule effects were analyzed.

## **6.2. Methods and materials**

### **6.2.1. Rainfall-Runoff models**

The Long and Short Terms model (LST model) was applied to simulate the inflow into the reservoir. The description of LST model was presented in chapter III. The model was evaluated and calibrated by DE optimization. The reservoir operating policies are based on the reservoir rule curves and the principles of water balance concept. The daily discharge was simulated by using both LST model and reservoir operation model.

### **6.2.2. Data**

The current (1981-2000) and future (2046-2065) precipitation by GCM as presented in chapter V were used in this study.

As mentioned in chapter V, the initial water storage levels at the beginning of the dry seasons are needed to be identified for simulation. In this study, the initial condition of storage in every year that was  $1291.68 \times 10^6 \text{ m}^3$  were set up considering the frequency of 50% relying on the observation data after eliminating the anomalous data.

### **6.2.3. Optimization and experiments**

The reservoir operation rule curves of the releasing-duration from December to Jun were derived for optimizing multi-objective of reservoir operation problem considering water shortage defined as water shortage index (*WSI*), annual power production (*APP*) and monthly power production stability (*PPS*) by DE. The descriptions of *WSI*, *APP*, *PPS* indices were presented in chapter V

At first, the optimization of the reservoir operation rule curves was respectively carried out under each of all current and future climate scenarios. The following three sets of rule curves were used for simulating dam-operation: (a) existing rule curves designed by the government (Existing Rule), (b) optimized rule curves on the basis of the

current hydrological data simulated by GCM (Current-Optimized-Rule), and (c) specially optimized rule curves for each climate condition simulated by the GCM under the current, RCP2.6, RCP4.5 or RCP8.5 scenario (Scenario-Specialized-Rule). The three sets of optimal rule curves were derived as trade-off solutions by multi-objective optimization. Reservoir operation was simulated under four GCM-simulated climate conditions, that is, under the current condition simulated by GCM (referred to as GCM-Current scenario), under the RCP2.6 scenario, under the RCP4.5, and under the RCP8.5.

Nine sets of objective weight  $(\alpha, \beta)$ , in which  $\alpha$  and  $\beta$  are respectively the contribution weights of water shortage and that of power production, were applied to search trade-off solutions for each climate scenario. They were set as  $(0, 0)$ ,  $(0, 1)$ ,  $(1, 0)$ ,  $(0.2, 0.2)$ ,  $(0.2, 0.4)$ ,  $(0.2, 0.6)$ ,  $(0.4, 0.2)$ ,  $(0.4, 0.4)$ , and  $(0.6, 0.2)$ . The results obtained from trade-off among nine above solutions of each climate scenario were used for analyzing and comparing impacts of climate change on the reservoir operation. On the other hand, the optimized trade-off solution of rule curves by each ensemble of GCM scenario was respectively applied for the reservoir operation simulation. The changes in the future performance were analyzed by comparing to the current performance. For comparison, the government's existing rule (Existing-Rule) was also applied for all climate scenario simulation, and their performances were evaluated. The performances by all three above applied rule cases for current and future scenarios were also evaluated and compared.

### **6.3. Results and discussions**

#### **6.3.1. Comparisons between the applied rules**

Figure 6.1 shows three indices of the reservoir operation results by following each of the three cases of dam-operation-rule under the four climate scenarios. It is evident from the Figure 6.1 that all the objective indices obtained by applying the Scenario-Specialized-Rule were significantly better than those by applying the Existing Rule. Those by using the Current-Optimized-Rule were slightly worse than those by the Scenario-Specialized-Rule.

By using the Existing Rule, the average values of the water shortage index (WSI) over three ensemble experiments, r1i1p1, r2i1p1, and r3i1p1, were respectively estimated as 0.0270 for the GCM-Current, and 0.0256, 0.0233 and 0.0227 respectively for the three future scenarios, RCP2.6, RCP4.5 and RCP8.5. In the case that the Current-Optimized-Rule applied to the current and future climate scenarios, the WSI was estimated to significantly decrease, on average, by 5.43, 3.73, 9.43 and 4.58 times, respectively. These projected indices were 0.0049, 0.0068, 0.0025 and 0.0049 correspondingly. By applying the Scenario-Specialized-Rule, the average values of the WSI were projected to be 0.0049, 0.0043, 0.0041 and 0.0043. There was a significant change compared to those by using the Existing-Rule with the improvement of 5.43, 5.89, 5.68 and 5.33 times and slightly changed compared to those by using the Current-Optimized-Rule of 57.77%, -39.75% and 16.32% for the RCP2.6, RCP4.5 and RCP8.5 scenarios, respectively.

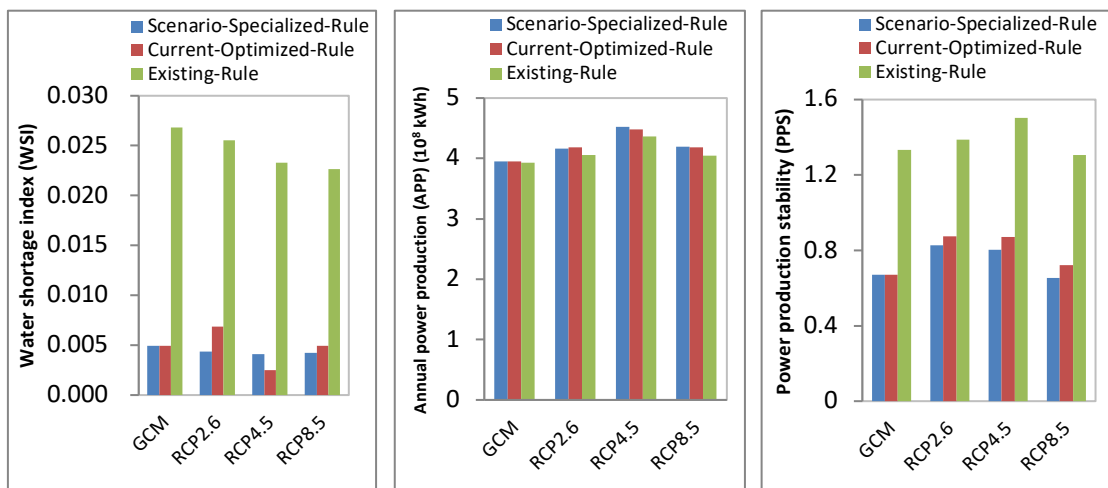


**Fig 6.1** Comparison of the reservoir operation objective indices for different cases of applied rule curves under the current (1981-2000) and future (2046-2065) climate scenarios

The average annual power production (*APP*) in the dry season by applying the Existing Rule were projected to be  $3.93 \times 10^8$  kWh/year,  $4.05 \times 10^8$  kWh/year,  $4.37 \times 10^8$  kWh/year and  $4.05 \times 10^8$  kWh/year for the GCM-Current, RCP2.6, RCP4.5 and RCP8.5 scenarios, respectively. The simulated power production by the Current-Optimized-Rule increased by 0.52%, 3.16%, 2.72% and 3.25% for the four above respective climate scenarios. By applying the Scenario-Specialized-Rule, the increase in these figures was 0.52%, 2.75%, 3.70% and 3.67%.

The average of power production stability (*PPS*) over three ensembles for four climate scenarios was predicted to be 1.3324, 1.3860, 1.5029 and 1.3068 when the

Existing Rule was applied. Those by applying the Current-Optimized-Rule were projected to decrease considerably by 1.99, 1.59, 1.73 and 1.81 times. The decrease by using the Scenario-Specialized-Rule was slightly larger with 1.99, 1.67, 1.87 and 2.0 times.

These above evidence demonstrated that the Scenario-Specialized-Rule was considerably efficient comparing to the Existing-Rule, and slightly better than the Current-Optimized-Rule.

### 6.3.2. Impact of climate change on reservoir operation objectives

Table 6.1. Percentage change in obtained objective indices by future climate scenarios

Ensemble	Operation rule	Water Shortage Index (WSI)			Annual Power Production (APP) (kWh)			Power Production Stability (PPS)			Balance distance		
		RCP2.6	RCP4.5	RCP8.5	RCP2.6	RCP4.5	RCP8.5	RCP2.6	RCP4.5	RCP8.5	RCP2.6	RCP4.5	RCP8.5
r1i1p1	Existing rule	8.07	-11.42	-8.77	-0.01	10.90	4.30	2.04	18.86	-9.04	1.81	-9.76	-13.01
	Current-Optimized-Rule	180.32	-14.72	79.39	-0.76	9.75	3.69	29.40	39.03	-1.48	8.41	-24.85	-12.39
	Scenario-Specialized-Rule	5.34	4.19	-46.69	-1.42	9.98	3.41	26.33	31.26	-9.25	8.47	-27.83	-12.88
r2i1p1	Existing rule	-29.26	-24.51	-33.87	5.64	7.54	5.57	7.57	4.45	3.21	-9.77	-14.30	-12.28
	Current-Optimized-Rule	-28.72	-81.64	-86.86	5.45	7.00	5.67	15.49	-8.09	6.64	-15.91	-24.46	-18.28
	Scenario-Specialized-Rule	7.61	-60.73	-74.48	4.78	8.45	6.13	1.76	-21.12	-13.76	-15.61	-30.02	-21.93
r3i1p1	Existing rule	11.13	-0.50	0.00	3.98	14.93	0.00	2.59	14.88	0.00	-4.91	-9.66	0.00
	Current-Optimized-Rule	-14.37	-49.08	17.93	13.20	24.31	8.67	48.63	63.28	18.85	-34.41	-52.41	-27.00
	Scenario-Specialized-Rule	-45.50	7.19	71.83	13.27	25.90	9.76	45.44	54.50	18.47	-35.82	-57.97	-29.81
Ensemble	Existing rule	-4.62	-13.17	-15.46	3.20	11.12	3.29	4.07	12.73	-1.94	-4.61	-13.30	-8.90
	Current-Optimized-Rule	38.74	-50.04	0.19	5.96	13.68	6.01	31.18	31.41	8.00	-14.90	-39.52	-19.51
	Scenario-Specialized-Rule	-12.06	-17.08	-13.87	5.55	14.78	6.43	24.51	21.55	-1.52	-15.39	-45.47	-22.13

Table 6.1 reports the changes in the objective indices obtained by applying the rule curves for the future (2046-2065) climate scenarios compared to the current (1981-2000) in three cases of the applied rule curves mentioned above. The balance distance in this table shows the three-dimensional distance between the solution point composed of the three objective indices and the origin, where the real values of three objectives were standardized into the same scale and unit. Results of the ensemble average as well as the individual members are presented in Table 6.1. The minus values of the change in water shortage index, WSI, power production stability, PPS, and the balance distance indicate the improvement, and the plus values indicate the deterioration. It is contrary to the

annual power production (*APP*). The smaller value of balance distance shows the better-balanced solution.

It is clear from the Table 6.1 that the water shortage index, *WSI*, and the annual power production, *APP*, of the future scenarios were estimated to be better than those under the current climate conditions simulated by the GCM in almost all cases of applied rule curves. Whereas, the power production stability (*PPS*) was projected to be deteriorated with more number of plus value than that of minus value as shown in Table 6.1.

In overall, the water shortage was predicted to decline if using the Existing-Rule in the future with changes of approximately -4.26%, -13.17% and -15.46% under RCP2.6, RCP4.5, and RCP8.5 scenarios, respectively. If applying the Current-Optimized rule curves to the future GCM climate data, the estimated water shortage was expected to be considerably improved for only RCP4.5 scenarios with the decrease of -50.04%. On the contrary, the remarkable increase in *WSI* value of 38.74% was found under RCP2.6 scenarios by this rule. The average of obtained *WSI* under the RCP8.5 scenario was comparable with 0.19%. If using the Scenario-Specialized-Rule for all climate scenarios, the predicted water shortage index, *WSI*, varied by -12.06%, -17.08% and -13.78% for three above respective future climate scenarios.

The annual power production (*APP*) was expected to increase in the future under all climate scenarios except the RCP2.6 r1i1p1. By using the Existing-Rule curves, the annual power production (*APP*) in the dry season was estimated to increase, on average, by 3.2%, 11.2% and 3.29% for RCP2.6, RCP4.5, and RCP8.5 scenarios, respectively. Those by applying the Current-Optimized rule curves were estimated to be rather higher of 5.96%, 13.68%, and 6.01%. Those by the Scenario-Specialized rule curves were slightly greater of 5.55%, 14.78%, and 6.43%.

It is interesting that the power production stability (*PPS*) in the future was projected to be greater than those at the current. Whereas to the water shortage index and the annual power production, the power stability changes resulted from the optimized rule curves were higher than those from the existing. It is evident that application of the Existing Rule curves resulted in the power production stability change of 4.07%, 12.73%

and -1.94% for three future climate scenarios while those by the Current-Optimized-Rule were 31.18%, 31.41%, and 8.00%, respectively. Those by the Scenario-Specialized-Rule were rather lower than by the Current-Optimized-Rule.

Remarkably, with three projected objective indices achieved under any climate scenario by all three cases of the applied rule curves, the predicted future reservoir operation was balanced better than those under the current scenario. The best results were expected under the RCP4.5 scenarios with a decrease in the balance distance by -13.30%, -39.52% and -45.47% for the Existing-Rule, the Current-Optimized-Rule, and Scenario-Specialized-Rule applications, respectively. The second better results were under the RCP8.5 scenario with the respectively obtained values of -8.90%, -19.51% and -22.13%, while those by RCP2.6 were rather higher of -4.61%, -14.90% and -15.19%.

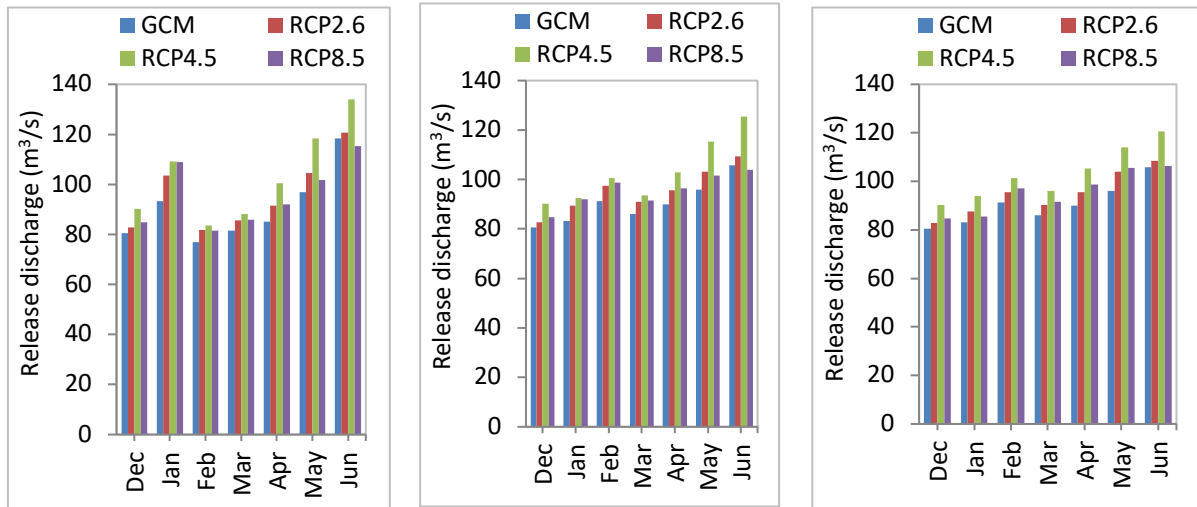
### **6.3.3. Impacts of climate change and optimization on the monthly released discharge control**

Figure 6.2 illustrates the average released discharge over three ensembles under the current and future climate scenarios by different solutions of applied rule curves, including (a) using the Existing-Rule curves, (b) using the Current-Optimized-Rule and applied them to the future scenarios, and (c) the Scenario-Specialized-Rule applied to all climate scenarios.

It is apparent from the figure that the monthly released discharge under the future climate scenarios was projected to be greater than that under the current climate condition simulated by the GCM in all three cases of applied operation rule. It is interesting that the released discharge in June was predicted to be the highest in the all three rule applications.

The RCP4.5 scenario resulted in the greatest released discharge and released discharge change in any months, the RCP8.5 scenario is shown as the second greater, especially in the case of using the Scenario-Specialized-Rule. There was a dramatic increase in released discharge in the late of releasing duration, especially for the RCP4.5 scenario. The predicted increases in this duration varied from 13.0% to 22.44% by the Existing-Rule, from 14.63% to 20.21% by the Current-Optimized-Rule and from 13.97% to 18.83% by the Scenario-Specialized-Rule application. Those in the previous months,

December, January, February, March, April, and May, were 8.24% to 12.08%, 8.73% to 12.08% and 11.12% to 12.97% respectively.



**Fig 6.2** Ensemble average released discharge by different solutions under the current (1981-2000) and future (2046-2065) climate scenarios for different cases of applied rule curves

Change in the monthly released discharge under the RCP2.6 scenario was estimated within the range from 1.92% to 8.07% by the Existing-Rule, 2.75% to 7.60% by the Current-Optimized-Rule, and a bit higher of 2.51% to 8.35% by the Scenario-Specialized-Rule applications. Those under the RCP8.5 scenario were 5.31% to 7.99%, 5.31% to 8.18% and 0.58% to 9.99%. Exceptionally, the change in February by the Existing-Rule under all three future scenarios was high of 10.83%, 19.09%, and 16.72%. Average release discharge in June under the RCP8.5 scenario was predicted to decrease by -2.67% and -1.79% by the Existing-Rule and the Current-Optimized-Rule, respectively.

By using the Existing-Rule curves, the released discharge by the current-GCM scenarios was estimated to vary from 77.0 m<sup>3</sup>/s to 118.5m<sup>3</sup>/s. The average released discharge over the seven months was predicted to be 90.4 m<sup>3</sup>/s. There was a decrease of 5.6% under the RCP2.6 scenario, 14.5% under the RCP4.5 scenario and 5.9% under the RCP8.5 scenario.

By applying the Scenario-Specialized-Rule, the range of obtained average released discharge under the current climate condition simulated by the GCM was smaller than that by applying the Existing Rule which was from 80m<sup>3</sup>/s to 105 m<sup>3</sup>/s. The similar phenomena were found in the results of the future climate scenarios with the clearly

narrower ranges of average monthly discharge. The differences between the lowest and the highest average monthly discharges in the dry season by the Existing-Rule were simulated to be 41.5, 39.1, 50.2 and 38.9 m<sup>3</sup>/s under the current, RCP2.6, RCP4.5 and RCP 8.5 climate scenarios, respectively, while those by the Current-Optimized-Rule were 25.3, 26.6, 35.0 and 19.1 m<sup>3</sup>/s. The increased percentage in average monthly discharge in the future compared to the current by using the Current-Optimized-Rule were 5.7%, 13.9%, 5.8% for the RCP2.6, RCP4.5 and RCP 8.5 climate scenarios, respectively. The average released discharge by this solution was slightly lower than that by the Existing-Rule. The consideration of water shortage and power production stability objectives for optimization in this case was the possible reason for those mentioned phenomena.

There was the insignificant difference between average released discharge by using all Scenario-Specialized-Rule and that by the Current-Optimized-Rule for the future RCP4.5 and RCP8.5 scenarios. Those were increase respectively 14.1% and 5.9% by the Scenario-Specialized-Rule. In contrast, change in the average discharge under the RCP2.6 scenario was estimated as lower as 4.9%. The effect of power production stability in optimization was the possible reason.

Interestingly, the pattern of simulated average monthly discharge by the Current-Optimized-Rule and Scenario-Specialized-Rule tended to increase from beginning to the end of the dry season with the greatest released discharge in June. That was similar to the results by the Existing-Rule except for January when the released discharge was projected to be higher than those in other months. It is because the precipitation depth is not small in January; however, the water level was set to dramatically low in this month in the Existing-rule. It is because of the impact of the consideration of the power production stability and the water shortage which is required to be about 60-65m<sup>3</sup>/s on average in optimization.

#### **6.4. Conclusions**

The objective of this study is to predict climate change impacts on reservoir operation and to evaluate mitigation of the impacts by optimization of reservoir operation rule curves. The efficiency of reservoir operation under current and several future climate scenarios was compared among several rule curves those were optimized for three

indices, water shortage index, annual power production, power production stability, by using multi-objective optimization approach under current and future climate conditions.

The results show that the multi-objective optimization of rule curves was successfully applied under both the current and the future climate scenarios. By applying the rule curves optimized using the current data to the future scenarios, the results were significantly better than those by applying the existing rule curves designed by the government. The results were proved to be slightly better when optimized rule curves are applied to the climate scenario that used for optimization.

The average of total power production in the future was estimated to increase by any applied operation rules while the water shortage was projected to be improved in most cases. The average power production stability was predicted to be better only in the RCP8.5 scenario by the existing rule and the all optimized rules. However, it was estimated that the future scenarios resulted in the better balance solution compared to the current ones with the decrease in the balance distance to the origin of 3-D scatter of standardized objectives.

The outflow to the downstream in the dry season was estimated to increase in the future by all applied operation. However, the optimized solutions were proved to result in slight increases of the average released discharge and significant improvement of the stability of release discharge in dry months.

Among three future climate scenarios, RCP4.5 was expected to result in the best solution of multi-objective reservoir operation with the performance of obtained objective and solution balance as well as the release into the downstream. The second better was suggested to be the RCP8.5 scenarios. These results were appropriate with the precipitation condition in which the RCP4.5 scenario data resulted in the larger amount of inflow into the reservoir than the RCP8.5 and RCP2.6.

## CHAPTER VII

### CONCLUSIONS AND RECOMMENDATIONS

#### 7.1. Conclusion

The objectives of this study were to evaluate the performance of Differential Evolution (DE) application in hydrological studies including rainfall-runoff model calibration and the reservoir operation optimization under current and future climate change condition at Thac Mo reservoir in Be River Catchment of the South Vietnam.

These objectives were achieved as follows:

- (1) Evaluation of the performances of DE in calibration of a rainfall-runoff model, Long-and-Short (LST) Term Runoff Model, by comparing with the performance of the Evolution Strategy (ES) algorithm

Comparison between the performance of DE and that of ES in the rainfall-runoff model calibration showed that both two evolutionary methods were successfully applied for calibrating LST model. It resulted in the simulated runoff closely matched the observed data with NSE approximate to 0.9 at Phuoc Hoa station for both calibration and validation periods. Obtained average of MAE and that of RMSE were 42.8 and 44.4 in calibration by DE. These results were slightly better than those by ES. The results of the best optimized indices and computation time also showed the slightly higher performance of DE in comparison with that of ES.

- (2) Analysis of climate change impact on streamflow and reservoir control of Thac Mo reservoir following historical operation rule

The investigation of effects of precipitation change due to climate change on inflow and reservoir control was carried out on the basis of the current climate conditions and the future climate scenarios, RCP2.6, RCP4.5, and RCP8.5. The LST model calibrated by DE was applied to simulate runoff of Thac Mo catchment. The flow coming into the

reservoir in the future, especially under the scenario RCP4.5, was estimated to dramatically increase in the rainy season. Some considerable increases were also found in dry season. The annual average inflow was projected to rise 6.4%, 18.5%, and 11.7% under the RCP2.6, RCP4.5, and RCP8.5 scenarios, respectively. The increases of inflow in several flood season months were predicted to increase up to 11.8% for the RCP2.6, 44.5% for RCP4.5 and 27% for RCP8.5. The raises in inflow, the water storage, release for hydropower and that through spillway were projected to change remarkably especially in flood season.

### (3) Evaluation of the performance of DE in reservoir operation optimization for Thac Mo reservoir

The performance of DE for optimizing Thac Mo reservoir operation was evaluated by using multi-objective including water shortage index (*WSI*), annual power production (*APP*) and power production stability (*PPS*) to optimize the rule curves in the dry season for the data period of 1995-2013. The optimized solutions resulted in the better-balanced objectives than those by the historical and the existing rule operation. The distance between trade-off solution and the origin (0, 0, 0) of the 3-D scatter of three standardized objectives was estimated to be 10 and 16 times shorter than those by the historical and the government existing rule operations. The individual objectives of optimized solutions were also found to be better than those by the existing and the historical operations. The improvements in the *WSI*, annual *PPS* of the trade-off compared to those by the existing-rule operation were estimated to be 178%, 3.88%, and 65.75% respectively. Those of the trade-off compared to the historical were 706%, -0.2% and 135%. The minus value of the difference in power production indicates the higher priority on power production.

### (4) Optimal operation rules under climate change conditions and its comparison with the current rule

DE application for reservoir operation optimization was successfully applied not only for the real current data as mentioned above but also for simulated data by GCM under current and future scenarios. Three cases of operation rule were used in reservoir balance model simulations. They are (a) existing rule curves designed by the government (Existing Rule), (b) optimized rule curves on the basis of the current hydrological data

simulated by GCM (Current-Optimized-Rule), and (c) specially optimized rule curves for each climate condition simulated by the GCM under current, RCP2.6, RCP4.5 or RCP8.5 scenarios (Scenario-Specialized-Rule). The results showed that the performance by the Scenario-Specialized-Rule was significantly better than that by the Existing Rule and slightly better than that of the Current-Optimized-Rule.

Under different climate conditions, the water shortage index (*WSI*) was estimated to change by -4.26%, -13.17% and -15.46% under RCP2.6, RCP4.5, and RCP8.5 scenarios, respectively. Those values were 38.74%, -50.04%, 0.19% by the Current-Optimized-rule and -12.06%, -17.08%, -13.78% by the Scenario-Specialized-Rule. The change in annual power production (*APP*) by the Existing-rule under three above climate scenarios were projected to be 3.2%, 11.2%, and 3.29%. Those were 5.96%, 13.68% and 6.01% by the Current-Optimized Rule and 5.55%, 14.78% and 6.43% by the Scenario-Specialized-Rule. Regarding power production stability (*PPS*), there were changes of 4.07%, 12.73% and -1.94% under the RCP2.6, RCP4.5, and RCP8.5 scenarios, respectively. Those by the Current-Optimized-Rule were 31.18%, 31.41%, and 8.00%, respectively. The RCP4.5 scenario resulted in the greatest change in the balance distance by -13.30%, -39.52% and -45.47% for the Existing-Rule, Current-Optimized-Rule, and Scenario-Specialized-Rule applications, respectively. The second better results were under RCP8.5. The release discharge to downstream was estimated to increase in dry season under future climate conditions especially by RCP4.5 scenario. The release stability was estimated to be improved under the Current-Optimized-Rule and Scenario-Specialized-Rule because of the consideration of water shortage index (*WSI*) and power production stability (*PPS*) in optimization.

The results of this study proved the efficiency of DE application for LST model calibration and for Thac Mo reservoir operation optimization for dry season simulation. These findings will contribute to the basic studies on applying DE in calibration of the other rainfall-runoff models of other catchments in Vietnam or around the world. Besides, the study helps to enhance the understanding of the impacts of climate change on inflow into the reservoir as well as reservoir control. The simulations using existing and optimized reservoir operation rules for the current and future climate conditions also gave the better understanding about the effect of DE optimization for the adaptive reservoir

operation rules for the future as well as figured out the future change in performances under the different existing rule and optimized rules.

## **7.2. Limitation and recommendation for future works**

The performances of DE in calibration of the LST model were compared with only ES technique. The comparison with other evolutionary methods such as genetic algorithm (GA), shuffled complex evolution (SCE-UA) would improve the evaluation of DE among evolutionary algorithms. For optimization of reservoir operation, the performance of DE needs to be compared with those of the other optimization technique.

The optimization for reservoir operation was carried out for the dry season. In future work, the optimization for flood season will be also investigated. Additionally, the available data in this study on specifically practical operation aims of Thac Mo reservoir such as produced electricity demand, practical operation rule was limited. The results of the study would be more helpful in practice if more data are collected. In this study, only two curves among four curves of operation rule were considered to be improved. The studies for improving all four curves will be considered to be investigated.

Moreover, only three future climate scenarios, RCP2.6, RCP.4.5 and RCP8.5 the duration 2046-2065 were used in this study. More investigations should be performed for further durations and scenarios.

## REFERENCES

- Afshar A, Shafii M, Bozorg Haddad O (2011) Optimizing multi-reservoir operating rules: an improved HBMO approach. *J Hydroinform* 13(1):121–139.
- Ahmadi M, Bozorg Haddad O, Loáiciga HA (2014a) Adaptive reservoir operating rules under climatic change. *Water Resour Manag* 29(4):1247–1266.
- Ahmadi M, Bozorg Haddad O, Mariño MA (2014b) Extraction of flexible multi-objective real-time reservoir operating rules. *Water Resour Manag* 28(1):131–147.
- Ahmadianfar I, Adib A, Taghian M (2016) Optimization of multi-reservoir operation with a new hedging rule: application of fuzzy set theory and NSGA-II. *Appl Water Sci* 7(6):3075–3086.
- Amjady N, Soleymanpour HR (2010) Daily hydrothermal generation scheduling by a new modified adaptive particle swarm optimization technique. *Electr Pow Syst Res* 80(6):723–732.
- Beyene T, Lettenmaier DP, Kabat P (2010) Hydrologic impacts of climate change on the Nile River basin: implications of the 2007 IPCC scenarios. *Climate Change* 100(3-4):433–461.
- Babel MS *et al.* (2012) Operation of a hydropower system considering environmental flow requirements: A case study in La Nga river basin, Vietnam. *J Hydro-environ Res* 6(1):63–73.
- Beyer H, Schwefel H (2002) Evolution strategies—A comprehensive introduction. *Nat. Comput* 1(1):3–52.
- Brekke LD, Maurer EP, Anderson JD, Dettinger MD, Townsley ES, Harrison A, et al. (2009) Assessing reservoir operations risk under climate change. *Water Resour Res* 45:W04411.
- Chakraborty UK (2008) *Advances in Differential Evolution*. Springer, Berlin.
- Chang FJ, Chen L, Chang LC (2005) Optimizing the reservoir operating rule curves by genetic algorithms. *Hydrol Process* 19(11):2277–2289.

- Chang LC, Chang FJ (2009) Multi-objective evolutionary algorithm for operating parallel reservoir system. *J Hydrol* 377(1):12–20.
- Chau KW (2007) A split-step particle swarm optimization algorithm in river stage forecasting. *J Hydrol* 346(3–4):131–135.
- Chen T, Hsu Y (2006) A multiobjective optimization solver using rank-niche evolution strategy. *Adv Eng Softw* 37(10):684–699.
- Chen L, McPhee J, Yeh WWG (2007) A diversified multiobjective GA for optimizing reservoir rule curves. *Adv Water Resour* 30(5):1082–1093.
- Chu JG *et al.* (2015) Improving multi-objective reservoir operation optimization with sensitivity-informed problem decomposition. *Hydrol Earth Syst Sci* 12(4): 3719–3752.
- Celeste AB, Billib M (2009) Evaluation of stochastic reservoir operation optimization models. *Adv Water Resour* 32(9):1429–1443.
- Castelletti A *et al.* (2012) Assessing water reservoirs management and development in northern Vietnam. *Hydrol Earth Syst Sci* 16(1):189–199.
- Cioffi F, Gallerano F (2012) Multi-objective analysis of dam release flows in rivers downstream from hydropower reservoirs. *Appl Math Modell* 36(7):2868–2889.
- Cohen W, Ollington R & Ling F (2013) Hydrologic Model Parameter Optimisation. *International Congress on Modelling and Simulation* pp1–6.
- CMIP5 data analysis system (n. d.) <http://apps.diasjp.net/modelvis/cmip5/> (accessed on November 15, 2018).
- Conway D (2005) From headwater tributaries to international river: observing and adapting to climate variability and change in the Nile basin. *Global Environmental Change* 15 (2):99–114.
- Dang TH *et al.* (2010) Long-term monitoring (1960–2008) of the river-sediment transport in the Red River Watershed (Vietnam): Temporal variability and dam-reservoir impact. *Sci Total Environ* 408(20):4654–4664.
- Data Integration and Analysis System (DIAS) (n. d.), <http://www.diasjp.net/en/> (accessed on November 15, 2018).

- Dawson CW, Abrahart RJ, See LM (2007) HydroTest: A web-based toolbox of evaluation metrics for the standardised assessment of hydrological forecasts. *Environ Model Softw* 22(7):1034–1052.
- DHI, 2005b, MIKE 11 – A modelling system for Rivers and Channels. DHI Software 2005, DHI Water and Environment, Hørsholm, Denmark.
- Duan Q, Sorooshian S and Gupta HV (1992) Effective and efficient global optimization for conceptual rainfall-runoff models. *Water Resour Res* 28(4):1015–1031.
- Duan Q, Sorooshian S and Gupta HV (1994) Optimal use of the SCE-UA global optimization method for calibrating watershed models. *J Hydrol* 158(3–4):265–284.
- Eiben AE, Smith JE (2003) *Introduction to Evolutionary Computing*. Springer, Berlin.
- Eum HI, Simonovic SP (2010) Integrated reservoir management system for adaptation to climate change: the Nakdong River Basin in Korea. *Water Resour Manag* 24(13):3397–3417.
- Fallah-Mehdipour E, Bozorg Haddad O, Rezapour Tabari MM, Mariño MA (2012) Extraction of decision alternatives in construction management projects: Application and adaptation of NSGA-II and MOPSO. *Expert Syst Appl* 39(3):2794–2803.
- Fill HD et al. (2013) Impact of climate change on hydropower production within the La Plata Basin. *International Journal of River Basin Management* 11(4):449–462.
- Fujihara Y, Tanakamaru H, Tada A, Hata T (2003) Calibration of rainfall-runoff models using the evolution strategy. *Proc 1st Int Conf Hydrology and Water Resources in Asia Pacific Region, Kyoto*, pp 885–890.
- Fujihara Y, Oda M, Horikawa N, Ogura C (2011) Hydrologic Analysis of Rainfed Rice Areas Using a Simple Semi-distributed Water Balance Model. *Water Resour Manag* 25(9):2061–2080.
- Gämperle R, Müller SD, Koumoutsakos P (2002) A parameter study for differential evolution. In: Grmela A, Mastorakis N (ed) *Advances in Intelligent Systems, Fuzzy Systems, Evolutionary Computation*. WSEAS Press, pp 293–298.

- Gill M K, Kaheil YH, Khalil A, McKee M, & Bastidas L (2006) Multiobjective particle swarm optimization for parameter estimation in hydrology. *Water Resour Res* 42(7) <http://dx.doi.org/10.1029/2005WR004528>.
- Glotić A, Zamuda A (2015) Short-term combined economic and emission hydrothermal optimization by surrogate differential evolution. *Appl Energy* 141:42–56.
- GoyalMK, Ojha CSP, Singh RD, Swamee PK, Nema RK (2013) Application of ANN, fuzzy logic and decision tree algorithms for the development of reservoir operating rules. *Water Resour Manag* 27(3):911–925.
- Gupta HV, Sorooshian S, and Yapo PO (1998) Toward improved calibration of hydrologic models; multiple and noncommensurable measures of information. *Water Resour Res* 34(4):751–763.
- Guo J, Zhou J, Lu J, Zou Q, Zhang H, Bi S (2014) Multi-objective optimization of empirical hydrological model for streamflow prediction. *J Hydrol* 511: 242–253.
- Hatanaka T, Uosaki K, Tanaka H, Yamada Y (1996) System parameter estimation by evolutionary strategy, *Proc. 35th SICE Annu Conf International Session Papers*, pp 1045–1048.
- Hejazi MI & Cai X (2011) Building more realistic reservoir optimization models using data mining - A case study of Shelbyville Reservoir. *Adv Water Resour* 34(6):701–717.
- Hien LT, Quy PN & Viet NT (2010) Assessment of Salinity Intrusion in the Red River under the Effect of Climate Change. *Journal of Civil Engineering and Architecture* 4(6):1–6.
- Ho VH, Kougias I & Kim JH (2014) Reservoir Operation using hybrid optimization algorithms. *Global NEST Journal* 17(1):1–15.
- Holland JH (1975) *Adaptation in Natural and Artificial Systems*. University of Michigan Press, Ann Arbor.
- Hormwichian R, Kangrang A. & Lamom A (2009). A conditional genetic algorithm model for searching optimal reservoir rule curves. *Journal of Applied Sciences* 9(19):3575–3580.

- IPCC (2014): Climate Change 2014: The Physical Science Basis. Contribution of Working Group I to the Fifth Assessment Report of the Intergovernmental Panel on Climate Change [Stocker T.F., D. Qin, G.-K. Plattner, M. Tignor, S.K. Allen, J. Boschung, A. Nauels, Y. Xia, V. Bex and P.M. Midgley (eds.)]. Cambridge University Press, Cambridge, United Kingdom and New York, NY, USA, 1535 pp.
- Japan Space System: ASTER Global Digital Elevation Model (GDEM), <http://gdem.ersdac.jspacsystems.or.jp/search.jsp> (accessed on November 17, 2015).
- Jiang Y, Hu TS, Huang CC, & Wu XN (2007) An improved particle swarm optimization algorithm. *Appl Math Comput* 193(1):231–239.
- Jiang Y, Liu CM, Huang CC, & Wu XN (2010) Improved particle swarm algorithm for hydrological parameter optimization. *Appl Math Comput* 217(7):3207–3215.
- Jiang Y, Li X & Huang C (2013) Automatic calibration a hydrological model using a master-slave swarms shuffling evolution algorithm based on self-adaptive particle swarm optimization. *Expert Syst Appl* 40(2):752–757.
- Kadoya M, Tanakamaru H (1989) Long-and-Short-term Runoff Model and its application to real-time flood forecasting. *Proc. Pacific International Seminar on Water Resources System, Tomamu*, pp 669–682.
- Kangrang A, Lehner A & Mayrhofer P (2011) An Improvement of Small Reservoir Rule Curves using Genetic Algorithms and Water Balance Equation. *Aust J Basic Appl Sci* 5(12):707–714.
- Karamouz M, Ahmadi A & Moridi A (2009) Probabilistic reservoir operation using Bayesian stochastic model and support vector machine. *Adv Water Resour* 32(11):1588–1600.
- Kennedy J, & Eberhart RC (1995) Particle swarm optimization. *Proceedings of IEEE international conference on neural networks* 4:1942–1948.
- Kim T, Heo JH, Jeong CS (2006) Multi-reservoir system optimization in the Hanjiang basin using multi-objective genetic algorithms. *Hydrol Process* 20(9):2057–2075.

- Kraue T, Cullmann J, Saile P & Schmitz GH (2011) Robust multi-objective calibration strategies-chances for improving flood forecasting. *Hydrol Earth Syst Sc Discussions* 8:3693–3741.
- Kumar ARS, Sudheer KP, Jain SK & Agarwal PK (2005) Rainfall-runoff modelling using artificial neural networks: Comparison of network types. *Hydrol Process* 19(6):1277–1291.
- Kuok KK, Harun S & Shamsuddin SM (2010) Particle swarm optimization feedforward neural network for modeling runoff. *Int J Environ Sci Technol* 7(1):67–78.
- Khoi DN, Suetsugi T (2012) Uncertainty in climate change impacts on streamflow in Be River Catchment, Vietnam. *Water and Environment Journal* 26(4):530–539.
- Khoi DN, Suetsugi T (2013) Assessment of climate change impacts on hydrology and sediment yield in the Be River Catchment, Vietnam. *Journal of Japan Society Civil Engineers* 69(4):31-36.
- Khoi DN, Suetsugi T (2014) The responses of hydrological processes and sediment yield to land-use and climate change in the Be River Catchment, Vietnam. *Hydrol Process* 28(3):640–652.
- Kişi Ö (2010) River suspended sediment concentration modeling using a neural differential evolution approach. *J Hydrol* 389(1-2):227–235.
- Labadie J (2004) Optimal operation of multi-reservoir systems: state-of-the-art review. *J Water Resour Plan Manag* 130(2):93–111.
- Le TPQ et al. (2007) The changing flow regime and sediment load of the Red River, Viet Nam. *J Hydrol* 334(1-2):199–214.
- Li L, Xu H, Chen X, Simonovic SP (2009) Streamflow forecast and reservoir operation performance assessment under climate change. *Water Resour Manage* 24:83 <https://doi.org/10.1007/s11269-009-9438-x>
- Lin S, Wu R & Chen S (2005). Study On Optimal Operating Rule Curves Including Hydropower Purpose in Parallel Multireservoir Systems. *Third International Conference on River* 83(1982):151–160.

- Liu Y, Khu ST, Savic D (2004) A Hybrid Optimization Method of Multi-objective Genetic Algorithm (MOGA) and K-Nearest Neighbor (KNN) Classifier for Hydrological Model Calibration. In: Yang ZR, Yin H, Everson RM. (eds) Intelligent Data Engineering and Automated Learning – IDEAL 2004. IDEAL 2004. Lecture Notes in Computer Science, vol 3177. Springer, Berlin, Heidelberg.
- Liu C, Wang ZG, Zheng HX, Zhang L, & Wu XF (2008) Development and application of HIMS system. *Science in China (E)* 38(3):350–360.
- Liu Y (2009) Automatic calibration of a rainfall-runoff model using a fast and elitist multi-objective particle swarm algorithm. *Expert Syst Appl* 36(5):9533–9538.
- Cruz LL, Willigenburg LGV, Straten GV (2003) Efficient Differential Evolution Algorithms for Multimodal Optimal Control Problems. *Appl Soft Comput* 3(2):97-122.
- Lu S, Sun C, & Lu Z (2010) An improved quantum-behaved particle swarm optimization method for short-term combined economic emission hydrothermal scheduling. *Energ Convers Manage* 51(3):561–571.
- López-Moreno JI et al. (2013) Impact of climate and land use change on water availability and reservoir management: Scenarios in the Upper Aragón River, Spanish Pyrenees. *Sci Total Environ* 493:1222–1231.
- Mao J et al. (2016) Optimal operation of a multi-reservoir system for environmental water demand of a river-connected lake. *Hydrol Res* 48(6):206–224.
- Madsen H (2000) Automatic calibration of a conceptual rainfall-runoff model using multiple objectives. *J Hydrol* 235(3-4):276–288.
- Mandal KK, Basu M, & Chakraborty N (2008) Particle swarm optimization technique based short-term hydrothermal scheduling. *Appl Soft Comput* 8(4):1392–1399.
- MONRE - Ministry of Natural Resources and Environment (2016) Climate change, sea level rise scenarios for Vietnam. The publisher of environmental resources and maps of Vietnam

- Moriasi DN, Arnold JG, Van Liew MW, Bingner RL, Harmel RD and Veith TL (2007) Model evaluation guidelines for systematic quantification of accuracy in watershed simulations, *Transactions of the ASABE* 50:885-900.
- Ndiritu JG, Africa S & Daniell TM (2001) An Improved Genetic Algorithm for Rainfall-Runoff Model Calibration and Function Optimization. *Math Comput Model* 33 (6-7):696–706.
- Oliveira R, Loucks DP (1997) Operating rules for multi-reservoir systems. *Water Resour Res* 33(4):839–852.
- Nash JE, Sutcliffe JV (1970) River flow forecasting through conceptual models: Part 1. A discussion of principles. *J Hydrol* 10(3): 282–290.
- Ngo LL, Madsen H & Rosbjerg D (2007) Simulation and optimisation modelling approach for operation of the Hoa Binh reservoir, Vietnam. *J Hydrol* 336(3-4):269–281.
- Ngoc TA, Hiramatsu K & Harada M (2013) Optimizing parameters for two conceptual hydrological models using a genetic Algorithm: A case study in the Dau Tieng River Watershed, Vietnam. *Japan Agricultural Research Quarterly (JARQ)* 47(1):85–96.
- Niu J, Zhong W, Liang Y, Luo N, Qian F (2015) Fruit fly optimization algorithm based on differential evolution and its application on gasification process operation optimization. *Knowl-based Syst* 88: 253–263.
- Olofintoye O, Adeyemo J, Otieno F (2013) Evolutionary Algorithms and Water Resources Optimization. In: Schütze O. et al. (eds) *EVOLVE - A Bridge between Probability, Set Oriented Numerics, and Evolutionary Computation II*. *Advances in Intelligent Systems and Computing*, vol 175. Springer, Berlin, Heidelberg.
- Pang H, Zhang Q, Wang W, Wang J, Li J et al. (2013) Calibration of three-axis magnetometers with differential evolution algorithm. *J Magn Magn Mater* 346:5–10.
- Perazzoli M, Pinheiro A. & Kaufmann V (2013) Assessing the impact of climate change scenarios on water resources in southern Brazil. *Hydrological Sciences Journal*, 58(1):77–87.

- QGIS Development Team (2015), QGIS Geographic Information System. Open Source Geospatial Foundation Project. <http://qgis.osgeo.org> (accessed on November 17, 2015).
- Price K, Storn R, Lampinen JA (2005) *Differential Evolution: A Practical Approach to Global Optimization*. Springer, Berlin.
- Rasmussen, P. et al., 2013. Assessing impacts of climate change, sea level rise, and drainage canals on saltwater intrusion to coastal aquifer. *Hydrol Earth Syst Sc* 17(1):421–443.
- Rechenberg I (1971) *Evolution strategies: Optimierung technischer Systeme nach Prinzipien der biologischen Evolution*. Dissertation, Technical University of Berlin.
- Reddy MJ and Kumar DN (2007) Multiobjective Differential Evolution with Application to Reservoir System Optimization. *J Civ Eng Manag* 21(2):136-146.
- Regulwar DG, Choudhari S & Raj PA (2010) Differential Evolution Algorithm with Application to Optimal Operation of Multipurpose Reservoir. *Journal of Water Resource and Protection (JWARP)* 2(6):560–568.
- Rosbjerg D, Ngo LL & Madsen H (2009) Optimisation of Hydropower in a Multi-Objective Context. International Conference "Water, Environment, Energy and Society", pp 1543-1553.
- Ronkkonen J, Kukkonen S, Price KV (2005) Real-parameter optimization with differential evolution, *Proc. IEEE CEC*, Edinburgh, 1: pp 506–513.
- Schaefli B (2015) *Projecting hydropower production under future climates: a guide for decision-makers and modelers to interpret and design climate change impact assessments*. Wiley Interdiscip Rev Water.
- Shokri A, Bozorg Haddad O, Mariño MA (2013) Algorithm for increasing the speed of evolutionary optimization and its accuracy in multi-objective problems. *Water Resour Manag* 27(7):2231–2249.
- Storn R (1996) On the usage of differential evolution for function optimization. *NAFIPS'1996*, pp 519–523.

- Storn R, Price K (1997) Differential evolution—A simple and efficient heuristic for global optimization over continuous spaces. *J Global Optim* 11(4):341–359.
- Sugawara M (1995) Tank model. In: V.P. Singh (ed) *Computer Models of Watershed Hydrology*. WRP, Baton Rouge, LA, pp 165–214.
- Tang Y, Reed P, and Wagener T (2006) How effective and efficient are multiobjective evolutionary algorithms at hydrologic model calibration? *Hydrol Earth Syst Sci* 10(2):289–307.
- Vasan and Raju KS (2004) Optimal Reservoir Operation Using Differential Evolution. *International Conference on Hydraulic Engineering: Research and Practice (ICON-HERP-2004)*, Indian Institute of Technology Roorkee, India.
- Vietnamese Government (2014): Decision on the issue of reservoir operation procedures for flood control in Dong Nai River Basin (Decision 1982/QD-TTg).
- Vrugt JA, Gupta HV, Bastidas LA, Bouten W, Sorooshian S (2003) Effective and efficient algorithm for multiobjective optimization of hydrologic models. *Water Resour Res* 39(8): 1–19.
- Vu VN, Nguyen HA (2015) Assessment of the Water Transfer Capacity from Be River Basin through Phuoc Hoa Hydraulic-Works. *CLEAN - Soil, Air, Water*, 43(5):645–651.
- Vu MT, Vo ND, Gourbesville P, Raghavan SV & Liong SY (2017) Hydro-meteorological drought assessment under climate change impact over the Vu Gia–Thu Bon river basin, Vietnam. *Hydrological Sciences Journal* 62(10).
- Wang QJ (1991) The genetic algorithm and its application to calibrating conceptual rainfall-runoff models. *Water Resour Res* 27(9):2467–2471.
- Wardlaw R, Sharif M (1999) Evaluation of genetic algorithms for optimal reservoir system operation. *J Water Res Plan Man* 125(1):25–33.
- Wu Y & Chen J (2013) Estimating irrigation water demand using an improved method and optimizing reservoir operation for water supply and hydropower generation: A case study of the Xinfengjiang reservoir in southern China. *Agric Water Manag* 116:110–121.

- Xie W et al. (2012) Short-term power generation scheduling rules for cascade hydropower stations based on hybrid algorithm. *Water Science and Engineering* 5(1):46–58.
- Yang G et al. (2016) Multi-Objective Operating Rules for Danjiangkou Reservoir Under Climate Change. *Water Resour Manag* 30(3):1183–1202.
- Yeh WWG (1985) Reservoir management and operations models: A state of the art review. *Water Resour Res* 21(12):1797–1818.
- Zahmatkesh Z, Karamouz M, Nazif S (2015) Uncertainty based modeling of rainfall-runoff: Combined differential evolution adaptive Metropolis (DREAM) and K-means clustering. *Adv Water Resour* 83:405–420.
- Zhang C, Wang R, Meng Q (2015) Calibration of conceptual rainfall-runoff models using global optimization. *Adv Meteorol*. doi:10.1155/2015/545376.
- Zhao C, Xu Q, Lin S, Li X (2013) Hybrid differential evolution for estimation of kinetic parameters for biochemical systems. *Chin J Chem Eng* 21(2): 155–162.
- Zhao T, Cai X & Yang D (2011) Effect of streamflow forecast uncertainty on real-time reservoir operation. *Adv Water Resour* 34(4):495–504.
- Zheng F, Zecchin A, Simpson A (2015) Investigating the run-time searching behavior of the differential evolution algorithm applied to water distribution system optimization. *Environ Model Softw* 69:292–307.
- Zhong J, Cai W (2015) Differential evolution with sensitivity analysis and the Powell's method for crowd model calibration. *J Comput Sci* 9:26–32.
- Zhou YL, Guo SL (2013) Incorporating ecological requirement into multipurpose reservoir operating rule curves for adaptation to climate change. *J Hydrol* 498:153–164.
- Zhang JY, Wang GQ, He RM, Liu CS (2009). Variation trends of runoffs in the Middle YellowRiver basin and its response to climate change. *Adv Water Sci* 20(2):153–8.